Journal of the
ENGINEERING MECHANICS DIVISION
Proceedings of the American Society of Civil Engineers

ENGINEERING MECHANICS DIVISION

EXECUTIVE COMMITTEE

Harry H. Hill, Chairman
John S. McNown, Vice Chairman
Daniel C. Drucker
Merit P. White, Secretary

WEST COAST COMMITTEE

Egor P. Popov, Chairman
John F. P. Brahtz
Boris Bresler
George W. Housner
James M. Gere

CONTENTS

January, 1957

Papers

Number

The Boundary Layer Development in Open Channels
by J. W. Delleur . . . . . 1138

Approximation to Plastic Behavior of Circular Membranes
by N. A. Weil . . . . . 1139

Lateral Buckling of Plane Frameworks
by E. F. Masur and A. Cukurs . . . . . 1140

Wind Induced Vibration of Cylindrical Structures
by Joseph Penzien . . . . . 1141

Discussion . . . . . 1154

A Pressure Line Concept for Inelastic Bending
by Frank Baron . . . . . 1157

The Infinite Elastic Beam on a Linear Viscoelastic Foundation
by Alfred M. Freudenthal and Harold G. Lorsch . . . . . 1158

Copyright 1957 by the American Society of Civil Engineers.

Paper 1138 EM 1

Journal of the
ENGINEERING MECHANICS DIVISION
Proceedings of the American Society of Civil Engineers

# THE BOUNDARY LAYER DEVELOPMENT IN OPEN CHANNELS

J. W. Delleur,[1] J. M. ASCE
(Proc. Paper 1138)

## SYNOPSIS

The development of a turbulent boundary layer is analyzed theoretically for the case of a steady flow in a horizontal open channel. The problem is solved for a rectangular cross-section, but the same scheme could be used for other sections. A simplified solution is given for a channel of large width. The theory is subsequently compared with experimental results.

## NOTATION

The letter symbols are defined where they first appear, and are listed in the Appendix for reference.

## INTRODUCTION

The theory is based on the principles of continuity, of constancy of energy in the potential flow, and of conservation of momentum in the boundary layer. Blasius' formula is used for computing the friction factor, and the 1/7 power law to describe the velocity field.

An interaction of the boundary layer and the main flow outside the layer is demonstrated, with the result that the layer develops more slowly than for a flat plate in an infinite fluid under similar flow conditions. For flows close to critical the boundary layer may reach a maximum and then decrease. For subcritical flow the boundary layer may reach the surface, after which the flow is fully developed and remains uniform.

The experiments have shown that the average behavior of the boundary layer is in close agreement with the theory. The tests also revealed

Note: Discussion open until June 1, 1957. Paper 1138 is part of the copyrighted Journal of the Engineering Mechanics Division of the American Society of Civil Engineers, Vol. 83, No. EM 1, January, 1957.

1. Asst. Prof. of Hydr. Eng., School of Civ. Eng., Purdue Univ., Lafayette, Ind.

the existence of secondary motions which affect the distribution of velocities as a result of which the displacement thickness is not constant across the channel at a given cross section.

For flows well in the tranquil range, the theory predicts where the boundary layer reaches a complete development, which is often of importance in certain laboratory investigations. For flows close to critical, the theory contributes to a better understanding of the mechanism of the establishment of flow over broad crested weirs, for example, and yields a simple way of computing a discharge coefficient.

## Background of the Problem

Some free-surface problems are customarily solved by assuming an ideal non viscous fluid. The usual equation for the discharge over a broad crested weir, for example, is derived in this manner. The neglect of the friction may, however, be corrected by considering a layer of shear flow along the boundary. The flow is thus separated into two regions: a boundary layer, where the viscous effects are confined, and a region of potential flow outside the layer, where the flow behaves as if it were non viscous. The two regions of flow are treated separately, as originally suggested by Prandtl[2] in his theory of the boundary layer.

Consider a steady flow in a horizontal open channel. The flow outside the boundary layer is essentially frictionless. Bernoulli's theorem applies, and the specific energy, $E_s$, of the potential flow remains constant, that is:

$$E_s = h + u_1^2/2g = \text{constant} \qquad (1)$$

where h is the depth of flow, and $u_1$ is the velocity outside the boundary layer. Furthermore, the principle of continuity, or constancy of the discharge, must apply along the channel.

The boundary layer thickness is designated by $\delta$. Two parameters are used to describe the boundary layer: the displacement thickness and the momentum thickness. The displacement thickness $\delta_*$ is the distance by which the potential flow has been displaced from the boundary due to the presence of the boundary layer, and is defined by

$$\delta_* = \int_0^h \left(1 - \frac{u}{u_1}\right) dy \qquad (2)$$

where u is the velocity at the distance y from the boundary. The momentum thickness $\theta$, is a similar length parameter associated with the momentum defect suffered by the fluid because of friction; it is defined by

$$\theta = \int_0^h \frac{u}{u_1}\left(1 - \frac{u}{u_1}\right) dy \qquad (3)$$

2. Prandtl, L. "Uber Flussigkeiten bei sehr kleiner Reibung" Verhandlung, Third International Matmematics Congress, Heidelberg, 1904.

The determination of a turbulent boundary layer development by semi-empirical methods usually involves the use of the so-called boundary layer momentum equation. It is a differential equation derived from the equation of motion or making use of the momentum principle.[3] It was originally derived by von Karman[4] for two-dimensional laminar boundary layers:

$$c = \frac{\tau_o}{\rho u_1^2} = \frac{\partial \theta}{\partial x} + \frac{1}{u_1} \frac{\partial u_1}{\partial x} (2\theta + \delta_*) \qquad (4)$$

where $\tau_0$ is the boundary shear, $\rho$ is the density of the fluid, and c is a friction factor. Assuming no transverse flow, this equation holds for a flow in a straight open channel due to the symmetry of the flow. Furthermore, it also holds for turbulent boundary layers, by taking $u_1$ as the temporal mean velocity outside the boundary layer. Expressions for the corrective terms taking into account the anisotropy of the turbulence have been derived by Ross[5] and Robertson[6]. These are shown to be negligible for zero pressure gradient. The use of Eq. (4) to describe the conservation of momentum in a turbulent boundary layer in open channel flow is, therefore, justified. Furthermore, in this particular problem the details of the turbulent flow are not known and not required; only the development of the boundary layer is sought.

In order to integrate von Karman's momentum equation, some relations must be assumed or derived between $\delta_*$, $\theta$ and c. It is known that for flows with small pressure gradients, the shape parameter, k, of the boundary layer remains approximately constant, that is

$$\frac{\theta}{\delta_*} = k = \text{constant} \qquad (5)$$

The only remaining difficulty in applying Eq. (4) is the determination of a suitable expression for the wall shear stress coefficient. For the range of Reynolds numbers expected in open channel flow, Blasius formula[7] is the most convenient. Blasius formula was originally derived for turbulent flow in smooth pipes for $R_e = \frac{ud}{\nu} \leqslant 100{,}000$ as

$$f = 0.3164 \left(\frac{ud}{\nu}\right)^{-\frac{1}{4}} \qquad (6)$$

3. See, for example, "Modern Development in Fluid Dynamics," edited by S. Goldstein, Oxford, 1938, p. 131.
4. von Karman, Th., "Uber laminare und turbulente Reibung," Zeitschrift fur angewandte Mathematik und Mechanik, Vol. 1, p. 235-252, 1921.
5. Ross, D., "Integration of the Reynolds Equation for Incompressible Turbulent Boundary Layers," Ordnance Research Laboratory, The Pennsylvania State College, Rept. No. 2, Project NR 062-139; 1953.
6. Ross, D., and Robertson, J. M., "An Empirical Method for Calculation of the Growth of a Turbulent Boundary Layer," Jour. of Aero. Sc., Vol. 21, p. 355, 1954.
7. Blasius, H., Forschungsheft 131 des Vereins deutscher Ingen. 1911.

where d is the pipe diameter and $\nu$ the kinematic viscosity, and f is the pipe resistance coefficient in

$$\frac{p_1 - p_2}{L} = \frac{f}{d} \rho \frac{u^2}{2}$$

Blasius' formula (6) may be adapted for use in flows along a flat plate, in which case it becomes[8]

$$c = \frac{\tau_o}{\rho u_1^2} = 0.0225\, m^{1/4} \left( \frac{u_1 \delta_*}{\nu} \right)^{-\frac{1}{4}} \tag{7}$$

where $m = \frac{\delta_*}{\delta}$

Blasius' formula is often used in conjunction with the 1/7th power law which describes the velocity field in a single function

$$\frac{u}{u_1} = \left( \frac{y}{\delta} \right)^{1/7} \tag{8}$$

for which

$$m = \frac{\delta_*}{\delta} = \frac{1}{8} \quad ; \quad k = \frac{\theta}{\delta_*} = \frac{7}{9} \tag{9}$$

Blasius' friction coefficient formula and the 1/7th power law are known to be reliable for Reynolds numbers, $Re_x = \frac{u_1 x}{\nu}$,

$$5 \times 10^5 < Re_x < 10^7$$

## The Concept of Virtual Channel

The principles of constant discharge may be combined with the boundary layer displacement thickness. Calling q the discharge per unit width,

$$q = \int_0^h u\, dy = \int_0^h (u - u_1)\, dy + u_1 h$$

or, by virtue of the definition of the displacement thickness

$$q = u_1 (h - \delta_*) \tag{10}$$

Eq. (10) states that the actual discharge in a two-dimensional flow is

8. Schlichting, H., "Lecture Series 'Boundary Layer Theory,' Part II, Turbulent Flows," NACA TM No. 1218, 1949, p. 21.

equivalent to that of an ideal fluid flowing in a virtual channel of depth $h - \delta_*$. This conclusion may be generalized to a three-dimensional channel for which the actual discharge is that of an ideal fluid in a virtual channel, the boundaries of which are moved inward by an amount $\delta_*$. The expression of the discharge is thus

$$Q = A u_1 \tag{11}$$

where A is the cross sectional area of the virtual channel.

Close to the corner there is a zone of mutual interference of the layers developing along the wall and along the corner. The shape of the boundary layer near a corner has been investigated by Loitsianskii and Bolshakov.[9] Their results for a $90^0$ corner and a turbulent boundary layer have been used to sketch the edge of the displacement thickness in Fig. 1. The cross section of the virtual channel is

$$A = bh - b\delta_* - 2h\delta_* - 0.500\delta_*^2 \tag{12}$$

The term $0.5\ \delta_*^2$ is very small compared to the other terms of Eq. (12). In particular, for the experiments of series "A", to be described subsequently, $0.5\ \delta_*^2 < 0.001A$. Eq. (12) is then simplified to

$$A = bh - b\delta_* - 2h\delta_* \tag{13}$$

## The Interaction of the Boundary Layer and the Main Flow

Introducing the expression for the area of the virtual channel (13) into the equation of continuity (11), the latter becomes

$$Q = u_1 (bh - b\delta_* - 2h\delta_*) \tag{14}$$

The constancy of energy of the potential flow, outside the boundary layer requires

$$h + \frac{u_1^2}{2g} = E_s = \frac{3}{2} H \tag{15}$$

where H is the critical depth.

Eleminating h between (14) and (15), solving for $\delta_*$ and letting $q = Q/b$, it follows that

$$\delta_* = \frac{E_s - \frac{q}{u_1} - \frac{u_1^2}{2g}}{1 + \frac{2}{b}\left(E_s - \frac{u_1^2}{2g}\right)} \tag{16}$$

or

---

9. Loitsianskii, L. G. and Bolshakov, V. P.,"On the Motion of Fluids in Boundary Layer Near Line of Intersection of Two Planes," NACA TM 1308, 1951.

$$\delta_* = \frac{h - \frac{q}{u_1}}{1 + \frac{2h}{b}} \qquad (17)$$

Eq. (16) yields the average displacement thickness at any section when the specific energy, the surface velocity, and discharge are known, or when the surface velocity, depth and discharge are known. This shows the interaction of the boundary layer and the main flow, an important feature of the internal mechanism of the flow in open channels. It is this aspect that makes this boundary layer development different from that along flat plates or airfoils in an unconfined fluid. In an open channel the displacement thickness has a larger effect on the outside flow because it acts on a finite depth of fluid, whereas in an infinite flow, the effect of the displacement thickness is negligible as far as the change in the potential flow pattern is concerned. Regarding Eq. (17) the difference between the terms of the numerator is small, and therefore it yields good results only when they are known accurately.

Usually the precise measurement of h is difficult. Eq. (16) may be used where the specific energy can be measured with greater accuracy than the depth at the station, as is often the case in laboratory work.

## Equation of the Boundary Layer Development

The equation for the development of the boundary layer is obtained by introducing the expression for the displacement thickness, $\delta_*$, found above, (16), and its derivative into the boundary layer momentum equation (4). The velocity $u_1$ is taken as the independent variable, and the ratio of the momentum thickness $\theta$ to the displacement thickness $\delta_*$ is taken as a constant k, as stated in (5).

It is convenient, however, to use dimensionless parameters. The critical depth $H = \frac{2}{3} E_s$ is used as the reference length. The following dimensionless parameters are introduced:

$$\eta = \frac{\delta_*}{H} \; ; \quad \xi = \frac{x}{H} \; ; \quad \lambda = \frac{b}{H} \; ; \quad r = \frac{u_1}{\sqrt{gH}} \; ; \quad \sigma = \frac{Q}{bH\sqrt{gH}} \qquad (18)$$

$\eta$, $\xi$ and $\lambda$ are dimensionless displacement thickness, length and channel width, respectively; r is a Froude number in terms of the velocity of the main flow, and the critical depth; it will be the independent variable. Since the critical velocity is $u_c = \sqrt{gH}$, it follows that $r = 1$ corresponds to critical flow, $r < 1$ to subcritical flow, and $r > 1$ to supercritical conditions. Similarly, $\sigma$ has the form of a Froude number and has the value of unity for critical conditions. The parameter r may be interpreted as the Froude number of the potential or main flow, and $\sigma$ as the Froude number of the total flow.

Introducing the dimensionless parameters of (18) in the equation for the displacement thickness (16) and taking the derivative, it follows that

$$\eta = \frac{\frac{3}{2} - \frac{\sigma}{r} - \frac{r^2}{2}}{1 + \frac{1}{\lambda}(3 - r^2)} = \left[\frac{3}{2} - \left(\frac{\sigma}{r} + \frac{r^2}{2}\right)\right]\left[1 - \frac{3 - r^2}{\lambda + 3 - r^2}\right] \tag{19}$$

and

$$d\eta = \frac{\frac{\sigma}{r} - r^2 + \frac{2r^2\eta}{\lambda}}{1 + \frac{1}{\lambda}(3 - r^2)} \frac{dr}{r}$$

$$= \left(\frac{\sigma}{r} - r^2\right)\left[1 - \frac{3 - r^2}{\lambda + 3 - r^2} - \frac{\lambda(3 - r^2)}{(\lambda + 3 - r^2)^2} + \frac{3\sigma\lambda(1 - r^2)}{(\sigma - r^3)(\lambda + 3 - r^2)^2}\right]\frac{dr}{r} \tag{20}$$

where the second form in each case is written to simplify the computation of the limit as $\lambda$ approaches $\infty$, for the case of a two-dimensional flow, which will be considered in a subsequent section—

The Karman momentum equation (4), in terms of the new variables becomes

$$c\,d\xi = k\,d\eta + (2k+1)\,\eta\,\frac{dr}{r} \tag{21}$$

The differential equation governing the growth of the boundary layer is now obtained by replacing the values of $\eta$ and $d\eta$ in (21) by (19) and (20):

$$c\,d\xi = \left\{\frac{3}{2}\left(\frac{2k+1}{r}\right) - (4k+1)\frac{r}{2} - (k+1)\frac{\sigma}{r^2} - \frac{(3 - r^2)\left[k\left(3 - \frac{\sigma}{r} - 2r^2\right) + \left(\frac{3}{2} - \frac{\sigma}{r} - \frac{r^2}{2}\right)\right]}{r(\lambda + 3 - r^2)}\right.$$

$$\left. - \frac{\lambda k(2\sigma - 3r + r^3)}{(\lambda + 3 - r^2)^2}\right\} dr. \tag{22}$$

If Blasius' friction factor (7) is used, it may be expressed in terms of the dimensionless parameters (18) as

$$c = 0.0225\, m^{1/4}\left[\frac{r(3 - r^2)}{2} - \sigma\right]^{-\frac{1}{4}}\left[1 - \frac{3 - r^2}{\lambda + 3 - r^2}\right]^{-\frac{1}{4}}\left[\frac{H\sqrt{gH}}{\nu}\right]^{-\frac{1}{4}} \tag{23}$$

which may be introduced in (22) to yield

$$\left[\frac{H\sqrt{gH}}{\nu}\right]^{-\frac{1}{4}} d\xi = \frac{1}{0.0225\, m^{1/4}}\left[\frac{r(3 - r^2)}{2} - \sigma\right]^{\frac{1}{4}}\left[1 - \frac{3 - r^2}{\lambda + 3 - r^2}\right]^{\frac{1}{4}} \cdot$$

$$\cdot \left\{\frac{3}{2}\left(\frac{2k+1}{r}\right) - (4k+1)\frac{r}{2} - (k+1)\frac{\sigma}{r^2} - \frac{(3 - r^2)\left[k\left(3 - \frac{\sigma}{r} - 2r^2\right) + \left(\frac{3}{2} - \frac{\sigma}{r} - \frac{r^2}{2}\right)\right]}{r(\lambda + 3 - r^2)}\right.$$

$$\left. - \frac{\lambda k(2\sigma - 3r + r^3)}{(\lambda + 3 - r^2)^2}\right\} dr \tag{24}$$

Equations (19) and (24) completely define the growth of the boundary layer in terms of the discharge parameter $\sigma$, and the aspect ratio $\lambda$. The rate of growth of the boundary layer may be represented graphically by plotting $\frac{x}{H}\left(\frac{H\sqrt{gH}}{\nu}\right)^{-1/4}$ against $\eta$, where $\frac{x}{H}$ is a dimensionless length along the channel, $H\sqrt{gH}/\nu$ is a Reynolds number in terms of the critical depth and critical velocity, and $\eta$ is a dimensionless displacement thickness (see Fig. 8). Equations (19) and (24) will be referred to as the three-dimensional equations of the boundary layer growth.

## Boundary Layer Development in a Wide Channel

The equations of the boundary layer development may be greatly simplified in the case of a two-dimensional flow. When the flow is close to critical, and when the channel is very wide compared to its depth, the aspect ratio $\lambda = \frac{b}{H}$ is large. Letting $\lambda$ or b approach infinity, the equations (16), (17), (19) reduce to

$$\delta_* = E_s - \left(\frac{q}{u_1} + \frac{u_1^2}{2g}\right) \tag{25}$$

$$\delta_* = h - \frac{q}{u_2} \tag{26}$$

$$\eta = \frac{3}{2} - \left(\frac{\sigma}{r} + \frac{r^2}{2}\right) \tag{27}$$

Equation (21) of the boundary layer growth becomes, for $\lambda \to \infty$,

$$c\,d\xi = \left[\frac{3}{2}\frac{(2k+1)}{r} - (4k+1)\frac{r}{2} - (k+1)\frac{\sigma}{r^2}\right] dr \tag{28}$$

so that the differential equation (24) of the boundary layer development, in which Blasius' friction factor formula has been used to evaluate c, is:

$$\left(\frac{H\sqrt{gH}}{\nu}\right)^{-\frac{1}{4}} d\xi = \frac{1}{0.0225\,m^{1/4}}\left[\frac{r(3-r^2)}{2} - \sigma\right]^{\frac{1}{4}}\left\{\frac{3}{2r}(2k+1) - \frac{r}{2}(4k+1) - \frac{\sigma}{r^2}(k+1)\right\} dr \tag{29}$$

Equations (27) and (28) completely define, in a parametric form, the growth of the boundary layer, and yield a family of curves of $\frac{x}{H}\left(\frac{H\sqrt{gH}}{\nu}\right)^{-\frac{1}{4}}$ vs. $\eta$ in terms of the discharge parameter $\sigma$, (Fig. 2). Comparing equations (27) and (29) to (19) and (24), it appears that the bulk of the solution is given by the two dimensional equation, and the effect of the side walls and corners appears as a correction. The magnitude of this correction permits one to evaluate the effect of the sides and corner, (see Fig. 8).

## General Properties of the Boundary Layer Development in an Horizontal Channel

For simplicity the general properties of the boundary layer development will be analyzed in terms of the two-dimensional theory; they may be extended to the three-dimensional theory, in which the effect of the sides and corners appear as a correction to the two-dimensional theory.

At the origin of the boundary layer $\delta_* = 0$, and Eq. (25) yields a relation between $\sigma$ and r:

$$\frac{r(3-r^2)}{2} - \sigma = 0 \tag{30}$$

The plot of Eq. (30) is shown as curve I on Fig. 3. Curve I has two branches, the left branch for $r < 1$ and the right branch for $r > 1$, which correspond to subcritical and supercritical conditions respectively. Therefore for each value of the discharge parameter $\sigma$, there are two possible values of the velocity parameter, namely, $r_0$ and $r_3$, which correspond to subcritical and supercritical conditions respectively.

Under certain conditions, the development of the boundary layer may reach a maximum. Assuming that such a maximum exists, at that point $d\eta/dr = 0$ for which Eq. (27) yields

$$\sigma = r^3 \tag{31}$$

The plot of Eq. (31) is shown as curve II in Fig. 3, and $r_1$ is the value of r which satisfies Eq. (31). Using the definitions (18), it follows that the condition (31) is equivalent to $u_1^3 = gq$. But since it was established in (10) that $q = u_1(h - \delta_*)$, the condition (31) yields.

$$u_1 = \sqrt{g(h-\delta_*)} \tag{32}$$

This indicates that the flow is critical in the virtual channel of depth $h - \delta_*$, at the point of maximum development of the boundary layer. The boundary layer thus grows to a maximum, producing a throat in the virtual channel. This throat is the control of the discharge. When the existence of this maximum is physically possible, the discharge establishes itself in such a manner that the flow is critical at the maximum.

Eq. (27) and (29), which describe the development of the boundary layer have a physical significance only when the boundary layer thickness $\delta$ is less than the depth of water h. That is the limit of validity of the theory reached when $m = \frac{\delta_*}{\delta} = \frac{\delta_*}{h}$, or by (15), (16) and (18), when

$$\frac{\sigma}{1-m} = \frac{r(3-r^2)}{2} \tag{33}$$

In the limiting case of the boundary layer becoming tangent to the free surface, $r = 1$, and the condition for existence of the maximum of the layer is

$$1 - m < \sigma < 1 \tag{34}$$

Beyond its maximum, the boundary layer decreased until it reaches a point where the tangent is vertical. This occurs when $\frac{d\xi}{d} = 0$ or by (29) when

$$\sigma = \left(\frac{3}{2}\,\frac{2k+1}{k+1} - \frac{4k+1}{2(k+1)}\,r^2\right)r \qquad (35)$$

The plot of Eq. (35) is shown as curve III in Fig. 3, for $k = \frac{7}{9}$, and where $r_2$ is the value of r which satisfies (35). The section of the curve of the growth of the boundary layer, between the maximum and the point of vertical tangent, that is for $r_1 < r < r_2$, is not accurate, because of the rapid increase in velocity between $r_1$ and $r_2$ which requires a rapid change of surface slope. This would necessitate taking into account the curvature of the flow. This situation may occur when the channel ends with a free overfall.

Due to the confinement of the flow and the effect of the free surface, the rate of growth of the boundary layer in open channels is slower than along a flat plate in an infinite fluid. For the purpose of comparison the development of the boundary layer along a flat plate is shown in Fig. 2.[10]

## Laboratory Set-Up

The general layout of the laboratory equipment is shown in Fig. 4. The main feature of the equipment is the test channel which is 15' - 7-1/2" long and 13-11/16" wide. It is part of a closed circuit formed by the reservoir, the pump, the constant head tank, the entrance section with gravel baffles and screens, the test section of the channel, the exit of the channel with a measuring weir, and finally, a return channel leading back to the reservoir.

The measuring equipment consisted of a pitot tube with its traversing mechanism, a micromanometer, and point gages. The pitot tube consisted of a hypodermic needle inserted in a streamlined lucite stem. Two sizes of needles were used: 0.027" O.D. and 0.060" O.D. Almost all data presented herein were taken with the 0.060" tube, which had an inside diameter of 0.041". The traversing mechanism controlled the vertical position of the pitot tube to the nearest 0.001", and the micromanometer was designed to indicate pressure differentials of 0.001" of water.

The discharge was controlled by maintaining a constant pool elevation at the entrance section. The elevation was measured with a point gage which permitted the reproduction of the pool elevation for consecutive experiments on the same flow.

The investigation being focussed on the development of a turbulent boundary layer, it was deemed desirable to ensure that the transition from a laminar to a turbulent flow in the boundary layer always occurred at the same point. The point selected was the end of the curved inlet, so that the boundary layer would be turbulent throughout the length of the channel proper. A 1/16" wire was found convenient for the range of experiments.

## Experiments

Four series of experiments were carried out, with the following characteristics:

10. Schlichting, H., "Lecture Series 'Boundary Layer Theory,' Part II, Turbulent Flows," NACA TM 1218, 1949, Eq. (17.9).

| Series | Type of Flow | Total Energy E | Discharge Parameter | Aspect Ratio |
|---|---|---|---|---|
| A | Subcritical | .218' | .84 | 7.85 |
| B | Subcritical | .259' | .50 | 4.41 |
| C | Subcritical | .2505' | .855 | 6.83 |
| D | Supercritical | .6835' | .158 | 2.49 |

Series "A" is the most complete of the four series of experiments. It was designed to check thoroughly the theory for a particular flow condition. Series "B", "C" and "D" are more qualitative and were intended to explore other flow conditions. Velocity profiles were taken at the center of the channel ($z = 0$) and at $z = \pm .1'$; $\pm .2'$; $\pm 3'$; $\pm 4'$, where z is measured normal to the axis of the channel, at 4 stations: $x = 52''$; $99.75''$; $135.75''$ and $171.5''$, where x is measured from the beginning of the channel. In addition, centerline velocity profiles were taken at $x = 4''$; $25''$; $63.875''$; $81.75''$; $123.5''$ and $153.69''$. Typical data are presented in Figs. 5 to 7.

The displacement thicknesses $\delta_*$ were computed by numerical integration from the velocity profiles. Where several profiles were taken at the same station, the average $\delta_*$ was computed (a weight of 1 was given to each value of $\delta_*$, except those pertaining to outer profiles which were assigned a relative weight of 1/2). These average displacement thicknesses were then expressed in dimensionless form and compared with the values predicted by the theory. The displacement thicknesses were also evaluated from Eq. (16). The results are summarized in Table 1, and in Fig. 8.

Series "B" has a low value of $\sigma$, indicating a very tranquil flow, the velocity being far from critical. The boundary layer in this case would pierce the surface before reaching its maximum. The experimental channel was too short to reach the point of full development of the flow. (See Fig. 9.)

Series "C" was intended for the check of formula (16). The local depths were measured with a point gage indicating the nearest 0.001". The displacement thicknesses, computed by this formula, are compared with the experimental data, and the theoretical curve of the boundary layer growth in Fig. 9.

Series "D" was intended to check the theory in the case of supercritical flow. The supercritical condition was obtained by placing a sluice gate at the entrance of the channel. The rough surface for this type of flow made the observations difficult; the results are shown in Fig. 9.

## Analysis of Data

Examinations of Fig. 8 reveal the main conclusions to be drawn from the experimental investigation. The average displacement thickness confirms the three-dimensional theory. The shape of the theoretical curve of the boundary layer development, the existence of the maximum point and the subsequent decrease of the boundary layer thickness are also confirmed. The curve through the average experimental displacement thickness is consistently slightly below the theoretical curve. The individual experimental data from points across the channel at a given station are scattered about their mean. This scatter is attributed to the presence of secondary motions. The theory

thus predicts the mean behavior of the boundary layer, but does not show the detail of the boundary layer distribution as influenced by the secondary flow. Motion pictures of tracer particles have shown the existence of these secondary flows.

The boundary layer experiments also showed that formula (16), which also evaluates the mean behavior of the boundary layer, yields results which are in close agreement with the theory.

The experiments show that the 1/7th power law describes adequately the average velocity field. The 1/7th power law has been generalized to a power formula of the type $\frac{u}{u_1} = \left(\frac{y}{\delta}\right)^n$, for which

$$m = \frac{\delta^*}{\delta} = \frac{1}{\frac{1}{n} + 1} \qquad \text{and} \qquad K = \frac{\theta}{\delta_*} = \frac{\frac{1}{n}}{\frac{1}{n} + 2}$$

The experimental data indicate that n varies from a maximum of $\frac{1}{5.5}$ to a minimum of $\frac{1}{7.70}$; the average n for the experiment was $\frac{1}{6.85}$. The numerical computation could have been carried out with this value of n instead of 1/7. However, this slight deviation does not affect the results, because in the equation for the growth of the boundary layer n occurs indirectly in $m^{\frac{1}{4}}$ and k, which are not very sensitive to small changes in n.

It may also be remarked that the equations (19) and (24) governing the development of the boundary layer do not contain explicitly the length of the channel. This is due to the fact that the specific energy $E_s$, the discharge parameter $\sigma$ and the length L of the channel are not independent. For example, if the energy $E_s$ and the length L are specified, the discharge parameter $\sigma$ is determined. In other words, $\sigma$ is not a free parameter when $E_s$ and L are given. This fact may be used to analyze, for example, how the discharge establishes itself over a broad crested weir, and yields a theoretical way of computing a discharge coefficient, thus relating the fixed geometry of this hydraulic device and the discharge when the boundary layer is the governing factor.[16] The governing influence of the boundary layer on the rate of flow over embankment shaped weirs has also been substantiated in the comprehensive experiments carried out by Sigurdsson.[17]

He also confirms the use of the 1/7th power law to describe the velocity distribution. It must be pointed out that the application of the boundary layer theory to broad crested weirs has certain limitations. In fact, other phenomena may play an important role in the hydraulics of broad crested weirs, such as the curvature and possible undulation of the surface. There may also be a separation at the entrance if it is not rounded, which would have a predominant effect. The theory is applicable only where the flow is essentially parallel and free from undulation and separation.

For flows well in the tranquil range, the boundary layer grows until it reaches the surface, after which the flow becomes uniform. The determination of the distance to the point of uniform flow in intake section of open

16. Delleur, J. W., "The Boundary Layer Development on Broad Crested Weirs," Fourth Midwestern Conference on Fluid Mechanics, Purdue University, 1955.
17. Sigurdsson, G., "Discharge Characteristics of an Embankment-shaped Weir," M. S. Thesis, Georgia Inst. of Tech., June, 1955.

channels is important in certain laboratory investigations.[18] Or, inversely, the discharge which will yield a uniform flow in an open channel may be required.

## CONCLUSIONS

The development of a turbulent boundary layer is treated for steady flow in a rectangular open channel. A simplified solution is given for a channel of large width.

The theory shows an interaction of the boundary layer and the main flow outside the layer, with the result that the layer develops more slowly than for a flat plate in an infinite fluid under similar flow conditions. For flows close to critical the boundary layer may reach a maximum and then decrease. For flows less than critical the theory predicts where the boundary layer reaches the surface.

The experiments have shown that the average behavior of the boundary layer is in close agreement with the theory. The tests revealed that there are secondary motions which affect the distribution of velocities. As a result the displacement thickness is not constant at any one cross section, but the average displacement thickness is in close agreement with the theory.

Two applications of the theory are mentioned: the distance to uniform flow in the intake section of open channel, which is sometimes an important factor in laboratory investigations; and the computation of a theoretical discharge coefficient for flows over horizontal broad crested weirs.

From a broader point of view, the consideration of the boundary layer in open channel opens new horizonts for a better understanding of the internal mechanism of this type of flow.

## ACKNOWLEDGMENTS

This paper is based on a dissertation submitted in April 1955 to the School of Engineering at Columbia University in partial fulfillment of the requirements for the degree of Doctor of Engineering Science. The research was initiated under the guidance of Professor A. E. Craya, formerly Visiting Professor at Columbia University,[19] and to whom the author is very grateful. This work was partially sponsored by the Office of Naval Research under Contract Nonr 266 (10).[20]

## NOTATION

A : cross section of virtual channel

b : width of channel

c : friction coefficient for flow along flat plates

18. Delleur, J. W., Discussion to ASCE Transaction paper 2716, 1954, p. 1167.
19. At the present at the University of Grenoble, France.
20. Craya, A. E., and Delleur, J. W., "An Analysis of Boundary Layer Growth in Open Conduits Near Critical Regime," Dept. of Civil Engineering, Columbia Univ., Contract Nonr 266 (10), 1952. A copy of this report has been deposited at the Engineering Societies Library in New York City.

f : friction coefficient for pipe flow

h : depth of flow

H : critical depth

k : shape parameter of velocity profile

l : length of zone of interference of bottom and wall boundary layers

n : ratio

q : discharge per unit width

Q : total discharge

r : velocity parameter, dimensionless

Re : Reynolds number

u : longitudinal velocity

$u_1$ : velocity at the edge of the boundary layer

x : distance along the channel

$\delta$ : boundary layer thickness

$\delta_*$ : displacement thickness

$\eta$ : ratio $\delta_*/H$

$\lambda$ : ratio b/H

$\nu$ : kinematic viscosity

$\xi$ : ratio x/H

$\rho$ : density

$\sigma$ : discharge parameter, dimensionless

$\tau$ : boundary shear stress

TABLE 1

Series "A"

COMPARISON OF THEORETICAL AND EXPERIMENTAL DATA

| x (in.) | 4 | 25" | 52" | 63.88 | 81.75 | 99.75 | 123.50 | 135.75 | 153.69" | 171.50 |
|---|---|---|---|---|---|---|---|---|---|---|
| $\delta^*$ computed from velocity profiles Iin.) | .061 (C.L.) | .085 (C.L.) | .136 (Avg.) | .110 (C.L.) | .111 (C.L.) | .186. (Avg.) | .080 (C.L.) | .201 (Avg.) | .103 (C.L.) | .163 (Avg.) |
| $\delta^*$ computed by approximate formula (in.) | .051 | .090 | .142 | .157 | .179 | .182 | .217 | .218 | .218 | .216 |
| $\delta^*$ computed from velocity profiles | .0351 | .0489 | .0782 | .0628 | .0634 | .1066 | .0460 | .1153 | .0589 | .0933 |
| $\eta$ computed by approximate formula | .0292 | .0518 | .0815 | .0898 | .1025 | .1044 | .1247 | .1249 | .1253 | .1239 |
| $\eta$ computed by theoretical formula | .0125 | .0480 | .0778 | .0883 | .1017 | .1130 | .1232 | .1272 | .1298 | .1267 |
| $\frac{x}{H}\left(\frac{H\sqrt{gH}}{\nu}\right)^{-\frac{1}{4}}$ | .172 | 1.073 | 2.233 | 2.742 | 3.510 | 4.283 | 5.302 | 5.828 | 6.599 | 7.363 |

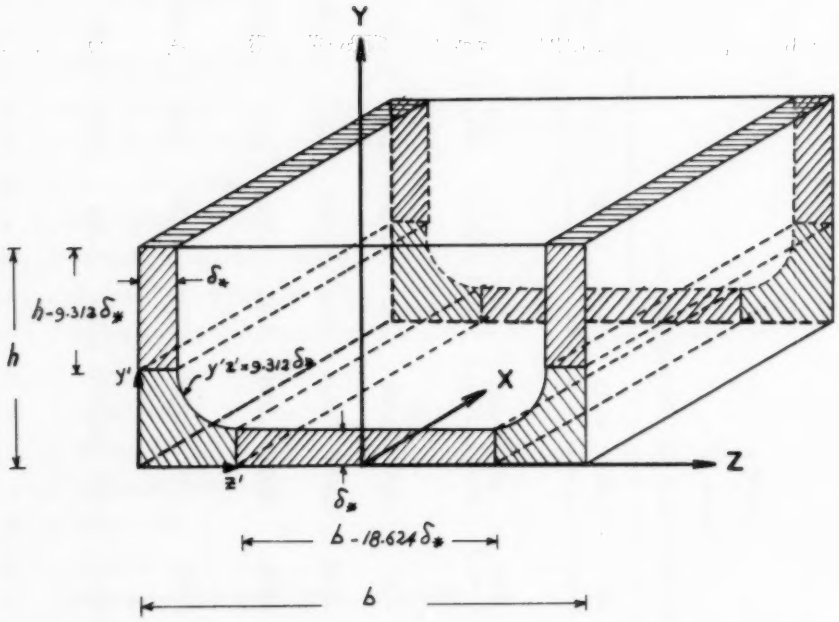


FIG. 1. VIRTUAL CHANNEL

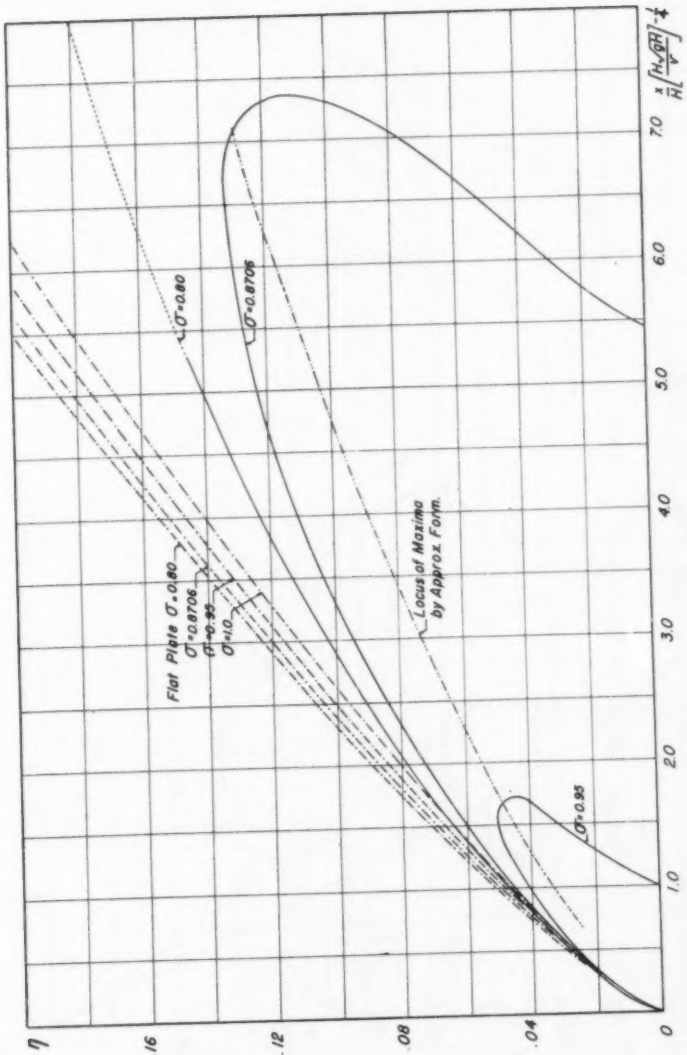


FIG.2

Boundary Layer Growth

Two-Dimensional Flow

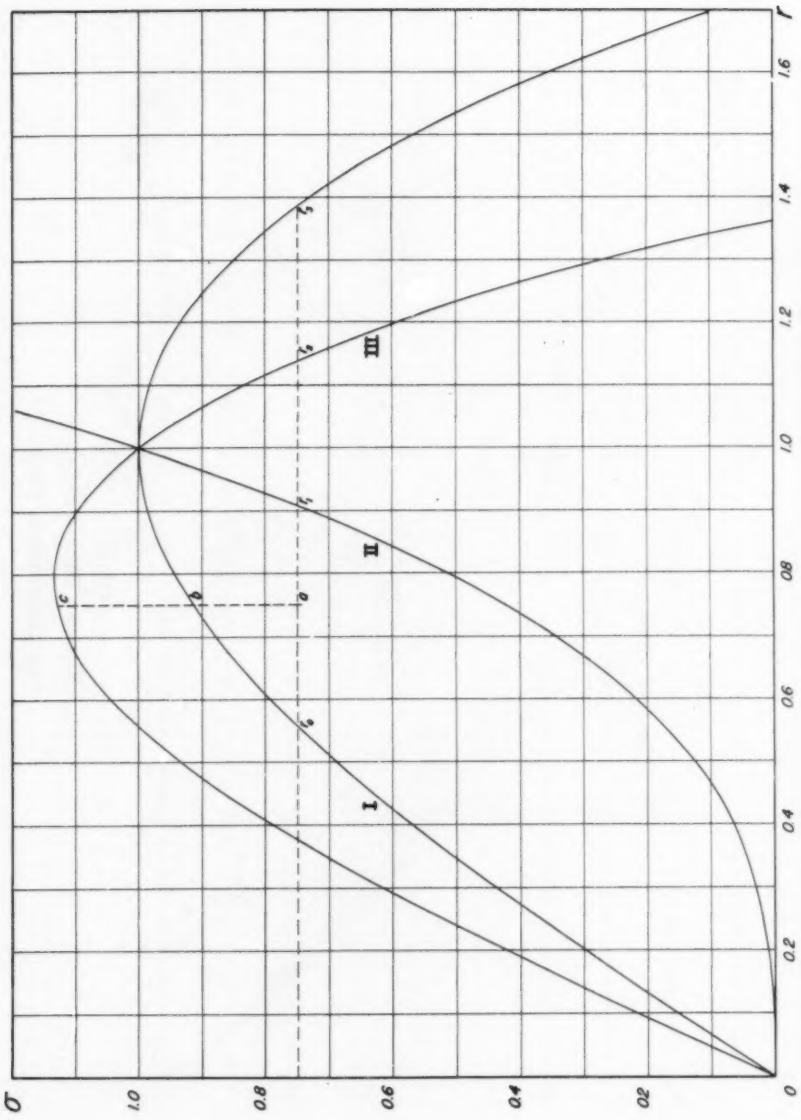


FIG. 3. Relation between $r_0, r_1, r_2, r_3$ and $\sigma$

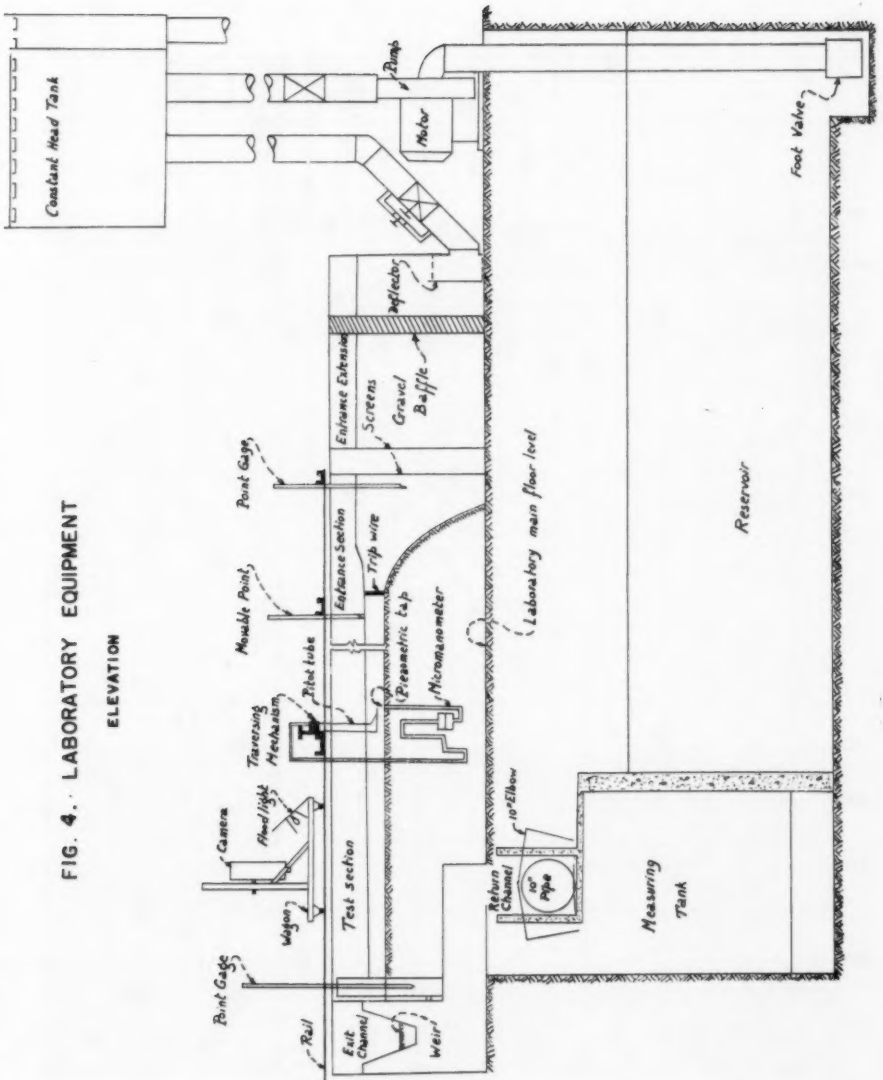


FIG. 4. - LABORATORY EQUIPMENT

ELEVATION

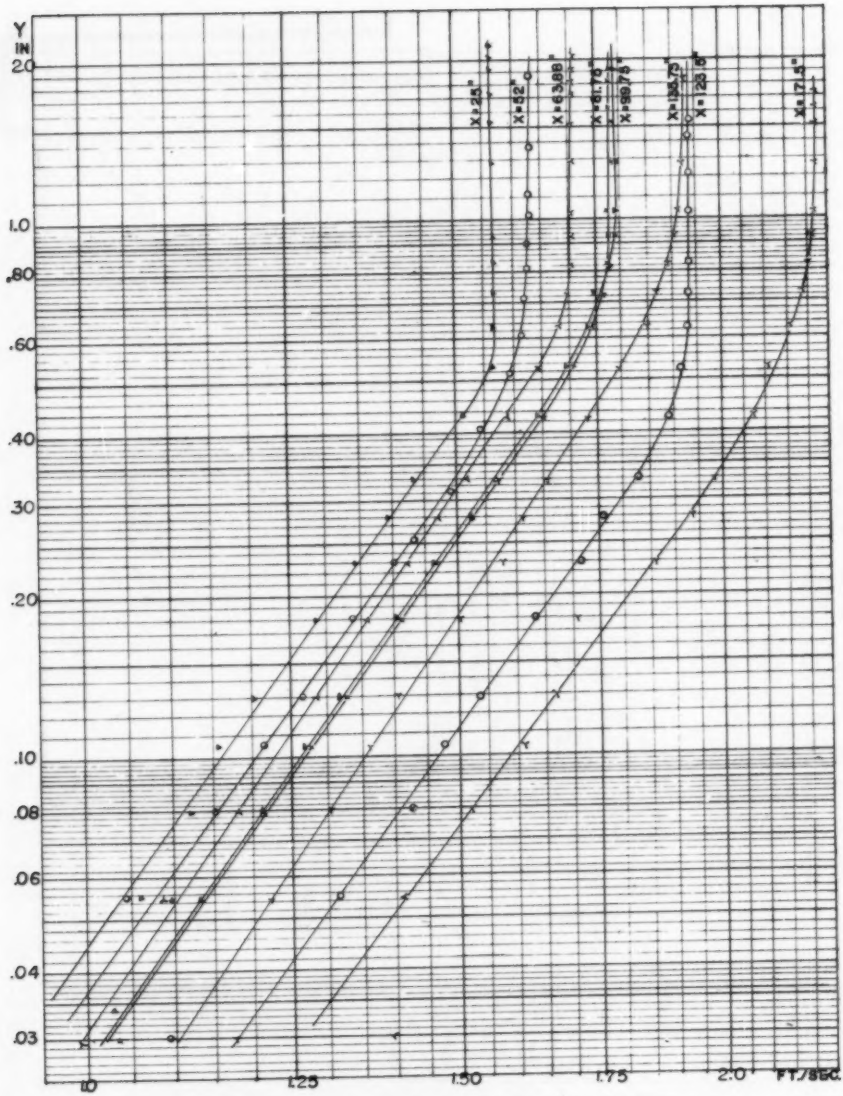


FIG 5 VELOCITY MEASUREMENTS ALONG CENTER LINE

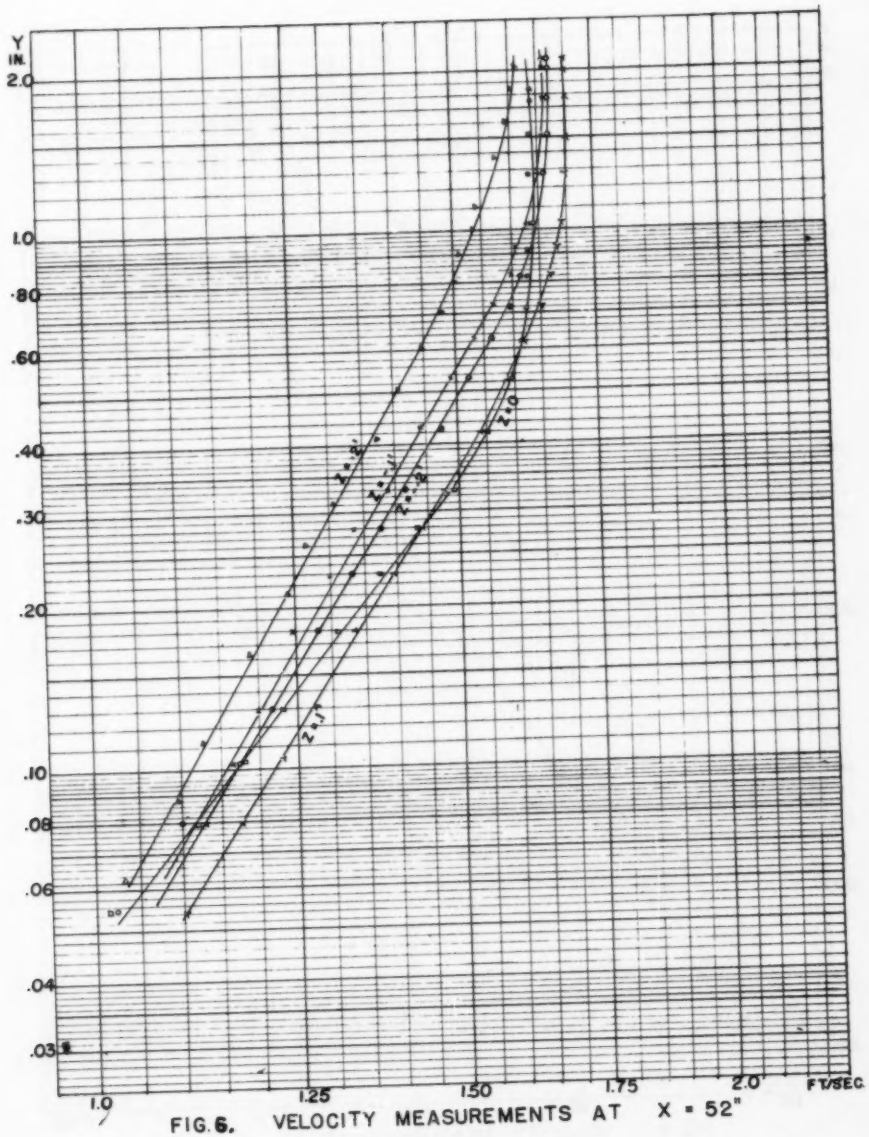


FIG. 6. VELOCITY MEASUREMENTS AT X = 52"

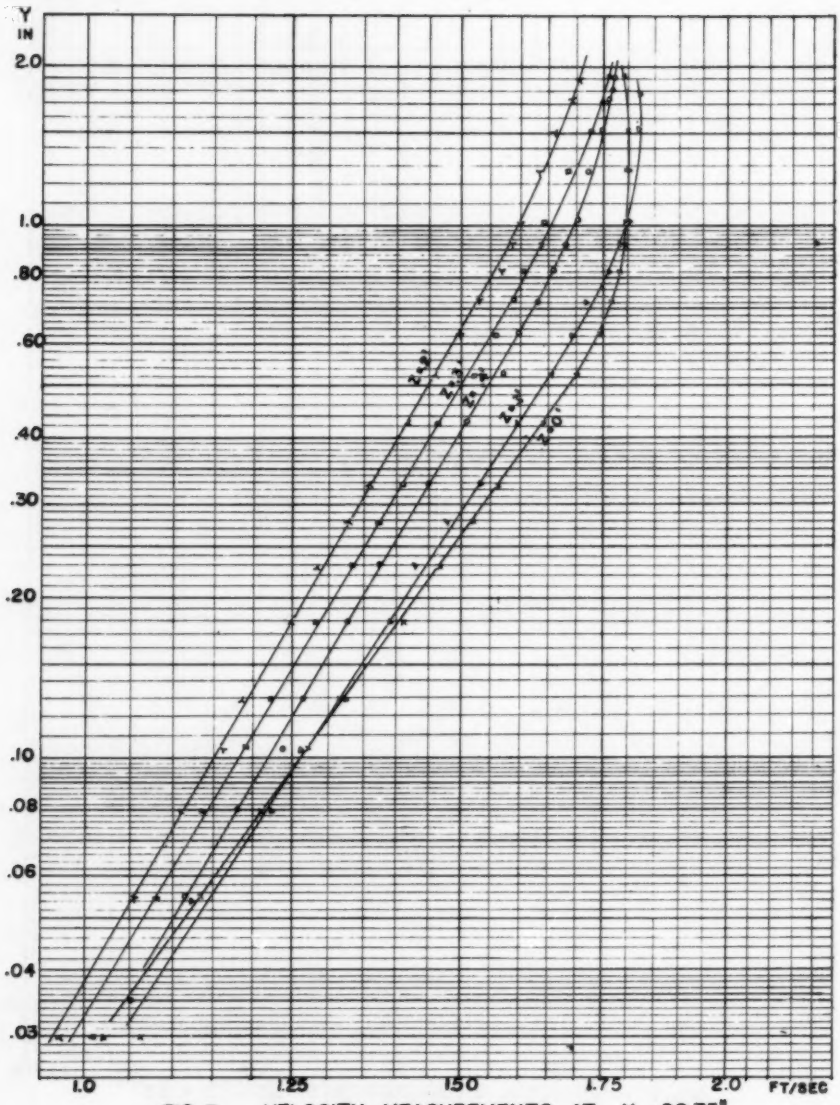


FIG. 7. VELOCITY MEASUREMENTS AT X =99.75"

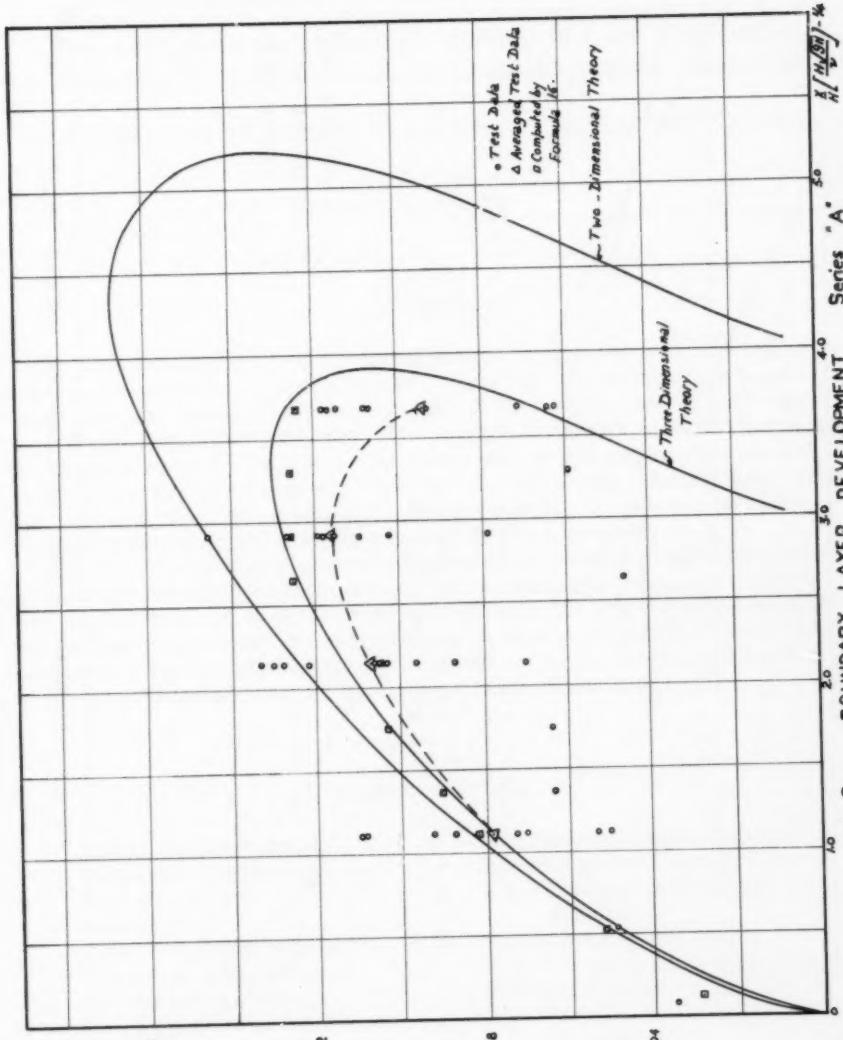


FIG. 8. BOUNDARY LAYER DEVELOPMENT

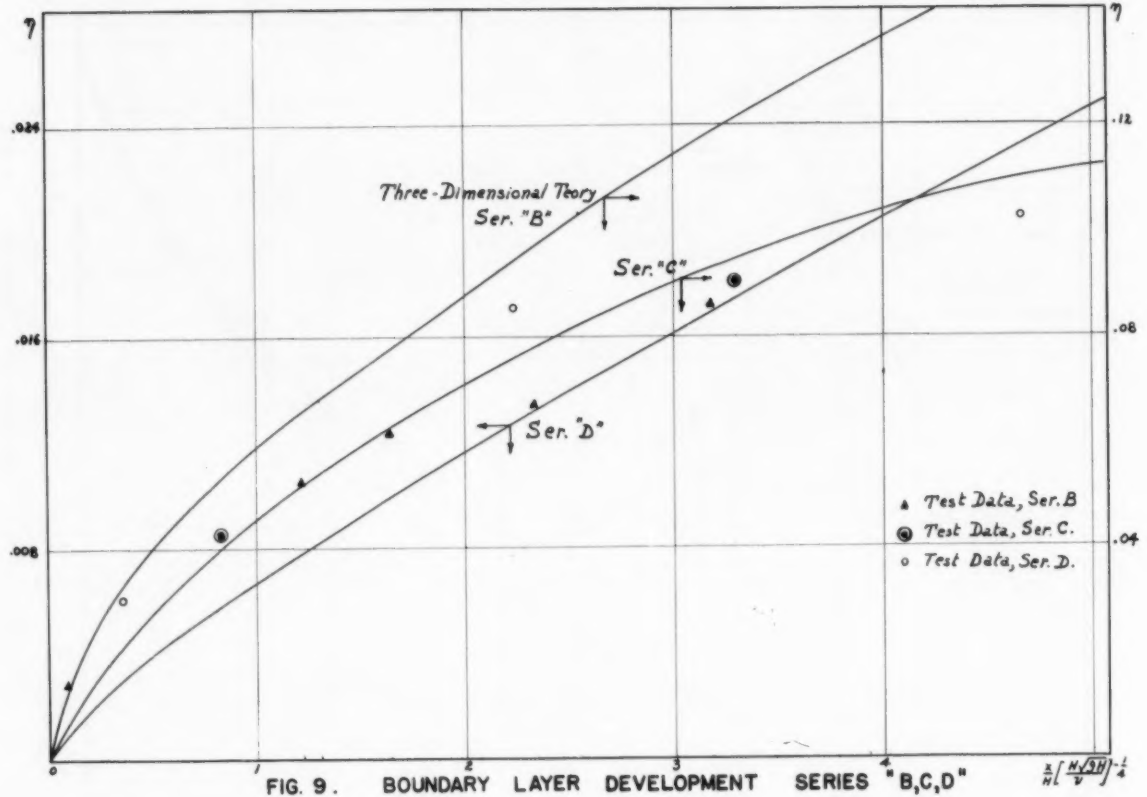


FIG. 9. BOUNDARY LAYER DEVELOPMENT SERIES "B,C,D"

Paper 1139 EM 1

Journal of the
ENGINEERING MECHANICS DIVISION
Proceedings of the American Society of Civil Engineers

# APPROXIMATION TO PLASTIC BEHAVIOR OF CIRCULAR MEMBRANES

N. A. Weil,[1] J. M. ASCE
(Proc. Paper 1139)

## SYNOPSIS

An approximate theory is presented for the plastic behavior of clamped circular membranes subjected to lateral hydrostatic pressures. It is assumed that the actual stress-strain curve of the material can be well represented by a parabolic expression. The von Mises-Hencky relations are taken to govern the plastic behavior of the material; suitable approximations are then adopted for the biaxial stress-strain and strain-displacement laws. The derivation is based on infinite power series expansions, wherein terms containing the higher powers of small quantities are neglected.

The predictions of this approximate theory are compared with experimental results obtained from bulge tests of annealed copper diaphragms. Theory and experiments are in satisfactory agreement in the low and medium pressure ranges. In the vicinity of instability the theory gradually deviates from experimental observations; this is accounted for by the increased contribution of the omitted terms near the bursting pressure of the diaphragm.

## NOMENCLATURE

$a$ = Radius of diaphragm, in
$h$ = Thickness of diaphragm, in
$\sigma$ = True stress, psi
$\epsilon$ = Natural strain
$\tau$ = Octahedral shear stress, psi
$\gamma$ = Octahedral shear strain
$P$ = Hydrostatic pressure, psi
$p$ = $Pa/\overline{h}$ = Relative pressure, psi
$\eta$ = $h/\overline{h}$ = Dimensionless thinning
$r$ = Radial distance from pole, in
$\rho$ = $r/a$ = Dimensionless radial distance
$w$ = Vertical deflection, in
$\omega$ = $w/a$ = Dimensionless deflection
$u$ = Horizontal displacement, in
$v$ = $u/a$ = Dimensionless horiz. displacement
$m$ = Strain hardening exponent
$A$ = Hardness factor, psi

Note: Discussion open until June 1, 1957. Paper 1139 is part of the copyrighted Journal of the Engineering Mechanics Division of the American Society of Civil Engineers, Vol. 83, No. EM 1, January, 1957.

1. Design Engr., M. W. Kellogg Co., New York, N. Y.

Subscripts r, $\theta$, z denote entities acting in meridional, circumferential and normal (i.e. principal) directions. Bars above symbols represent entities in the original (undeformed) plate; the subscript o refers to variables at the center (pole) of the bulge.

## INTRODUCTION

The problem of the plastic behavior of clamped membranes is important from two structural viewpoints: to determine the load-deflection relations in the plastic domain and to obtain an estimate on the ultimate load carrying ability (or the bursting pressure in the case of fangible disks) of circular plates. Rheologically this problem is used to examine the validity of various plasticity laws over a wide range of strains.

All of the aforementioned aspects of this problem have received the attention of investigators. An analytical treatment, based on the Hencky-Mises plasticity laws and strain-displacement relations valid for large deformation in the plastic domain, was recently presented in the literature.(1) This solution, hereinafter referred to as the "exact theory," is in good agreement with experimental results, and predicts the significant values at instability with a fair degree of accuracy. The solution itself, however, is cumbersome, requiring a numerical iteration scheme between two simultaneous integral equations.

To avoid the difficulties inherent in an exact solution, Hill (2) proposed an approximate solution, whose results are given in closed form. This solution is based on the Levy-Mises plasticity laws (i.e. strain-rates rather than strains are considered), and is valid only for materials whose stress-strain curve can be well approximated by a linear relationship.

Most materials, especially annealed metals, do not possess a constant rate of strain hardening. For materials with a decreasing rate of strain hardening the Hill-theory, as will be shown later, may be insufficiently accurate to be used even as a crude approximation. In this case the assumption of a power-function (parabola) for the stress-strain relation would lead to a closer correlation with the physical behavior of the structure investigated.

This assumption forms the core of the current work. To comply with the nature of the problem, strain-displacement relations valid for large deformations were adopted, although their form was somewhat simplified from that used in the exact solution (1) to lessen the complexity of the derivation. The material is also assumed to be insensitive to rate of straining. The laws of static equilibrium are observed and the plasticity laws are approximately satisfied. The solution is obtained in the form of successive approximations, in which higher powers of small quantities are ignored. The current work is restricted to the full development of the second approximation. The dimensionless notation used in the derivation allows for an immediate application of the results to diaphragms of various radii and thicknesses.

### Solution of the Approximate Theory

The von Mises flow condition postulates that plastic deformation will occur when the octahedral shear stress

$$\tau = \frac{1}{3}\left[ (\sigma_1 - \sigma_2)^2 + (\sigma_2 - \sigma_3)^2 + (\sigma_3 - \sigma_1)^2 \right]^{1/2} \qquad (1)$$

exceeds a given limiting value. The magnitude of flow is measured by the octahedral shear strain

$$\gamma = \frac{2}{3}\left[ (\varepsilon_1 - \varepsilon_2)^2 + (\varepsilon_2 - \varepsilon_3)^2 + (\varepsilon_3 - \varepsilon_1)^2 \right]^{1/2} \quad (2)$$

where the yield curve $\tau = \tau(\gamma)$ is assumed to be known. Assuming volume constancy

$$\varepsilon_1 + \varepsilon_2 + \varepsilon_3 = 0 \quad (3)$$

the flow condition for a uniaxial stress $\sigma_1$ and a longitudinal strain $\epsilon_1$ becomes

$$\left.\begin{aligned} \tau &= \frac{\sqrt{2}}{3}\sigma_1 \\ \gamma &= \sqrt{2}\,\varepsilon_1 \end{aligned}\right\} \quad (4)$$

In the case of biaxial stress ($\sigma_1 = \sigma_2$, $\epsilon_1 = \epsilon_2$), the flow condition modifies to

$$\left.\begin{aligned} \tau &= \frac{\sqrt{2}}{3}\sigma_1 \\ \gamma &= 2\sqrt{2}\,\varepsilon_1 = \sqrt{2}\,(-\varepsilon_3) \end{aligned}\right\} \quad (5)$$

Eqs. 4 and 5 show that plastic deformation is governed by identical relations under uniaxial and biaxial stresses, if in the latter case the negative through-thickness strain is taken as a measure of the amount of straining.

Assume now that uniaxial stress-strain relation for a given material follows the power-function law

$$\left.\begin{aligned} \sigma_1 &= A\varepsilon_1^{\,m} \quad \text{or} \\ \tau &= 2^{(1-m)/2}\, A\, \gamma^m/3 \end{aligned}\right\} \quad (6)$$

where m is the strain hardening exponent and A is the stress value (hardness factor) at $\epsilon_1 = 1$.

In a clamped diaphragm subjected to lateral pressure, the stress distribution varies from a balanced biaxiality at the crown to a biaxiality ratio of 1/2 at the edge. It is, therefore, a reasonably good simplification to assume that the yield criterion will be given by

$$\frac{\sigma_r + \sigma_\theta}{2} = A(-\varepsilon_z)^m \quad (7)$$

Let the finite strain-displacement relations be given by the approximate dimensionless form:

$$\left.\begin{aligned} \varepsilon_r &= v' + \tfrac{1}{2}(\omega')^2 \\ \varepsilon_\theta &= v/\rho \\ \varepsilon_z &= \ln \eta \end{aligned}\right\} \qquad (8)$$

where primes denote differentiation with respect to $\rho$.

Hill's first approximation,(2) postulating a constant stress throughout the diaphragm, shows that the through-thickness strain will be given by (to this approximation)

$$\varepsilon_z = -2\omega_o^2 (1 - \rho^2) \qquad (9)$$

Adopting this criterion as the starting point for the second approximation, Eq. 7 assumes the form

$$\sigma_r + \sigma_\theta = 2^{1+m} A \omega_o^{2m} (1 - \rho^2)^m \qquad (10)$$

The equilibrium of normal forces yields [see Eq. 13 of Ref. (1)]

$$\sigma_\theta = \left(1 + \frac{\eta'\rho}{\eta}\right)\sigma_r + \rho\sigma_r' \qquad (11)$$

One can eliminate $\sigma_\theta$ from Eqs. 10 and 11 to obtain

$$\sigma_r' + \left(\frac{2}{\rho} + \frac{\eta'}{\eta}\right)\sigma_r = 2^{1+m} A \omega_o^{2m} \frac{(1 - \rho^2)^m}{\rho} \qquad (12)$$

Furthermore, Eq. 9 and the last of Eqs. 8 can be combined to give

$$\eta'/\eta = \varepsilon_z' = 4\omega_o^2 \rho \qquad (13)$$

which substituted into Eq. 12 leads to

$$\sigma_r' + 2\left(\frac{1}{\rho} + 2\omega_o^2 \rho\right)\sigma_r = 2^{1+m} A \omega_o^{2m} \frac{(1 - \rho^2)^m}{\rho} \qquad (14)$$

Eq. 14 is a first order differential equation with variable coefficients, $\rho$

being the independent and $\sigma_r$ the dependent variable. The explicit solution of this type of differential equation is well known; however, the integrals appearing in this solution cannot be evaluated in closed form.

Therefore, in what follows, infinite series expansions will be used, unless the problem lends itself to a solution in closed form. In doing so, only those terms of the infinite series are retained which involve powers of the variables no higher than $\rho^5$, $\omega_o{}^5$ or $m^2$.

These assumptions merit more detailed consideration. The range of the dimensionless radial distance is $0 \leq \rho \leq 1$. In the vicinity of the clamping edge, $\rho \leq 1$, stresses and strains are relatively small, so that omission of terms containing the sixth or higher powers of $\rho$ should not introduce serious errors.

For annealed materials one commonly finds that $m \leq 0.4$ and for severely cold-rolled materials $m < 0.1$. Hence the error due to the omission of terms in $m^3$ or higher will generally stay below 7 per cent; in most instances the error will be much less, remembering that most series expansions have inverse factorial coefficients.

$\omega_o$ varies from 0 at the beginning of the experiment to a maximum possible value of 1; most engineering materials fail at about $\omega_o \leq 0.6$. At low pressures the contribution of terms of order $\omega_o{}^6$ or higher is entirely negligible. At increasing pressures, however, the error due to the omission of these terms becomes more significant. This will lead to a gradual deviation of the actual values from the results predicted by this approximate theory, the error being largest at instability.

Proceeding on the principles set down above, and disallowing infinite stresses at the pole, the solution of Eq. 14 yields $\sigma_r$; $\sigma_\theta$ can then be obtained from Eq. 10. The stresses will therefore be given by the expressions

$$\left.\begin{aligned} \sigma_r &= 2^m A\omega_o{}^{2m}\left\{1 - (0.5m+\omega_o{}^2)\rho^2 - \left[0.5m(1-m) - m\omega_o{}^2 - 2\omega_o{}^4\right]\frac{\rho^4}{3}\right\} \\ \sigma_\theta &= 2^m A\omega_o{}^{2m}\left\{1 - (1.5m-\omega_o{}^2)\rho^2 - \left[2.5m(1-m) + m\omega_o{}^2 + 2\omega_o{}^4\right]\frac{\rho^4}{3}\right\} \end{aligned}\right\} \quad (15)$$

The relationship between pressure and vertical deflection can be obtained in the following manner. Eq. 15 of Ref. 1 can be modified to

$$\omega' = -\frac{\rho p}{2\sigma_r \eta}\left(1 - \frac{\rho^2 p^2}{4\sigma_r{}^2 \eta^2}\right)^{-1/2}$$

and expanding

$$\omega' = -\frac{\rho p}{2\sigma_r \eta} - \frac{\rho^3 p^3}{16\sigma_r{}^3 \eta^3} \quad (16)$$

The term containing $\rho^5$ has been omitted in Eq. 16 because otherwise the solution would become extremely complex. This step, however, is justified,

since the numerical coefficient of this term is exceedingly small (1/128).

Eq. 13 can be readily solved for $\eta$ subject to the boundary condition that $\eta = 1$ at $\rho = 1$. Expanding this solution in series one obtains

$$\eta = 1 - 2\omega_o^2(1-\rho^2) + 2\omega_o^4(1-\rho^2)^2 \tag{17}$$

Inserting now $\sigma_r$ from the first of Eqs. 15 and $\eta$ from Eq. 17 into Eq. 16, results, to this approximation

$$\left.\begin{aligned}\omega' = -\Bigg\{ & 1 + 2\omega_o^2 + 2\omega_o^4 + \left[0.5m - (1-m)\omega_o^2 - (2-m)\omega_o^4\right]\rho^2 + \\ & + \left[m(1+0.5m) + m^2\omega_o^2 + (2-2m+m^2)\omega_o^4\right]\frac{\rho^4}{6}\Bigg\}\frac{\rho\rho}{2^{1+m}k\omega_o^{2m}} - \\ & - \Bigg\{1 + 6\omega_o^2 + 18\omega_o^4 + \left[0.5m - (1-3m)\omega_o^2 - (6-9m)\omega_o^4\right]3\rho^2 + \\ & + \left[m(0.5+m) - m(1-6m)\omega_o^2 + (4-15m+18m^2)\omega_o^4\right]\rho^4\Bigg\}\left(\frac{\rho\rho}{2^{1+m}k\omega_o^{2m}}\right)^3\end{aligned}\right\} \tag{18}$$

For a constant pressure the only independent variable in this equation is $\rho$. Hence it can be integrated to yield

$$\left.\begin{aligned}\omega = -\Bigg\{ & (0.5+\omega_o^2+\omega_o^4)\rho^2 + \left[0.5m - (1-m)\omega_o^2 - (2-m)\omega_o^4\right]\frac{\rho^4}{4} + \\ & + \left[m(1+0.5m) + m^2\omega_o^2 + (2-2m+m^2)\omega_o^4\right]\frac{\rho^6}{36}\Bigg\}\frac{p}{2^{1+m}k\omega_o^{2m}} - \\ & - \Bigg\{(1+6\omega_o^2+18\omega_o^4)\frac{\rho^4}{4} + \left[0.5m - (1-3m)\omega_o^2 - (6-9m)\omega_o^4\right]\frac{\rho^6}{2} + \\ & + \left[m(0.5+m) - m(1-6m)\omega_o^2 + (4-15m+18m^2)\omega_o^4\right]\frac{\rho^8}{8}\Bigg\}\left(\frac{p}{2^{1+m}k\omega_o^{2m}}\right)^3 + C\end{aligned}\right\} \tag{19}$$

In Eq. 19 $\omega_o$ appears as a parameter. Its value can be obtained from the boundary conditions:

$$\omega = \omega_o \quad \text{at} \quad \rho = 0$$
$$\omega = 0 \quad \text{at} \quad \rho = 1$$

Substitution of the boundary values and elimination of C from the resulting two expressions of Eq. 19 leads to

$$\left[1 + 1.25m^2 + 0.5m + (4+5.5m+2m^2)\omega_o^2 + (8+10.5m+9m^2)\omega_o^4\right]\left(\frac{p}{2^{2+m}A\omega_o^{2m}}\right)^3 + \left[1 + 0.3056m + 0.0278m^2 + (1.5+0.5m+0.0556m^2)\omega_o^2 + (1.1111+0.3889m+0.5m)\omega_o^4\right]\frac{p}{2^{2+m}A\omega_o^{2m}} - \omega_o = 0 \quad (20)$$

The above expression is cubic in the relative pressure, p. Treating this quantity as the independent variable ($\omega_o$ being fixed for a given pressure) and using the Newton-Raphson method,(3) Eq. 20 can be solved to yield

$$p = \left[1 - 0.3056m + 0.0656m^2 - (2.5-0.3889m-0.1184m^2)\omega_o^2 + (6.139+0.5332m-2.886m^2)\omega_o^4\right]2^{2+m}A\omega_o^{1+2m} \quad (21)$$

Having obtained the value of C from the boundary conditions and p from Eq. 21, one can return to Eq. 19 to obtain an explicit expression for the dimensionless deflection:

$$\omega = \left\{1 + \left[0.3056m - 0.0656m^2 + (0.5+0.222m-0.296m^2)\omega_o^2 + (1.8611-0.6998m+2.518m^2)\omega_o^4\right]\rho^2 + \left[0.0556m + 0.0108m^2 + (1.1111m-0.6373m^2)\omega_o^2 + (3.111-1.8457m+1.2495m^2)\omega_o^4\right]\rho^4\right\}(1-\rho^2)\omega_o \quad (22)$$

Furthermore, Eq. 21 can be inverted to solve for $\omega_o$ in terms of p. There results

$$\omega_o = \left[1 + 0.3056m - 0.5833m^2 + (2.5-2.333m+1.1678m^2)\left(\frac{p}{2^{2+m}A}\right)^{\frac{2}{1+2m}} + (12.611-33.99m+79.56m^2)\left(\frac{p}{2^{2+m}A}\right)^{\frac{4}{1+2m}}\right]\left(\frac{p}{2^{2+m}A}\right)^{\frac{1}{1+2m}} \quad (23)$$

Adopting now the Hencky deformation theory for the yield criterion

$$\left.\begin{aligned} \varepsilon_i &= \frac{\gamma}{3\tau}\left[\sigma_i - \frac{1}{2}(\sigma_j+\sigma_k)\right] \\ i,j,k &= 1,2,3 \quad ; \quad i \neq j \neq k \end{aligned}\right\} \tag{24}$$

and using the law of volume constancy, Eq. 3, the following identity can be derived to relate principal strains and stresses

$$\varepsilon_r = \frac{2\sigma_r - \sigma_\theta}{2\sigma_\theta - \sigma_r}\,\varepsilon_\theta \tag{25}$$

and by substitution of Eqs. 15 and the second of Eqs. 8

$$\varepsilon_r = \left[1 + (3m-6\omega_o^2)\rho^2 + (2m+5.5m^2-22m\omega_o^2+22\omega_o^4)\rho^4\right]\frac{v}{\rho} \tag{26}$$

The first of Eqs. 8, in turn, can be rewritten as

$$v' = \varepsilon_r - \tfrac{1}{2}\omega'^2$$

which, upon substitution of Eqs. 22 and 26, leads to the first order differential equation

$$\left.\begin{aligned} v' - \left[1 + (3m-6\omega_o^2)\rho^2 + (2m+5.5m^2-22m\omega_o^2+22\omega_o^4)\rho^4\right]\frac{v}{\rho} &= \\ = -\Big\{1 - 0.6111m + 0.2245m^2 - (1+0.1389m-0.5694m^2)\omega_o^2 - & \\ - (3.472-1.6219m+5.235m^2)\omega_o^4 + & \\ + \left[m - 0.6111m^2 + (2-4.667m+2.705m^2)\omega_o^2 - \right. & \\ \left. - (6-5.583m-5.095m^2)\omega_o^4\right]\rho^2 + & \\ + \left[0.3333m + 0.2130m^2 + (7m-9.222m^2)\omega_o^2 - \right. & \\ \left. - (10.333+2.620m-4.477m^2)\omega_o^4\right]\rho^4\Big\}\,2\rho^2\omega_o^2 & \end{aligned}\right\} \tag{27}$$

Solving Eq. 27 subject to the boundary condition that $v = 0$ at $\rho = 1$ provides the expression for $v$. Then, by the second of Eqs. 8,

$$\varepsilon_\theta = \Big\{ 1-0.9167m-0.5471m^2 + (1.5+0.2778m-2.498m^2)\omega_o^2 - \\ - (9.75-18.079m-113.65m^2)\omega_o^4 + \\ + \Big[ 1.1944m-2.147m^2 - (0.5-5.417m+1.0097m^2)\,\omega_o^2 - \\ - (10.778-0.9992m-130.42m^2)\,\omega_o^4 \Big]\rho^2 + \\ + \Big[ 0.4444m+0.6590m^2 - (1.6667m-11.134m^2)\,\omega_o^2 - \\ + (0.7222-28.44m+103.12m^2)\,\omega_o^4 \Big]\rho^4 \Big\} (1-\rho^2)\omega_o^2 \qquad (28)$$

and, from Eq. 26

$$\varepsilon_r = \Big\{ 1 - 0.9167m - 0.5471m^2 + (1.5+0.2778m-2.498m^2)\omega_o^2 - \\ - (9.75-18.079m-113.65m^2)\omega_o^4 + \\ + \Big[ 4.194m - 4.897m^2 - (6.5-15.417m-3.106m^2)\omega_o^2 - \\ - (21+29.92m-199.65m^2)\omega_o^4 \Big]\rho^2 + \\ + \Big[ 2.444m + 7.909m^2 - (29.33m-69.24m^2)\omega_o^2 + \\ + (25.72-124.45m+28.11m^2)\omega_o^4 \Big]\rho^4 \Big\} (1-\rho^2)\omega_o^2 \qquad (29)$$

The through-thickness strain, $\epsilon_z$, can be derived by simply adding Eqs. 28 and 29, and providing this sum with a minus sign, according to Eq. 3. The polar stress and the in-plane polar strain can be derived from Eqs. 15 and 28, respectively, by setting $\rho = 0$:

$$\sigma_o = 2^m \lambda \omega_o^{2m} \qquad (30)$$

$$\varepsilon_o = (1-0.9167m-0.5471m^2)\omega_o^2 + (1.5+0.2778m-2.498m^2)\omega_o^4 - \\ - (9.75-18.079m-113.65m^2)\omega_o^6 \qquad (31)$$

This completes the solution to the second approximation. The next

approximation would demand that Eqs. 15 be reintroduced into Eq. 10 in order to obtain a more defined relationship for the stresses.

## Comparison of Approximate Theory with Experiments

The experiments conducted on annealed copper membranes of two thicknesses were described in a previous paper.(1)

In brief, annealed electrolytic copper plates of two thicknesses were tested: two "thin" plates with $\bar{h}$ = 0.02087 and 0.02020 in., respectively, and a "thick" plate with $\bar{h}$ = 0.1303 in. These plates were clamped into a device with a 11.5 in. aperture, rendering the radius a = 5.75 in.

Pressure was applied in predetermined steps to one side of the plates during the tests. After reaching a desired level, the pressure was released prior to any measurements, in agreement with theoretical considerations which ignored the contribution of elastic deformations. The initially flat plate deformed into a bulge as the test progressed; physical measurements (apart from pressure values) consisted of strain readings with the aid of a photogrid (20 lines per inch) using a microscope of about X9 magnification as well as clip strain-gages with a range of 0.20 in/in total strain capacity. Vertical and horizontal displacement were measured by means of a 0.0001" Ames dial mounted on a specially constructed bridge. These measurements were carried out over two mutually perpendicular radii of the plate, with clip gages applied to both the top and bottom surfaces.

In order to bring all tests to a common denominator, test results were plotted in terms of the "relative pressure," p. Conversion from actual pressure, P, to relative pressure was made through the relationship $p = Pa/\bar{h}$. Calculated numerical results are also expressed in terms of the relative pressure, p.

The stress-strain curve for this material is shown in Fig. 1. As can be seen in this figure, the actual stress-strain curve can be approximated by an expression of the type of Eq. 6, if the material constants are taken as

$$A = 65{,}500 \text{ psi} \; ; \; m = 0.375$$

Upon substitution of these numerical values into Eqs. 23, 31 and 30 in succession, the approximate theory yields the following expressions for the dimensionless crown deflection, polar strain and polar stress for this material:

$$\omega_o = \frac{7.132}{10^4} p^{0.5714} + \frac{5.898}{10^{10}} p^{1.7143} + \frac{17.385}{10^{16}} p^{2.857} \qquad (32)$$

$$\varepsilon_o = 0.5793\omega_o^{\,2} + 1.2529\omega_o^{\,4} + 13.011\omega_o^{\,6} \qquad (33)$$

$$\sigma_o = 8494\omega_o^{\,0.75} \qquad (34)$$

For given magnitudes of the relative pressure p, one can now calculate the dimensionless polar deflection from Eq. 32; in possession of this quantity the strain and stress at the crown are obtained from Eqs. 33 and 34 respectively.

The results of these calculations are shown in Figs. 2, 3 and 4,* along with the experimental values obtained from the tests. The agreement between the approximate theory and experiments is quite good at low and medium pressures. Near instability the agreement becomes less satisfactory; vertical deflection and stresses become too low, whereas predicted strains are excessive. Furthermore none of the curves exhibit a vertical rise, which characterizes the physical behavior of the membrane at instability.

Some of the reasons for the deviation of this theory from experiments in the vicinity of bursting have already been mentioned in the text. Among these are the approximate nature of the assumptions incorporated in Eqs. 6, 7, 8 and 9, the omission of higher order terms from the infinite series expansion and the fact that this solution was carried only to a second iterative step. The approximation involved in Eq. 6 could be improved by adopting a stress-strain expression of the type

$$\sigma = A\varepsilon^m + B\varepsilon^n$$

In view of the fact that even the simpler assumption for the stress-strain curve is quite close to the actual physical properties (see Fig. 1), this improvement is not felt to be significant. Rather, it seems that the approximations involved in Eqs. 7 and 8, and the sizeable contribution of the terms of order $\omega_o^6$ are the chief cause of the discrepancy near the limiting pressure.

As mentioned before, a different approximate theory was previously proposed by Hill.(2) It is based on the tenet that the actual stress-strain relation can be well approached by a linear expression of the type

$$\sigma = Y(1+H\varepsilon) \tag{35}$$

To the second approximation this assumption yields the following expressions for the significant variables:

$$(6H-10)\omega_o^3 + 4\omega_o = p/Y \tag{36}$$

$$\varepsilon_o = \omega_o^2 - \frac{3H-1}{4}\omega_o^4 \tag{37}$$

$$\sigma_o = (1+2H\omega_o^2)Y \tag{38}$$

For a given relative pressure level p, $\omega_o$ is obtained from the cubic expression given in Eq. 36 by some suitable method, say the Newton-Raphson method. $\epsilon_o$ and $\sigma_o$ can then be readily determined explicitly from Eqs. 37 and 38.

For the annealed copper used in this comparison, the material constants appearing in Hill's theory were assumed to be

$$Y = 15{,}000 \text{ psi} \; ; \; H = 6.1$$

* In Fig. 2 the dimensionless polar deflection, $\omega_o$, has been reconverted into actual center deflection, w.

The linear stress-strain curve based on these assumptions is also pictured in Fig. 1. It may be added that this line was obtained by choosing the best linear fit to the real $\sigma - \epsilon$ curve over the strain range $0 < \epsilon < 0.32$ encountered in the bulge tests. Finally the vertical center deflection, strain and stress predicted by Hill are shown in Figs. 2, 3 and 4 in dashed lines. The vertical center deflection and stress, Figs. 2 and 4, in the low and medium pressure range are predicted as well by Hill as by the theory described in this paper. At high pressures the Hill theory is less apt to follow actual physical behavior, insofar as these variables are concerned. For the polar strain, Fig. 3, Hill's approximation predicts a maximum, whereafter the polar strain is seen to diminish with increasing pressures. This is contrary to the physical behavior of disks subjected to lateral hydrostatic pressure.

The investigation of the instability condition and limiting pressures will be dealt with in a separate paper.

## REFERENCES

1. N. A. Weil and N. M. Newmark, "Large Plastic Deformations of Circular Membranes." Jour. App. Mech. Vol. 22, pp. 533-538 (1955).

2. R. Hill, "A Theory of the Plastic Bulging of a Metal Diaphragm by Lateral Pressure." Phil. Mag., Vol. 41, 7th Series, pp. 1133-1142 (Nov. 1950).

3. J. B. Scarborough, "Numerical Mathematical Analysis," The Johns Hopkins Press, Baltimore, Md., (1950).

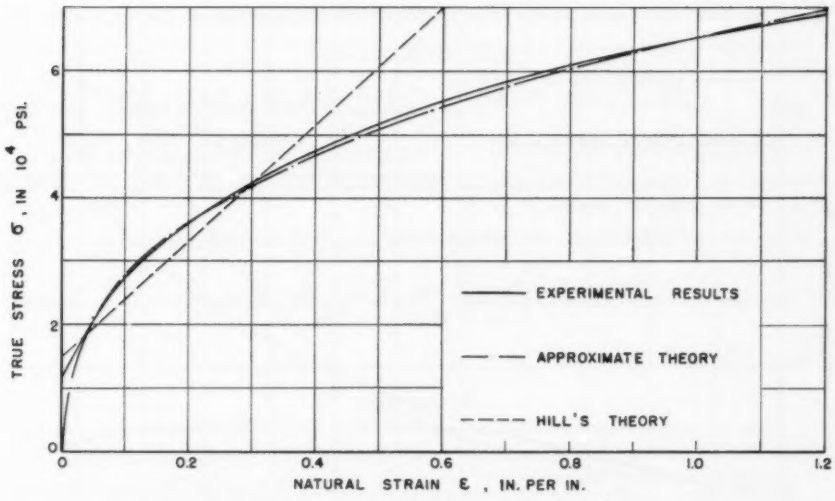


FIG. 1 STRESS-STRAIN CURVE FOR ANNEALED COPPER

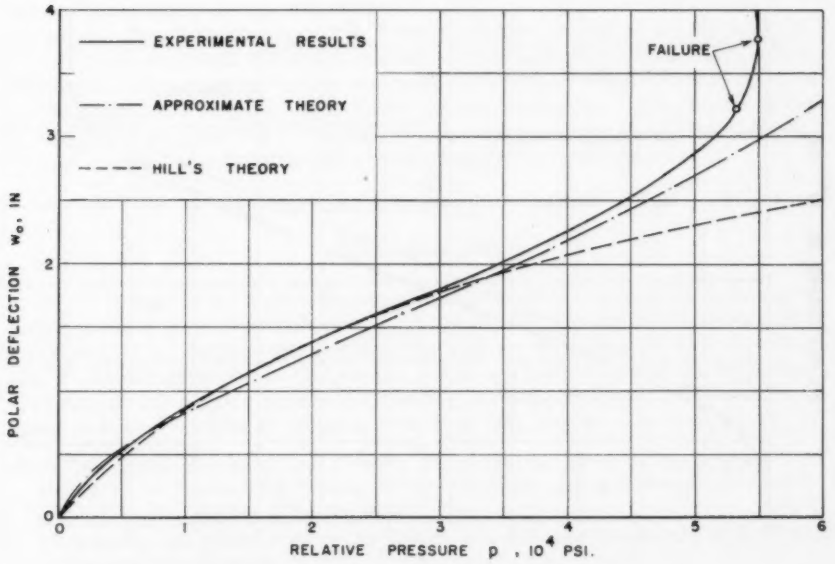


FIG. 2 POLAR DEFLECTION AS FUNCTION OF PRESSURE

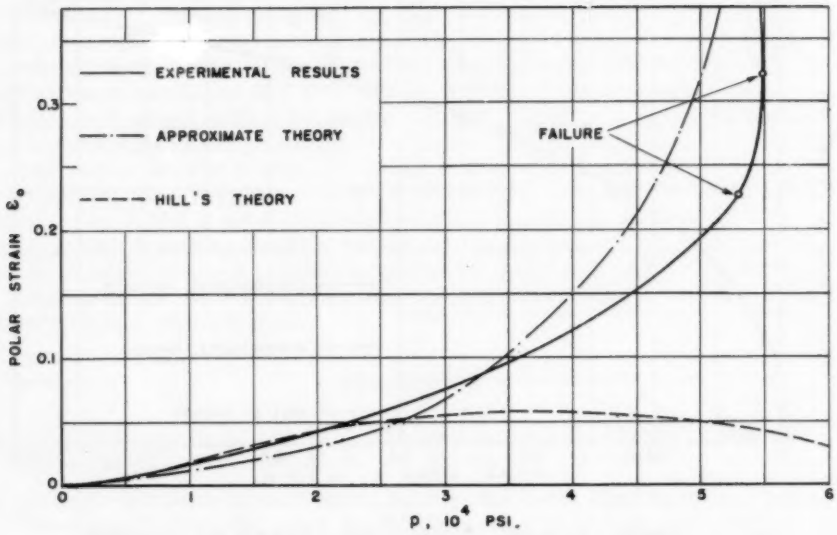


FIG. 3 POLAR STRAIN AS FUNCTION OF PRESSURE

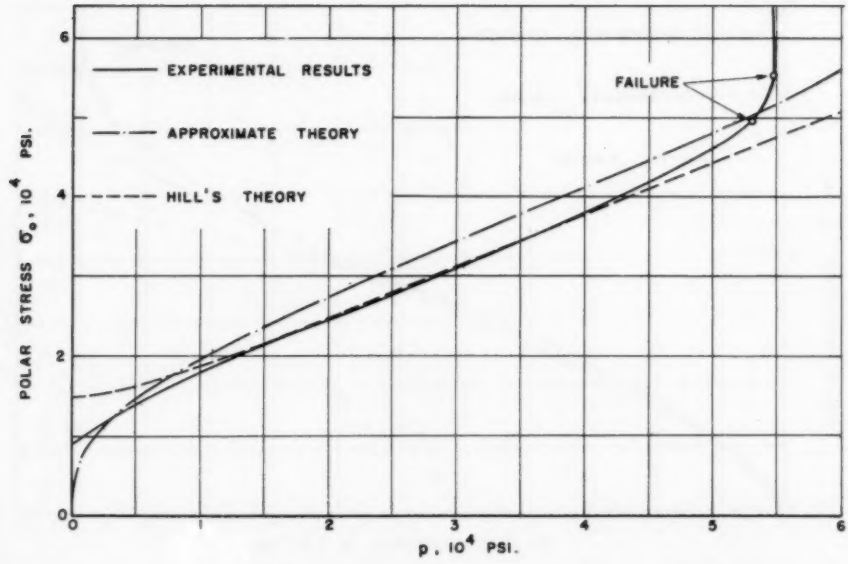


FIG. 4 POLAR STRESS AS FUNCTION OF PRESSURE

Journal of the
ENGINEERING MECHANICS DIVISION
Proceedings of the American Society of Civil Engineers

# LATERAL BUCKLING OF PLANE FRAMEWORKS[1]

E. F. Masur,[2] A.M. ASCE, and A. Cukurs[3]
(Proc. Paper 1140)

## SUMMARY

In current design practice it is generally assumed that a truss is equally safe against buckling in and out of its plane if its members have the same slenderness ratio in both directions. In this paper it is shown that the argument may be inapplicable to the customary rigid jointed type of structure. In fact it is demonstrated that this kind of truss, designed under present code requirements, may exhibit a much smaller factor of safety against buckling normal to its plane than in its plane.

The analysis of the lateral stability proceeds from the establishment of the basic equations to the derivation of a determinantal form of stability criterion. An alternate approach, pursued further in this paper because of its reduced numerical difficulty, utilizes a generalized moment distribution technique in the analysis of the response of the truss to applied unit couples whose planes are perpendicular to that of the structure. This results in the development of a "series criterion" which represents an extension and generalization of a similar criterion first proposed by Lundquist.

## INTRODUCTION

In the design of a compression member of a steel truss, it is customary, under present code requirements [1],[4] to consider the allowable axial stress a function of the largest slenderness ratio alone, without regard to the condition of elastic restraint at the joints. It follows therefore that an "efficient" member should display approximately the same slenderness ratio with respect to both principal directions; this, it is felt, should insure an equal

Note: Discussion open until June 1, 1957. Paper 1140 is part of the copyrighted Journal of the Engineering Mechanics Division of the American Society of Civil Engineers, Vol. 83, No. EM 1, January, 1957.

1. This work was sponsored by the Office of Ordnance Research, U.S. Dept. of the Army, Washington, D.C.
2. Associate Prof. of Eng. Mechanics, Univ. of Michigan, Ann Arbor, Mich.
3. Structural Eng., Procon, Inc., Chicago, Ill.
4. Numbers in brackets refer to the bibliography at the end of the paper.

factor of safety against buckling both in and out of the plane of the structure.

It is fairly obvious that this kind of reasoning cannot be applied to a large and common class of trusses without major modification. Even in the event of perfect pin connections at the joints, the argument is valid only if the centroid and shear center coincide. This is often not the case. The customary double-angle type of section, for example, buckles laterally in a mode which couples bending and twisting, and under an axial load which may be appreciably smaller than the Euler load, which is based on a bending mode alone.

If the bars are held rigidly at the joints, this discrepancy is likely to increase further. When buckling occurs in the elastic region (that is, for sufficiently slender elements) the critical compressive stress depends to a large extent on the degree of end restraint. This restraint, which is imposed on one member by the adjoining members, is generally less effective relative to lateral buckling that in relation to buckling in the plane of the structure. This is especially true of double-angle sections, whose torsional stiffness is negligible compared with their bending stiffness. It is therefore not implausible to expect trusses composed of such members to exhibit a greater tendency to buckle normal to their plane than in their own plane.

It is the purpose of this paper to investigate the conditions under which this type of instability will occur. In order to facilitate the analysis, a number of assumptions are made which, it is felt, are reasonable without reducing the generality of the approach to a significant extent. It is assumed, for example, that the members of the truss are joined rigidly at the panel points; the effect of the gusset plates is therefore disregarded. It is postulated further that the panel points are held rigidly against lateral translation by means of lateral cross bracing, which, however, does not contribute to the rotational joint stiffness. Since all members are composed of two angles, the further assumption that the shear center itself is held against lateral movement at the joints appears not unwarranted in view of the fact that the cross bracing is ordinarily connected to the outstanding legs.

The analysis in the form presented here is not confined to double-angle sections; it is restricted, however, to sections whose warping stiffness may be considered negligible in comparison with their torsional and bending stiffnesses. An extension to sections exhibiting appreciable warping resistance, such as, e.g., I-beams, may be effected at the expense of some of the numerical simplicity. On the other hand, this does not appear worthwhile since members of this type are rarely slender enough to be in danger of elastic buckling, at least so far as common structural practice is concerned.

It is finally assumed that, prior to lateral buckling, all members are subjected only to axial forces through their centroids. This implies, of course, that all external loads are applied at the joints, that all bars are initially straight, and that the effect of the joint translations within the plane of the framework may be neglected. Actually, "secondary moments" are inevitable and are likely to affect the condition of lateral instability to a significant extent. Nevertheless, this omission is not considered serious, as will be discussed in the Conclusion.

## Establishment of Basic Equations

In what follows, let a representative bar between joints i and j buckle laterally as shown in Fig. 1. The differential equations of equilibrium

governing the displacements (u,v) of the shear center S and the rotation $\beta$ are well-known and are given, for example, in [2], p. 132. For the case under consideration, in which the warping constant is assumed to vanish and in which, by virtue of the symmetry of all sections, buckling in the plane of the framework is uncoupled and may therefore be ignored, they read:

$$EI_y u^{iv} + P u'' + P y_o \beta'' = 0 \tag{1}$$

$$P y_o u'' + (P \rho^2 - G K)\beta'' = 0 \tag{2}$$

In these equations, the axial force P is considered positive in compression. E and G are the usual material constants, while $I_y$ and K are, respectively, the moment of inertia about the y-axis and the torsional stiffness constants.[5] The radius of gyration about the shear center is designated by $\rho$, and $y_o$ is the coordinate of the shear center relative to the centroid C. Primes, as usual, indicate differentiation with respect to the independent variable (z) along the axis of the bar.

Eqs. (1) and (2) can be simplified somewhat. If the dimensionless quantity $\mu$ is defined by

$$\mu = \frac{y_o^2}{GK/P - \rho^2} \tag{3}$$

it follows, from Eq. (2), that

$$y_o \beta'' = \mu u'' \tag{4}$$

and, upon substitution in Eq. (1), that

$$EI_y u^{iv} + N u'' = 0 \tag{5}$$

in which N is an "equivalent" axial force given by

$$N = P (1 + \mu) \tag{6}$$

The general solution of these linear homogeneous equations is readily established and involves six constants of integration. Basically, this process should now be repeated with each member. There results a large number of constants of integration, for which an equal number of linear homogeneous boundary conditions is available. The problem is to determine the smallest load for which the ensuing system of linear homogeneous equations admits a non-trivial solution; in this fashion, a typical determinantal stability criterion is established.

This represents a task of formidable numerical proportions. It can be simplified greatly, however, through a systematizing procedure which is analogous to the establishment of modified "slope-deflection" equations. To this end, the bar rotations $\beta$ and $\theta$ at the joints (representing twisting and

5. To be on the safe side, K for the section is assumed to be twice the value of the individual angle.

bending rotations, respectively) are introduced as independent variables, and Eqs. (4) and (5) are solved subject to the boundary conditions.

$$\begin{aligned} u(0) &= 0 & u(L) &= 0 \\ u'(0) &= \theta_{ij} & u'(L) &= -\theta_{ji} \\ \beta(0) &= \beta_{ij} & \beta(L) &= -\beta_{ji} \end{aligned} \tag{7}$$

in which L represents the length of the member. The choice of the sign convention is governed by considerations of consistency for the developments below.

The functions u(z) and $\beta(z)$ are thus established in terms of the four end rotations; their form is of no direct interest here and has therefore been omitted. However, it is now possible to express the twisting moment T and bending moment M at the joints in terms of these rotations. This is accomplished by letting

$$\begin{aligned} T_{ij} &= (GK - P\rho^2)\,\beta'(0) - Py_o\,u'(0) \\ T_{ji} &= (GK - P\rho^2)\,\beta'(L) - Py_o\,u'(L) \\ M_{ij} &= EI_y\,u''(0) \\ M_{ji} &= EI_y\,u''(L) \end{aligned} \tag{8}$$

In view of these equations, the moment-rotation relationships take the following simple form in the case of prismatic bars.

$$\begin{aligned} T_{ij} &= -S_t\,(\beta_{ij} - C_t\,\beta_{ji}) \\ M_{ij} &= -S_m\,(\theta_{ij} - C_m\,\theta_{ji}) \end{aligned} \tag{9}$$

with $T_{ji}$ and $M_{ji}$ obtained by inverting the subscripts (i,j) on the right side of Eqs. (9). It is of interest to note, and is physically plausible, that the choice of the shear center as reference point has led to an uncoupling of twisting and bending, so far as the joints are concerned. From this it is not to be inferred, however, that there is no coupling all along the bar; on the contrary, pure bending at the joints, for example, produces bending and twisting, unless the centroid and shear center coincide.

In Eqs. (9), the "stiffness factors" $S_t$ and $S_m$ and the "carry-over factors" $C_t$ and $C_m$ are given by the following equations:

$$\begin{aligned} S_t &= G\,K - P\,\rho^2 \\ C_t &= -1 \\ S_m &= \frac{EI_y}{L}\,\phi\,\frac{\sin\phi - \phi\cos\phi}{2 - 2\cos\phi - \phi\sin\phi} \\ C_m &= \frac{\phi - \sin\phi}{\sin\phi - \phi\cos\phi} \\ \phi^2 &= \frac{N\,L^2}{E\,I_y} \end{aligned} \tag{10}$$

In these equations, the trigonometric functions are replaced by the appropriate hyperbolic functions for negative values of N. When N vanishes, $S_m$ and $C_m$ assume the conventional values of $4EI/L$ and $1/2$, respectively. They have been tabulated, with slight modifications, in [3] for both tensile and compressive axial forces.

With the joint moments, both in twisting and in bending, thus established in terms of the joint rotations by means of Eqs. (9), there remain two major considerations to be observed. In the first place, the rotations ($\beta_{ij}$, $\theta_{ij}$) of all the bars joined at panel point i must be compatible with the rigidity of the joint; in other words, the angles between the individual members must be preserved during any rotation. Secondly, the total of all the bending and twisting moments must be in equilibrium.

To this end, it has been found that the employment of matrix notation leads to compactness of both conceptual and computational labor. Consider, for example, the typical bar connecting joints i and j (see Fig. 2), with its inclination $\alpha_{ij}$ relative to the positive x-axis defined as shown. All rotations and couples are assumed positive as indicated by the arrows, which are selected according to the usual right-hand-screw convention. This agrees, it may be noted, with the previous choice of boundary conditions and, in particular, with Eqs. (9).

If now a moment vector $m'$ and a rotation vector $\omega'$ are defined by[6]

$$m' = \begin{bmatrix} T \\ M \end{bmatrix} \qquad \omega' = \begin{bmatrix} \beta \\ \theta \end{bmatrix} \tag{11}$$

and if, further, a "stiffness matrix" $S'$ and a "carry-over matrix" $C'$ are introduced by means of

$$S' = \begin{bmatrix} S_t & 0 \\ 0 & S_m \end{bmatrix} \qquad C' = \begin{bmatrix} C_t & 0 \\ 0 & C_m \end{bmatrix} \tag{12}$$

then Eq. (9) may be written

$$m'_{ij} = -(S'\omega'_{ij} - C'S'\omega'_{ji}) \tag{13}$$

Let the rotation vector of a joint, if referred to the (x,y) coordinate system, be designated by $\omega$, and let similarly the moment vector $m$ refer to the same system, or

$$m = \begin{bmatrix} m_x \\ m_y \end{bmatrix} \qquad \omega = \begin{bmatrix} \omega_x \\ \omega_y \end{bmatrix} \tag{14}$$

It follows then, from considerations of statics and geometry, respectively, that

---

6. Where possible, the subscripts i and j, which identify the member but do not indicate components, will be dropped if no lack of clarity results from this omission.

$$m' = R\,m \qquad \omega' = R\,\omega$$
$$m = R^*m' \qquad \omega = R^*\omega' \tag{15}$$

in which the rotation matrix R and its transpose R* are defined by

$$R = \begin{bmatrix} \cos\alpha & -\sin\alpha \\ \sin\alpha & \cos\alpha \end{bmatrix} \tag{16}$$

When Eqs. (15) and (14) are substituted in Eq. (13), the "slope-deflection" equations in the (x,y) coordinate system read

$$m_{ij} = -(S\,\omega_i + C\,S\,\omega_j) \tag{17}$$

In Eq. (17), S and C are the stiffness and carry-over matrices in the new coordinate system, that is,

$$S = \begin{bmatrix} S_{xx} & S_{xy} \\ S_{yx} & S_{yy} \end{bmatrix} \qquad C = \begin{bmatrix} C_{xx} & C_{xy} \\ C_{yx} & C_{yy} \end{bmatrix} \tag{18}$$

which are related to the previous (primed) coordinate system by means of the transformation equations

$$S = R^*S'R \qquad C = R^*C'R \tag{19}$$

Hence, by Eqs. (12), (18), and (19), and after some trivial trigonometric transformations:

$$\begin{aligned} S_{xx} &= 1/2\,(S_t + S_m) + 1/2\,(S_t - S_m)\cos2\alpha \\ S_{yy} &= 1/2\,(S_t + S_m) - 1/2\,(S_t - S_m)\cos2\alpha \\ S_{xy} &= S_{yx} = -1/2\,(S_t - S_m)\sin2\alpha \end{aligned} \tag{20}$$

and an equivalent set of equations for the components of C. Since furthermore R is orthogonal, i.e., $RR^* = I$ (the unit matrix), the matrix $C'S'$ itself transforms similarly to Eq. (20). Finally, in developing Eq. (17), use was made of the fact that $\alpha_{ji} = \alpha_{ij} + \pi$ and that therefore $R_{ij} = -R_{ji}$; hence, in the new coordinate system, the i,j subscripts continue to be interchangeable for the stiffness and carry-over matrices.

In review, the relationships developed above insure that the end rotations $\beta_{ij}$ and $\theta_{ij}$ of all bars are compatible with a set of joint rotation vectors $\omega_i$. The establishment of the equations of equilibrium is now straightforward, since Eq. (17) expresses all the bar moment vectors with reference to the common (x,y) coordinate system. If n is the number of joints that are free to rotate, the following n vector equations (or 2n scalar equations) follow therefore immediately:

$$\sum_j m_{ij} = 0 \quad (i=1,2 \ldots n) \tag{21}$$

where the summation extends over all the bars joined together at i.

The equations of equilibrium (21) now lead directly to the determinantal stability criterion. In fact, define the "total joint stiffness" $K_{ii}$ by

$$K_{ii} = \sum_{j} S_{ij} \tag{22a}$$

and let further

$$K_{ij} = C_{ij} S_{ij} \qquad (i \neq j) \tag{22b}$$

Then substitution of Eq. (17) in Eqs. (21) results in the set of linear homogeneous equations

$$\sum_{j} K_{ij} \omega_j = 0 \quad (i=1,2 \ldots n) \tag{23}$$

This system has a nontrivial solution if, and only if, the 2n x 2n determinant of the coefficients of the joint rotations vanishes. The structure is therefore in neutral equilibrium under the smallest load for which

$$|K_{ij}| = 0 \tag{24}$$

## A Series Criterion of Stability

Eq. (24) represents a highly involved transcendental equation in terms of the external loads; to find its smallest root (that is, the smallest multiplier common to all loads) is therefore a task of forbidding numerical complexity. In this section, an alternate approach is presented, which constitutes a generalization of the "series criterion" of stability, which was first proposed by Lundquist [4] in connection with the stability of frameworks against buckling in their own plane.

Briefly, the suggested method proceeds as follows. Select a joint q (preferably the one most likely to buckle) and apply at q a unit moment about the x-axis. By means of a generalized moment distribution process which will be described in detail further below, this moment is distributed among the bars joined at q. This introduces unbalanced moments, generally about both the x and y axes, at the far ends of these bars. Holding now joint q fixed, these moments are all distributed in successive steps until all the other joints are balanced. If this process converges,[7] the only unbalanced joint will be the original joint q, toward which the residual moments $r_{xx}$ and $r_{yx}$ about the x- and y-axis, respectively, have been "washed back." If the same procedure is now repeated for an original applied unit moment about the y-axis at q, the wash-back moments will be, say, $r_{xy}$ and $r_{yy}$. Note that, in general, $r_{xy} \neq r_{yx}$.

If now the "residual matrix" r is defined by

---

7. In case of divergence, the structure is known to be unstable; in fact, it is unstable even with joint q fixed.

$$r = \begin{bmatrix} r_{xx} & r_{xy} \\ r_{yx} & r_{yy} \end{bmatrix} \tag{25}$$

then the structure is in general[8] stable if, and only if, the matrix I - r has a positive trace and determinant; hence

$$\begin{aligned} r_{xx} + r_{yy} &< 2 \\ (1 - r_{xx})(1 - r_{yy}) - r_{xy}\, r_{yx} &> 0 \end{aligned} \tag{26}$$

constitutes the desired series criterion of stability.

Suppose now that, for a given load parameter, the procedure described above yields a residual matrix which satisfies conditions (26); the structure is then known to be stable for this system of loads, and the process is repeated for a larger load multiplier, until one or the other of the conditions is violated. The exact value of the load parameter associated with neutral equilibrium can normally be estimated with a fair degree of accuracy through interpolation.

The joint balancing procedure itself represents an extension and generalization of the familiar moment distribution method; the employment of matrix notation makes it possible to describe it in almost identical terms. In fact, let the joint i undergo a rotation (vector) $\omega_i$, while all other joints remain fixed. It then follows, from Eq. (17), that each bar (i,j) exerts a moment $-S_{ij}\omega_i$ on this joint, while at the far end of the bars, say at (j), an unbalanced moment $-(CS)_{ij}\omega_i$ is introduced. It may be worth repeating, at this time, that all the vectors and matrices are expressed in relation to their common (x,y) coordinate system.

If now the rotation $\omega_i$ is so chosen as to balance the joint, it follows that all the new bar moments at i must equal the existing unbalanced moment $m_i^u$. If, further, the definition of the total joint stiffness $K_{ii}$ is recalled as given by Eq. (22a), the required joint rotation must be equal to $(K_{ii})^{-1}m_i^u$. Hence, whenever an unbalanced moment $m_i^u$ is removed at the joint i, while all the other joints remain temporarily fixed, the share taken by each bar at i is given by

$$m_{ij} = -S_{ij}(K_{ii})^{-1}\, m_i^u \tag{27}$$

while the new unbalanced moment introduced at the far end j of the bar is governed by

$$m_j^u = C_{ij}\, m_{ij} \tag{28}$$

The matrix $S_{ij}(K_{ii})^{-1}$ in Eq. (27) may be interpreted as a "generalized distribution factor," while $C_{ij}$ in Eq. (28), as mentioned before, represents a "generalized carry-over factor." In the problem under discussion, in which stability rather than stresses are being investigated, some saving in labor can be effected by combining steps (27) and (28)—that is, by transferring

8. A possible, though unlikely, exception occurs when the lowest buckling mode does not involve any joint rotation of q about either axis. In that case, Eqs. (26) constitute a necessary, but not sufficient condition of stability.

unbalanced moments directly from one joint to the other joints. This is achieved by letting

$$m_j^u = - T_{ij} m_i^u \tag{29a}$$

in which the "transfer matrix" $T_{ij}$ is defined by

$$T_{ij} = C_{ij} S_{ij} (K_{ii})^{-1} \tag{29b}$$

Note that this matrix is generally not symmetrical, nor is, in general, $T_{ij}$ equal to $T_{ji}$.

The numerical computation of the transfer matrices (two for each member of the framework) and the ensuing moment distribution procedure are reasonably simple and can be carried out on the slide rule. After all the matrices S and CS have been determined by means of Eqs. (20), the total joint stiffnesses K are calculated by adding the corresponding components of the stiffness matrices for any one joint. Letting $K_{xx}$, $K_{xy} = K_{yx}$, and $K_{yy}$ be the components of K for a given panel point, the inverse (flexibility) matrix $K^{-1}$ is given by

$$K^{-1} = 1/k \begin{bmatrix} K_{yy} & -K_{xy} \\ -K_{xy} & K_{xx} \end{bmatrix} \qquad k = K_{xx} K_{yy} - K_{xy}^2 \tag{30}$$

It is presumed here that all total joint stiffness matrices are positive definite, since otherwise the structure is known to be unstable, necessitating a (probably substantial) reduction in the load factor. Hence, $k \neq 0$ and $K^{-1}$ exists.

Let it now be assumed that the two moment distribution procedures have been carried out and the residual matrix r has been established as described at the beginning of this section. It is evident that if, instead of two unit moments, an arbitrary moment m of components $m_x$ and $m_y$ were applied at joint q, the residual moment vector would be rm. Since further $m = K\omega$, it follows that $(I-r)K\omega$ is the actual moment introduced at q. In other words, (I-r)K represents the equivalent stiffness of the joint q if all other joints are free to rotate. The positive definiteness of this matrix is therefore a necessary condition for the stability of the structure. The sufficiency condition, which is subject to the exception noted before,[8] can be proved by extending the argument employed in a similar problem in [5].

From this criterion of positive definiteness, conditions (26) can be derived directly. Use is made here of the symmetry of (I-r)K, which is a consequence of Maxwell's Theorem of Reciprocity and which, incidentally, also provides some means of checking the numerical work. It follows that the stability of the structure depends on the positiveness of the trace and determinant of (I-r)K. As for the latter, since K itself has a positive determinant, $|I-r|$ must also be positive. In regard to the trace, let the coordinate system be rotated so that K assumes a diagonal form; this is always possible on account of its symmetry. By examining the form of (I-r)K in this coordinate system, and by considering further that the diagonal terms of K are both positive, it can readily be verified that (I-r)K has a positive trace if, and only if, the trace of (I-r) itself is positive in this, and hence in the original, coordinate system. This completes the proof of the inequalities (26).

## Numerical Example

The method outlined above is now applied to the truss shown in Fig. 3. All joints are connected rigidly and are prevented from lateral sway by means of cross bracing (not shown), which, however, does not contribute to their rotational stiffness. All gusset plates are assumed to be 1/2" thick.

The purpose of the study is to determine the factor of safety against buckling—that is, the factor by which the given load must be multiplied to render the equilibrium of the structure neutral. In particular, it will be shown that although the compression members have been so selected as to make their L/r ratios about equal, the danger of buckling out of the plane of the truss is considerably greater than that within the plane, at least so far as the structure under consideration is concerned.

As for the stability within the plane of the framework, the investigation proceeds along the familiar lines as outlined originally in [4]. The applied load W = 50,000 lb was multiplied by several assumed values of the safety factor and, for each value, the stiffness and carry-over factors were computed with the aid of [3]. A unit moment in the plane of the truss was then applied at joint B, distributed among the three members joined at B, and, with B fixed, the remaining joints were balanced. If the effect of yielding is disregarded, it was found that the residual moment at joint B is 0.962 for a safety factor of 4.50, and 1.066 for 4.60. Hence, the load corresponding to plane instability lies between 225,000 and 230,000 lb.

The investigation of the lateral stability proceeded along an analogous path, as described in the previous section. For an assumed load multiplier, the axial bar forces were computed as well as the equivalent forces as given in Eqs. (3) and (6). The bending stiffness and carry-over factors $S_m$ and $C_m$ were next determined, as in the case of plane buckling. For the example of the double-angle section as used here, a measure of simplification is introduced by the fact that the torsional stiffness $S_t$ is negligible in comparison with $S_m$. The determination of the S and CS matrices in the (x,y) coordinate system, as given by Eqs. (20), is simplified accordingly.

Table I shows a representative portion of the constants involved for an assumed safety factor of 2.6. The material constants E and G were assumed to be equal to $29 \times 10^6$ psi and $11.6 \times 10^6$ psi, respectively. Since only relative stiffnesses are of concern in connection with this study, a number of common factors were disregarded in the establishment of $S_m$. However, it is important to retain the correct proportionality in computing $S_t$ (not needed here) from Eqs. (10), particularly since the tables in [3] give values of $S_m$ which are only one-fourth of those corresponding to Eqs. (10).

The total joint stiffness is now determined by adding the corresponding components of the S matrices of all the bars connected at a particular joint. For example, the stiffness matrix $K_A$ of panel point A is obtained as the sum of $S_{AB}$ and $S_{AD}$; this leads to

$$K_A = \begin{bmatrix} 0.45 & 0.45 \\ 0.45 & 1.29 \end{bmatrix}$$

which is positive definite and has an inverse [see Eq. (30)]

$$K_A^{-1} = \begin{bmatrix} 3.40 & -1.29 \\ -1.29 & 1.29 \end{bmatrix}$$

The stiffness matrices of all the other joints, and their inverse, are then computed in the same fashion.

TABLE I

STIFFNESS AND CARRY-OVER CONSTANTS FOR A SAFETY FACTOR OF 2.6

| Bar | Force | N | ø | $C_m$ | $S_m$ | α | S | | | CS | | |
|---|---|---|---|---|---|---|---|---|---|---|---|---|
| | | | | | | | xx | xy | yy | xx | xy | yy |
| AB | 91.9 | 105.2 | 3.62C | 1.48 | 0.90 | 45 | .45 | .45 | .45 | .67 | .67 | .67 |
| CB | 91.9 | 105.2 | 3.62C | 1.48 | 0.90 | 135 | .45 | -.45 | .45 | .67 | -.67 | .67 |
| BD | -130 | -118 | 2.70T | 0.37 | 3.40 | - 90 | 3.40 | 0 | 0 | 1.26 | 0 | 0 |
| AD | - 65 | - 63.4 | 4.16T | 0.26 | 0.84 | 0 | 0 | 0 | .84 | 0 | 0 | .22 |
| CD | - 65 | - 63.4 | 4.16T | 0.26 | 0.84 | 180 | 0 | 0 | .84 | 0 | 0 | .22 |

The final step consists in the establishment of the transfer matrices defined by Eqs. (29). This is achieved by multiplying the CS matrix of a member, as given in Table I, by the inverse stiffness matrix of the joint from which the unbalanced moment is to be transferred. For example, $T_{AB}$ represents the effect of the balancing of joint A on the unbalanced moment at B; it is given by

$$T_{AB} = (CS)_{AB} K_A^{-1} = \begin{bmatrix} .67 & .67 \\ .67 & .67 \end{bmatrix} \begin{bmatrix} 3.40 & -1.29 \\ -1.29 & 1.29 \end{bmatrix} = \begin{bmatrix} 1.42 & 0 \\ 1.42 & 0 \end{bmatrix}$$

It should be emphasized once again that two such transfer matrices must be computed for each bar since, in general, $T_{AB} \neq T_{BA}$.

Fig. 4 shows all the transfer coefficients for a safety factor of 2.6; it also demonstrates the moment distribution procedure, which in this case turns out to be exceptionally simple owing to the symmetry of the structure. A brief description at this point, it is felt, may elucidate the simple, but perhaps somewhat unfamiliar steps. The introduction and balancing of a unit moment about the x-axis at point B produces unbalanced moments about both axes at joints A, D, and C, as shown in the first line. When the unbalanced moment $m_x = -0.15$ at A is removed, the moments about both axes, which are transferred back to B, are each equal to $-(1.42)(-0.15) = +0.21$; at the same time, a moment vector is transferred to joint D whose x-component is zero and whose y-component is given $-(-0.28)(-0.15) = -0.04$. Similarly, the balancing of $m_y = -0.15$ at A produces (0,0) at B and (0, +0.04) at D.

The process is repeated for joint C, with analogous results. The unbalanced moments at D now are -0.29 and 0, respectively, about the x- and

y-axes. The removal of the former introduces an unbalancing effect only at joint B, to which an additional moment vector is transferred, whose x-component equals $-(0.37)(-0.29) = 0.11$ and whose y-component vanishes.

With all joints other than B balanced, it is seen that the latter is now subjected to a residual unbalanced moment whose components are 0.53 and 0, respectively. If the same process is carried out after an initial unit moment about the y-axis is balanced at B, it can be demonstrated that the residual moment vector is given by (0, 2.10). Hence, the residual matrix, as defined by Eq. (25), is

$$r = \begin{bmatrix} 0.53 & 0 \\ 0 & 2.10 \end{bmatrix}$$

which is seen to violate the stability criterion (26). In other words, the structure is laterally unstable under a load of 130,000 lb.

The same procedure, if carried out for a safety factor of 1.8 (corresponding to a load of 90,000 lb), leads to

$$r = \begin{bmatrix} 0.35 & 0 \\ 0 & 0.80 \end{bmatrix}$$

which satisfies both criteria (26). The actual factor of safety of the structure is therefore known to lie between 1.8 and 2.6. While its exact value is not important in connection with the general discussion in this paper, it does seem noteworthy that it is very significantly smaller than its counterpart against plane buckling.

## CONCLUSION

As pointed out already in the Introduction, the present theory is based on the assumption that, prior to lateral buckling, all members are subjected to axial forces through their centroids. What effect, if any, the presence of so-called secondary moments in the plane of the structure has on the condition of lateral stability is difficult to assess without considering a specific example. It is known, however [6], that structures whose bending moments are statically indeterminate do not ordinarily collapse under loads which are associated with incipient lateral instability. The type of framework under consideration represents such an example; hence, it is reasonable to expect the actual collapse load to exceed the theoretical buckling load.

In any event, the factor of safety which is computed on the basis of the simplifying assumption of this paper must represent a lower bound to the factor of safety based on the collapse load. Indeed, as pointed out in [6], any safety factor based on statically admissible bending moments represents such a lower bound; obviously, a set of identically vanishing bending moments is statically consistent in the absence of loads other than those applied at the joints.

Whether the startlingly large discrepancy between the safety factors against buckling in and out of the plane of the structure can be extended to trusses of different geometry, or of greater torsional resistance, or

composed of members heavy enough to correspond to plastic buckling, can of course not be answered summarily at this point. On the other hand, the results of this study seem to indicate that the current design practice of equalizing the slenderness ratios of compression members in both directions may not necessarily lead to an efficient functioning of the structure. Perhaps it may not be unreasonable to suggest that the pertinent features of the present code be subjected to further scrutiny in this respect.

## REFERENCES

1. "Steel Construction," American Institute of Steel Construction, 5th Ed., 1950.
2. "Buckling Strength of Metal Structures," by F. Bleich, McGraw-Hill Book Co., Inc., 1952.
3. "Tables of Stiffness and Carry-Over Factors for Structural Members under Axial Load," by E. E. Lundquist and W. D. Kroll, NACA Tech. Note 652, 1938.
4. "Stability of Structural Members under Axial Load," by E. E. Lundquist, NACA Tech. Note 617, 1937.
5. "On the Fundamental Frequencies of Vibration of Rigid Frames," by E. F. Masur, Proceedings of the First Midwestern Conference on Solid Mechanics, p. 89-94, Urbana, 1953.
6. "The Collapse Strength of Redundant Structures after Lateral Buckling," by E. F. Masur and K. P. Milbradt, submitted for publication to Journal of Applied Mechanics, ASME.

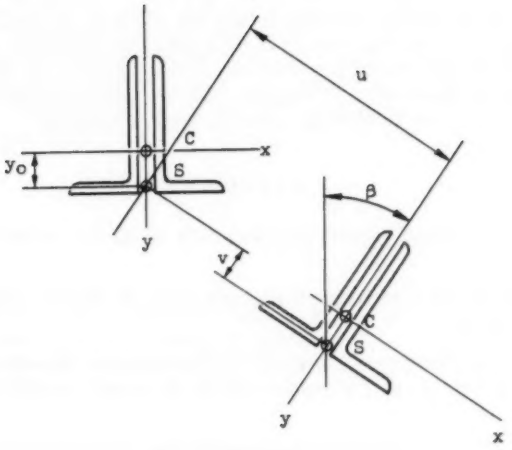


Fig. 1
Typical buckled cross section.

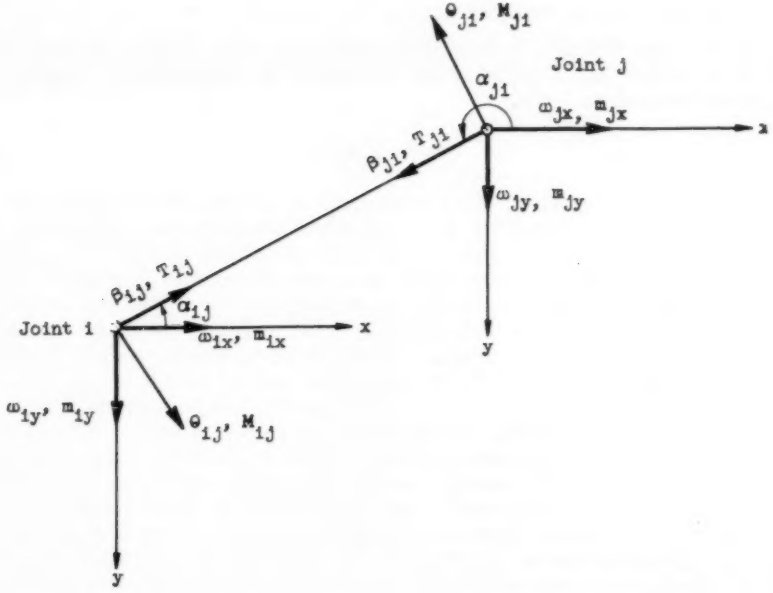


Fig. 2
Positive rotation and moment vectors in representative bar.

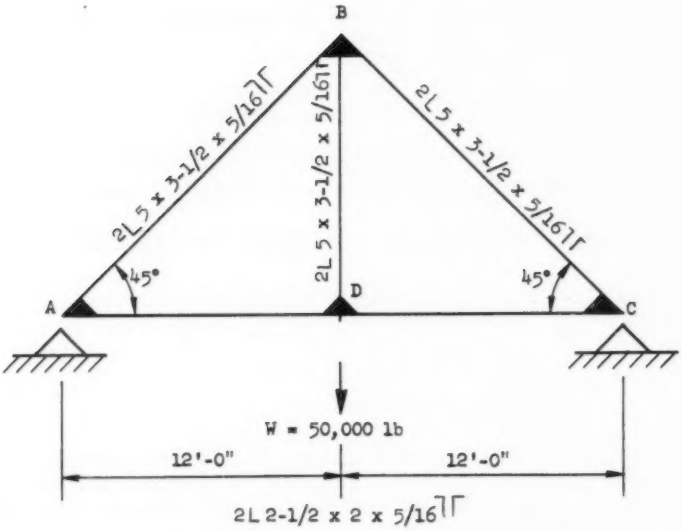


Fig. 3
Example of framework.

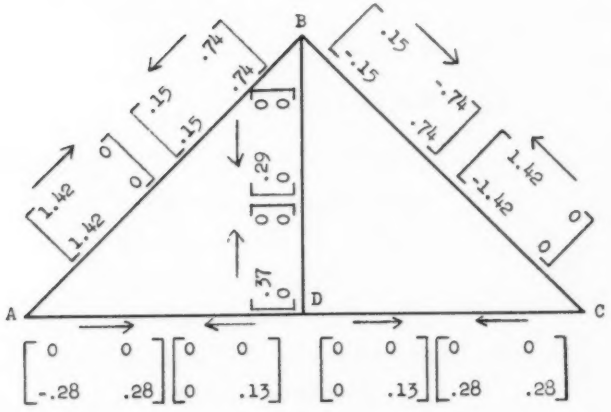


B

| $m_x$ | $m_y$ |
|---|---|
| 1.00 | |
| .21 | .21 |
| 0 | 0 |
| .21 | -.21 |
| 0 | 0 |
| .11 | 0 |
| .53 | 0 |

A

| $m_x$ | $m_y$ |
|---|---|
| -.15 | -.15 |

D

| $m_x$ | $m_y$ |
|---|---|
| -.29 | 0 |
| 0 | -.04 |
| 0 | +.04 |
| 0 | +.04 |
| 0 | -.04 |

C

| $m_x$ | $m_y$ |
|---|---|
| -.15 | .15 |

Fig. 4
Moment distribution.

Paper 1141 EM 1

Journal of the
ENGINEERING MECHANICS DIVISION
Proceedings of the American Society of Civil Engineers

# WIND INDUCED VIBRATION OF CYLINDRICAL STRUCTURES

Joseph Penzien,* J. M. ASCE
(Proc. Paper 1141)

## SYNOPSIS

This paper presents the results of a wind tunnel investigation to determine the dynamic behavior of cylindrical sections under the action of wind at high Reynold's numbers. These results show that wind induced vibration normal to the direction of wind is "self excited" rather than "forced". Two critical wind velocities were observed. The lower critical velocity appears to be associated with the von Karman vortex street. However, the basic aerodynamic phenomenon associated with the higher and more severe critical velocity is not presently understood.

## SYMBOLS AND NOTATION

| Symbol | Definition |
|---|---|
| $f_v$ | Frequency of vortex shedding |
| V | Wind velocity |
| D | Cylinder diameter |
| S | Strouhal Number |
| $F_L$ | Unit lateral force resulting from vortex shedding |
| $C_L$ | Lateral force coefficient |
| t | Time |
| $\rho$ | Mass density of air—0.00238 slugs |
| $X_D$ | Maximum dynamic response amplitude |
| $X_{DR}$ | Static response amplitude due to lateral force at resonance |

Note: Discussion open until June 1, 1957. Paper 1141 is part of the copyrighted Journal of the Engineering Mechanics Division of the American Society of Civil Engineers, Vol. 83, No. EM 1, January, 1957

*Asst. Prof. of Civ. Eng., Univ. of California, Berkeley, Calif.

| Symbol | Definition |
|---|---|
| R | Reynolds number |
| $\nu$ | Kinematic viscosity |
| $C_D$ | Drag coefficient |
| $F_D$ | Total maximum dynamic reaction of cylinder |
| $f_S$ | Natural frequency of cylindrical system |
| $\zeta$ | Logarithmic decrement of damping |

## INTRODUCTION

The general problem of designing tall stacks which are dynamically stable under the action of wind is becoming increasingly important due to the demand by industry for taller stacks. Until recent years, it has been the general practice to design stacks conservatively for a static load equal to the wind drag at a wind velocity considerably above the maximum velocity expected. However numerous cases[1,2,3,4,5]* of serious wind-induced vibration have been experienced and in some cases failures have occurred, thus pointing out the inadequacy of designing stacks on this basis.

Numerous papers have been published on this subject recently which point out the tendency of stacks to vibrate in a direction normal to the wind. These papers usually associate such behavior with the well known von Karmon vortex street.[6] This phenomenon is a periodic shedding of vortices alternately from the cylinder at a frequency ($f_v$) as given by Eq. 1.

$$f_v = S(V/D) \tag{1}$$

This periodic shedding of vortices produces a change in the particle velocities on opposite sides of the cylinder and by Bernoulli's theorem similar changes in pressures result. Thus, it is generally assumed an alternating unit force ($F_L$) normal to the direction of the wind is produced as described by Eq. 2.

$$F_L = C_L \rho \frac{V^2}{2} \sin 2\pi f_v t \tag{2}$$

This periodic forcing function gives rise to forced vibration, the amplitude of which varies with wind velocity as shown in Fig. 1 and the frequency of which is equal to that of the forcing function itself. The maximum response with this type of excitation is reached when the vortex shedding frequency is equal to the natural frequency of the stack.

Much of the discussion in the literature on this problem has been concerned with the numerical values which should be assigned to the Strouhal Number S and the Lateral Force Coefficient $C_L$.

*Numbers in parentheses refer to the bibliography.

It has been concluded by some writers that above the critical range of Reynold's numbers ($R = \frac{VD}{\nu}$), the shedding of vortices become aperiodic. In view of this one would conclude that a truly resonant condition would never be reached and excessive vibrations would not build up. Experience however shows that excessive vibrations can occur at Reynold's numbers considerably above the critical range.

Recently a paper[3] by Ozker and Smith has presented a new concept of the dynamic response of tall stacks to wind action. By measuring the dynamic response of a full scale stack to a wide range of wind velocities they concluded that wind induced vibrations of a stack are "self excited" rather than "forced" as discussed above. With this type of oscillation the frequency of vortex shedding is controlled by the response of the stack itself. That is, the stack vibrates at its own natural frequency at all times and is independent of wind velocity. Similar response measurements were made by Amori[4] in 1918 which support the above concept.

Presented in this paper are the results of a wind tunnel investigation of the dynamic behavior of cylindrical sections under the action of wind. In general these data support the concept of self excitation set forth by Ozker and Smith. There are however differences in the response—wind velocity relationship.

## Experimental Techniques

Three aluminum cylinders 44 inches long and having diameters of 3, 6, and 9 inches were tested in a 3 foot open throat wind tunnel. Each cylinder was supported by a cantileverbeam at each end as shown in Fig. 2. These beams were placed parallel to the direction of the wind and outside the main air stream. In this manner the rigidity of the test specimen was kept high in the direction of the wind while its rigidity normal to the wind was kept relatively low. By changing the width and length of these supporting beams a wide range of frequencies could be obtained for each cylinder.

The dynamic response was measured by SR-4 gages mounted on each side of the supporting beams. These gages were wired into a bridge in such a way that only a transverse displacement of the cylinder as a whole would be recorded, i.e., a rotation of the cylinder about an axis parallel to and midway between the supporting beams would not change the bridge balance. Fortunately, however, because of symmetry of structure and loading, rotations of this type were negligible. The strain gage bridge was connected to a Sanborn Recorder which produced a continuous record of dynamic response for a given system.

A total of twenty tests were conducted as shown in Table 1. Each test represents a given cylinder with a given support rigidity. A continuous record of dynamic response was recorded for each test during which the wind velocity was increased in increments of 5 ft/sec from zero to 115 ft/sec.

Vertical fins were attached to the 6 inch cylinder for three tests. These fins projected 5/8 of an inch from the cylinder and were spaced every 30 degrees around its perifery as shown in Fig. 3. These tests were conducted to check the effect of fluting on dynamic response.

TABLE 1 - TEST PROGRAM

| Test No. | Cylinder Diameter In. | Natural Frequency Cycles/Sec. | Test No. | Cylinder Diameter In. | Natural Frequency Cycles/Sec. |
|---|---|---|---|---|---|
| 1 | 9 | 43.0 | 11 | 6 | 10.5 |
| 2 | 9 | 27.0 | 12 | 6 | 6.5 |
| 3 | 9 | 12.5 | 13 | 3 | 43.0 |
| 4 | 9 | 10.0 | 14 | 3 | 28.0 |
| 5 | 9 | 7.5 | 15 | 3 | 17.0 |
| 6 | 9 | 4.7 | 16 | 3 | 15.0 |
| 7 | 6 | 38.0 | 17 | 3 | 9.0 |
| 8 | 6 | 29.5 | 18* | 6 | 15.0 |
| 9 | 6 | 19.7 | 19* | 6 | 9.5 |
| 10 | 6 | 13.0 | 20* | 6 | 5.2 |

*5/8 inch fins attached every 30 degrees around perifery of cylinder.

## DISCUSSION OF TEST RESULTS

### Type of Response

It was clearly shown in this series of tests that the response frequency of a cylindrical system under the action of wind remains constant regardless of wind velocity and is equal to the natural frequency of the system. This indicates that the vibration of tall stacks are "self excited" rather than "forced" as generally assumed.

A typical record of cylinder response normal to the direction of wind is shown in Fig. 4. This figure shows a portion of the continuous record of response for the 3 inch cylinder ($f_s = 17$ c/s) subjected to a steady wind velocity of 65 ft/sec.

In addition to the fact that each cylinder responded at its natural frequency, another important fact is immediately apparent from these records. That is, the vibration amplitude is generally not constant during a condition of steady wind as one might expect. Instead the oscillation increases rapidly and then decreases in a similar manner. While this behavior is somewhat random, it does indicate that energy is suddenly fed into the system from the airstream. Some of this energy is dissipated through structural and aerodynamic damping, while the remainder is suddenly fed back into the airstream.

The basic aerodynamic phenomenon causing the above alternate conditions of stability and instability is unknown at present. One might set forth several hypotheses as possibilities; however there is no experimental or theoretical evidence to support them. One possibility is that there is sufficient periodic shedding of vortices on alternate sides of the cylinder to build up the vibration. After a number of cycles the shedding becomes out of phase with response, thus reducing the vibration. Another possibility is that at these high Reynold's numbers an alternating force is produced due to flow changes resulting from an alternate shifting of the separation point on the boundary layer. Shedding of vortices in this case would be considered aperiodic. This shifting of separation point can be alternately in and out of phase with response.

It should be noted that the type of response reported above is very similar to the full scale stack response as reported by Ozker and Smith. This indicates that the aerodynamic phenomenon existing for these tests is similar to that for full scale stacks. One difference to be questioned however in correlating these data with full scale is that while these data are in the critical range of Reynold's numbers ($10^5$ - $10^6$), full scale stacks usually vibrate at Reynold's numbers above the critical range ($> 10^6$).

## Strouhal Number[7]

The relationship between Strouhal number and Reynold's number has been measured experimentally by Relf and Simmons[8] in the critical range for rigid cylinders. This relationship is shown in Fig. 5 along with the relationship between drag coefficient and Reynold's number. The change from "laminar" to "turbulent" flow in the critical range results in a sudden reduction of drag coefficient and an increase in Strouhal number.

Since the response as reported above for non-rigid cylinders is "self excited," the Strouhal number might appear to be of little significance. However, when considering the rapid increase and decrease of response as described above, one might expect the periodic force to remain in resonance through more and more cycles as the wind velocity gets nearer and nearer to the resonant wind velocity as given by Equation 1. This condition would result in a build up of response at this wind velocity. The value of Strouhal number used in calculating this resonant wind velocity would be that obtained experimentally for rigid cylinders.

As a check on Strouhal frequency, a test was conducted in this investigation for which a cylinder was made sufficiently rigid so that it responded not at its natural frequency but at a frequency assumed to be the Strouhal frequency. The 9 inch cylinder which was used for this test had a natural frequency of 43 cycles/second. A portion of the response record for a wind velocity of 35 ft/sec is shown in Fig. 6. This response record indicates a somewhat steady condition. Therefore, one can get a measure of the predominant frequency of the forcing function.

These frequencies as obtained from this test are plotted in Fig. 5. While these results deviate somewhat from those of Relf and Simmons, they do indicate a sudden increase of Strouhal number in the critical range.

Also plotted in Fig. 5 are the values of Strouhal number as calculated using Equation 1 and the lowest wind velocity at which a resonant condition was reached as shown by Point No. 1 on the response curves in Figs. 7, 8, and 9. The correlation between the values of Strouhal number obtained in this manner and those obtained from the rigid cylinder test described above is reasonably good. This indicates that a first resonant point will be reached at the resonant wind velocity as associated with the von Karmon vortex street.

## Amplitude of Response

The experimental relationship between cylinder response and steady wind velocity is given in Figs. 7, 8, and 9 for the 3, 6, and 9 inch smooth cylinders, respectively. Each curve represents a different degree of stiffness for the system as indicated by the given natural frequency $f_s$. The amplitude of response is shown by plotting the maximum total dynamic reaction force ($F_D$) normal to the direction of the wind for each increment of wind velocity tested. This force is equivalent to that static force which would be required to

produce the same stress as the maximum dynamic stress.

Although, it is difficult to find correlation among these data, the following important facts are indicated by these results.

(1) The wind velocity at which the first peak response occurs (Pt. No. 1, Figs. 7, 8, and 9) agrees reasonably well with the resonant wind velocity as calculated using Equation 1 provided allowances are made for the change of Strouhal number with Reynold's number as previously discussed.

(2) A more severe resonant condition may be reached at a higher wind velocity than in (1) above. This condition is most clearly shown in Fig. 8 at a wind velocity of approximately 60 ft/sec. The vibration became so severe in this velocity region that it had to be stopped to prevent yielding of the supporting beams.

(3) Maximum response in general does not continue to increase with wind velocity, but does reach a maximum at certain critical velocities.

(4) There appears to be a certain critical stiffness or rigidity for which vibration due to wind is most severe.

(5) Stresses produced by vibration of a cylinder normal to the direction of the wind can be much larger than those produced by the steady drag force provided the right combination of wind velocity, structural stiffness, and structural geometry is present. Low structural damping, as is usually the case in tall steel stacks, is also necessary for this condition to exist.

### Effect of Surface Roughness on Dynamic Response

Response curves for the fluted 6 inch cylinder (Fig. 3) are shown in Fig. 10. A comparison of these data with those for the smooth 6 inch cylinder shows an appreciable reduction of vibration. This fact indicates that while roughness or projections from a smooth cylinder increases the steady drag load it does have a stabilizing effect on vibration normal to the wind.

## GENERAL CONCLUSIONS AND RECOMMENDATIONS

From the results of this investigation, the following general conclusions may be deduced:

(1) Wind induced vibrations of cylindrical sections normal to the wind are "self excited" rather than "forced".
(2) These wind induced vibrations build up rapidly at certain critical wind velocities.
(3) A lower critical wind velocity exists which corresponds to that associated with the von Karman vortex street. The oscillation which builds up at this velocity is usually not too severe.
(4) A high critical wind velocity can exist which may produce very severe oscillations. The basic aerodynamic phenomenon causing this behavior is not presently understood.

In view of the present state of knowledge regarding wind induced vibration of tall stacks, it is very desireable that further research be conducted to clarify the basic aerodynamic phenomenon associated with this behavior.

Since it is very difficult to conduct wind tunnel studies above the critical range of Reynold's number, it will be necessary that full scale tests be made. These tests should be so designed to provide a clear understanding of the

aerodynamic forces involved. Only after such studies are successfully completed will the designer have the necessary information to arrive at economical and safe designs of tall stacks.

## REFERENCES


1. Dickey, W. L. and Woodruff, G. B., The Vibration of Steel Stacks, A.S.C.E. Separate No. 540, November, 1954.
2. Dockstader, E. A. and Swiger, W. F., Resonant Vibration of Steel Stacks, A.S.C.E. Separate No. 541, November 1954.
3. Ozker, M. S. and Smith, J. O., Factors Influencing the Dynamic Behavior of Tall Stacks Under the Action of Wind, A.S.M.E. Paper No. 55-A-69.
4. Omori, F., Wind Pressure on Tall Chimneys, Engineering, Vol. 106, 1918, pp. 334-336.
5. Frank, W., Stromungerregte Schornsteinschwingungen, Journal Archiv Fur Warmewirtschaft und Dampfkesselwesen, vol. 22, February, 1941, pp. 33-35.
6. Karman, Th. von, Flussigkeits—u. Luftwiderstand, Physik. z. 13, 49, 1911.
7. Strouhal, V., Uber eine besondere Art der Tonerregung, Wied, Ann. Physik u. Chem., Neue Folge, Band V., 1878, pp. 216-251.
8. Relf, E. F. and Simmons, L. G. F., The Frequency of the Eddies Generated by the Motion of Circular Cylinders through a Fluid—London, Edinburgh, and Dublin Philosophical Magazine, Sixth Series, Vol. 49, 1925.
9. Sherlock, R. H. and Stalker, A Study of Flow Phenomena in the Wake of Smoke-Stacks, Engineering Research Bulletin, No. 29, University of Michigan, March, 1941.
10. Steinman, D. B., Problems of Aerodynamic and Hydrodynamic Stability, Bulletin 31, University of Iowa Studies in Engineering, 1947.
11. Den Hartog, J. P., Recent Technical Manifestations of von Karman's Vortex Wake, Proc. Natl. Acad. Sci., vol. 40, 1954, pp. 155-157.

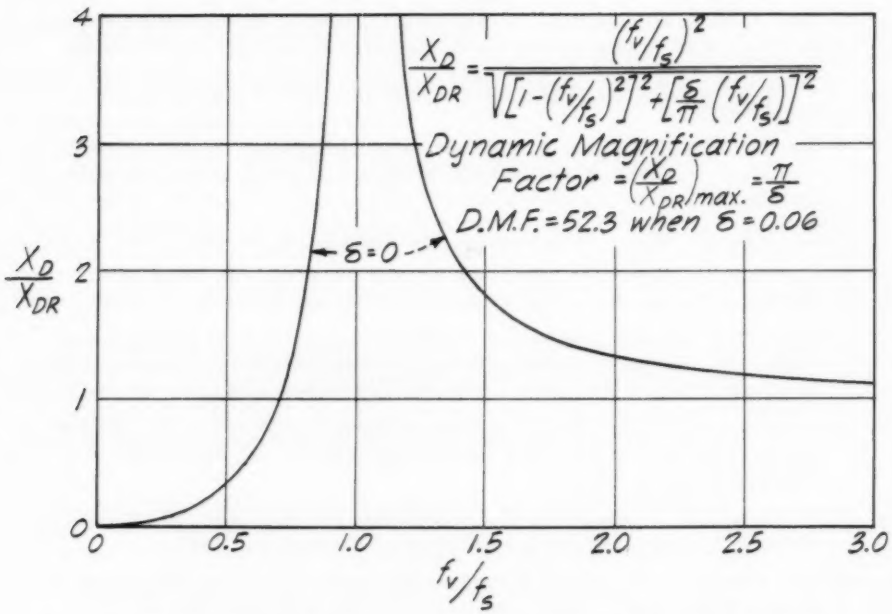


Fig. 1 - Dynamic Response Resulting from Periodic Forcing Function as Described by Equation 2.

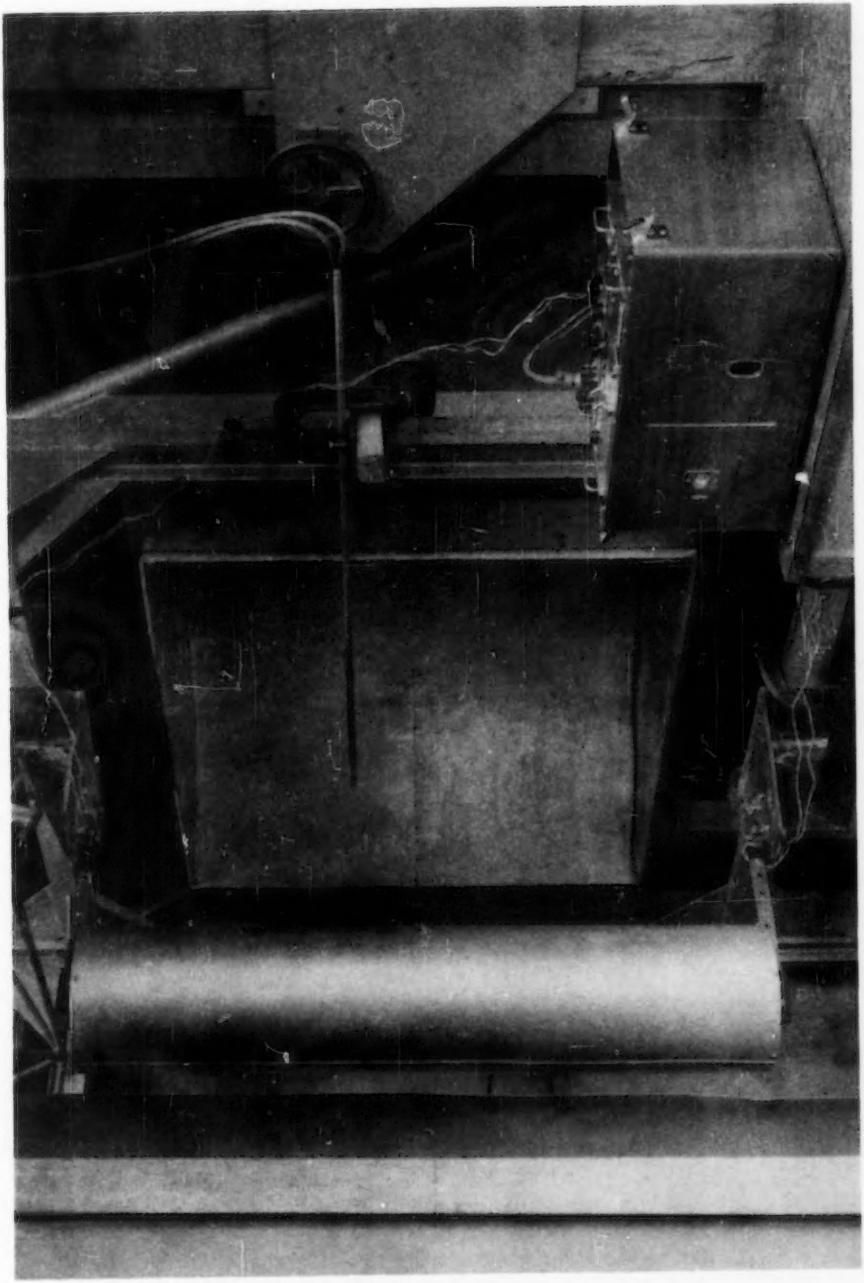

Fig. 2 - Test Section of Wind Tunnel with 9 inch fluted cylinder in place.

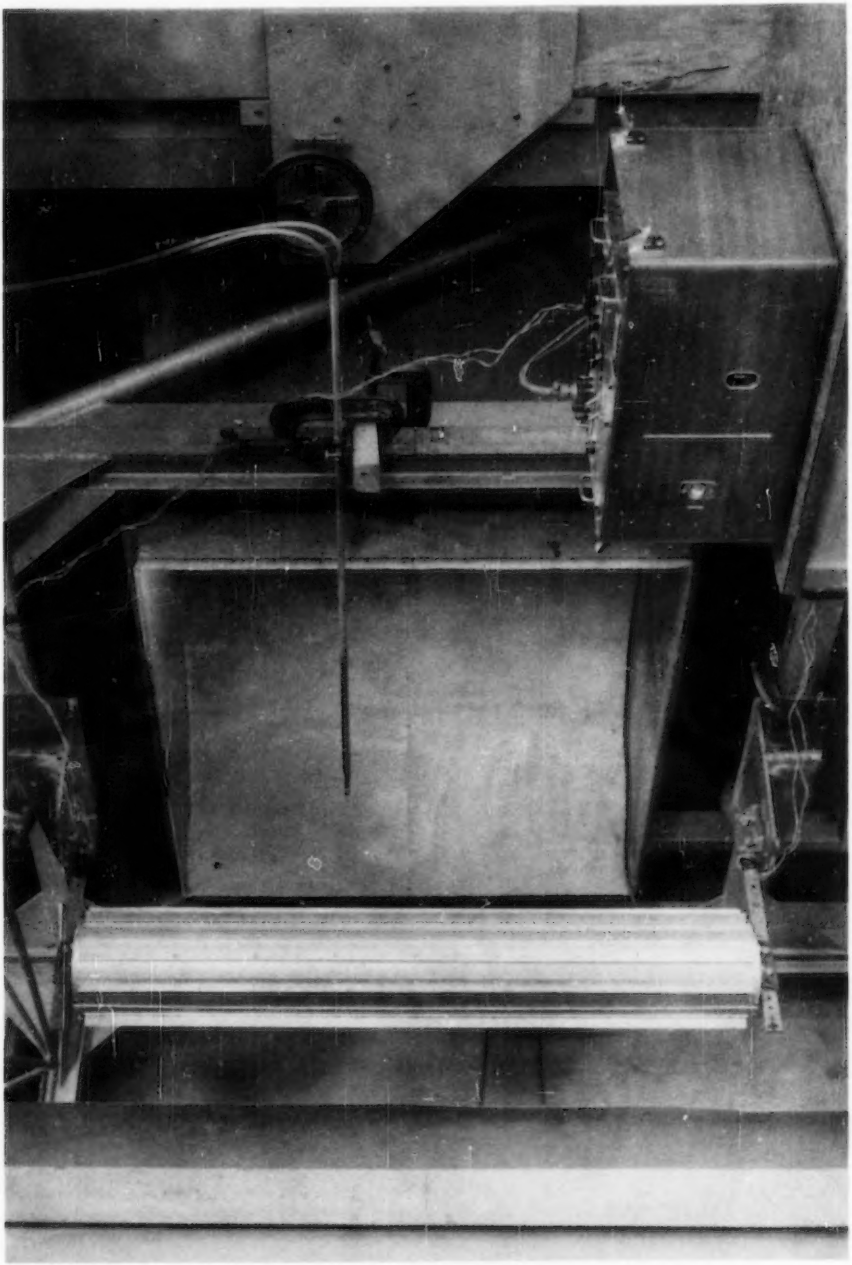

Fig. 3 - Test Section of Wind Tunnel with 6 inch fluted cylinder in place.

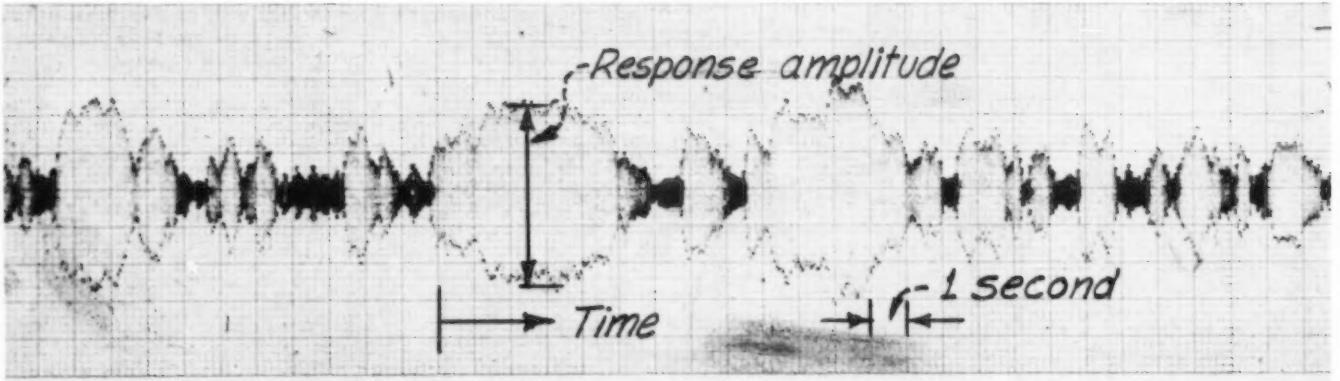


3-in. dia. cylinder
cylinder frequency ($f_s$) = 17 cycles per sec.
wind velocity (V) = 65 ft. per sec.

Fig. 4 - Typical Oscillograph Record of Cylinder Response Normal to Wind.

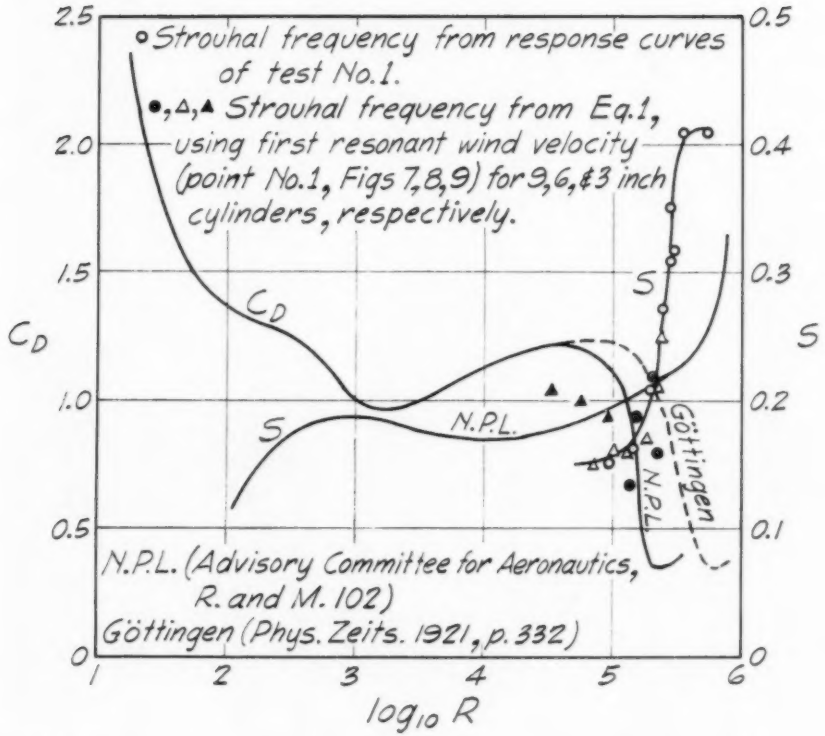


FIG.5- Variation of Drag Coefficient and Strouhal Number with Reynold's Number for Circular Cylinder.

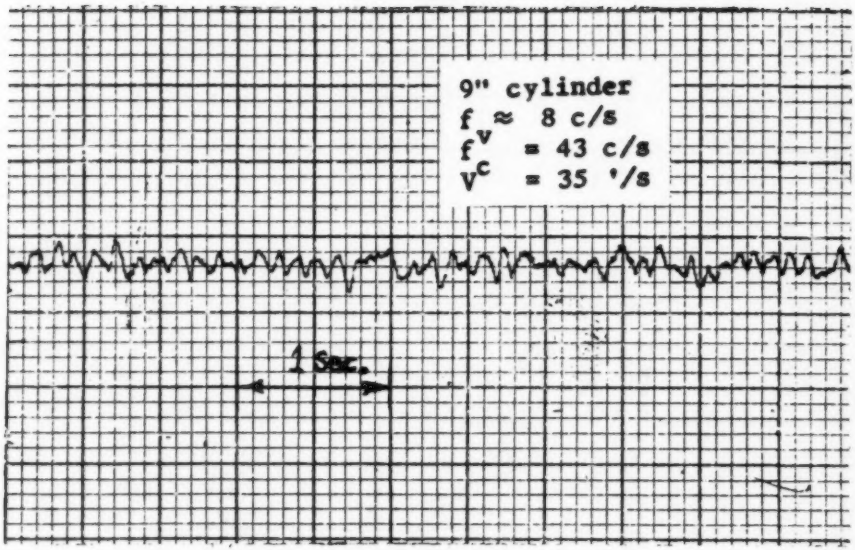


Fig. 6 - Dynamic Response of Rigid Cylinder.

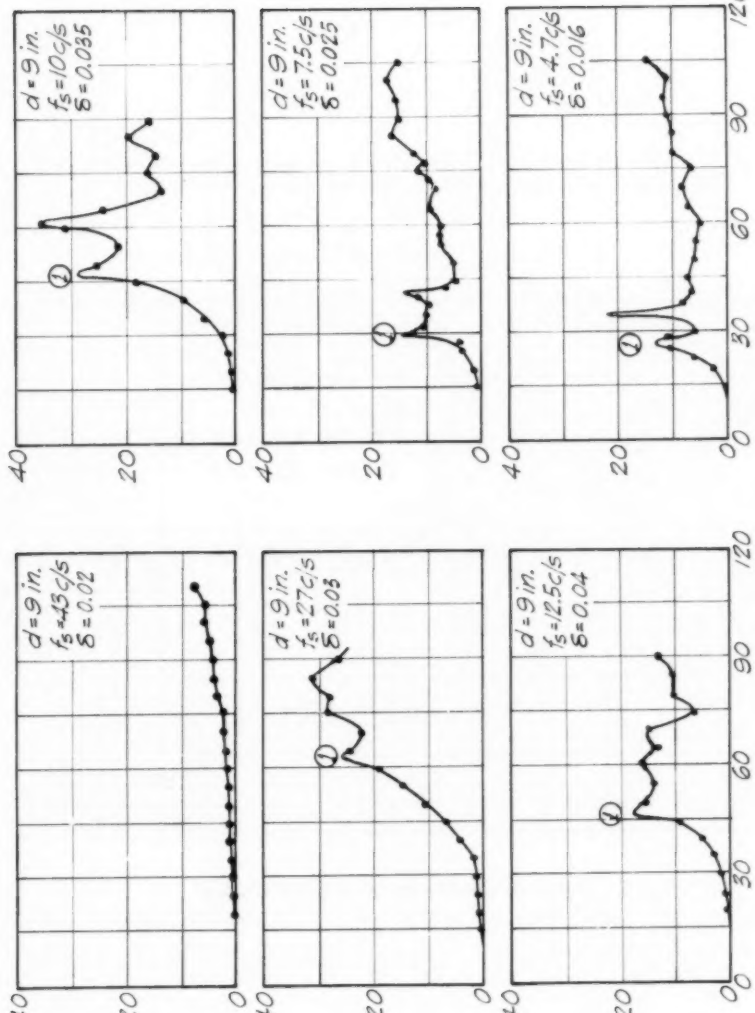


Fig. 7-Dynamic Response Curves for 9-in. Smooth Cylinder.

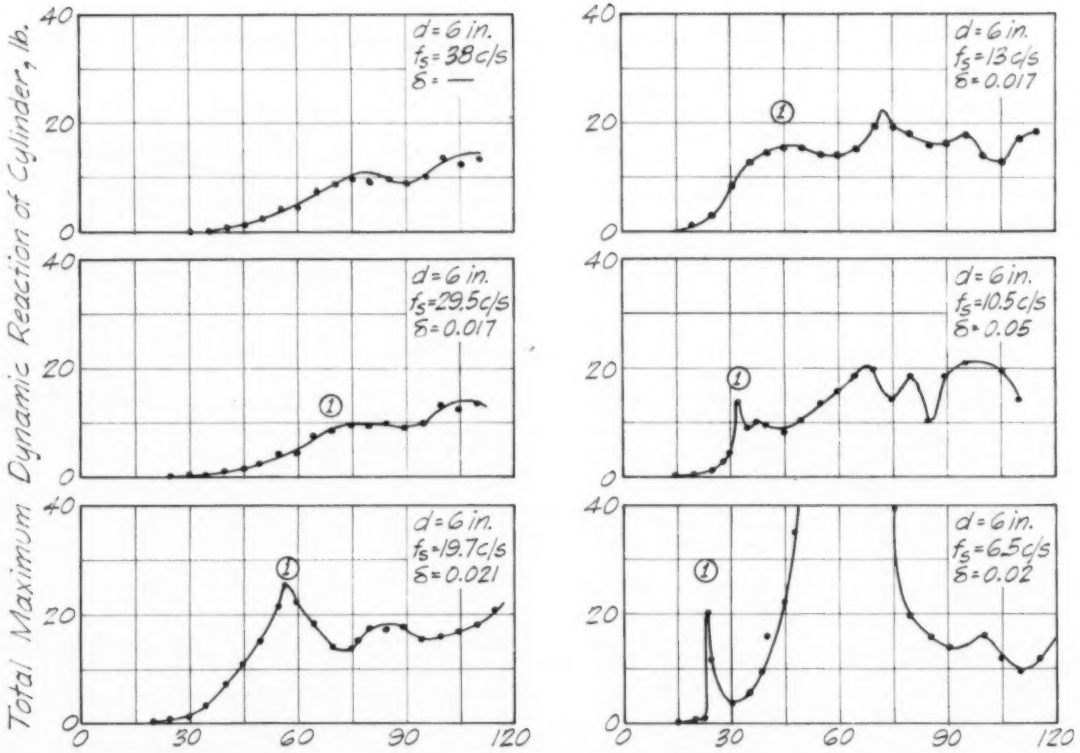


Fig. 8 - Dynamic Response Curves for 6-in. Smooth Cylinder.

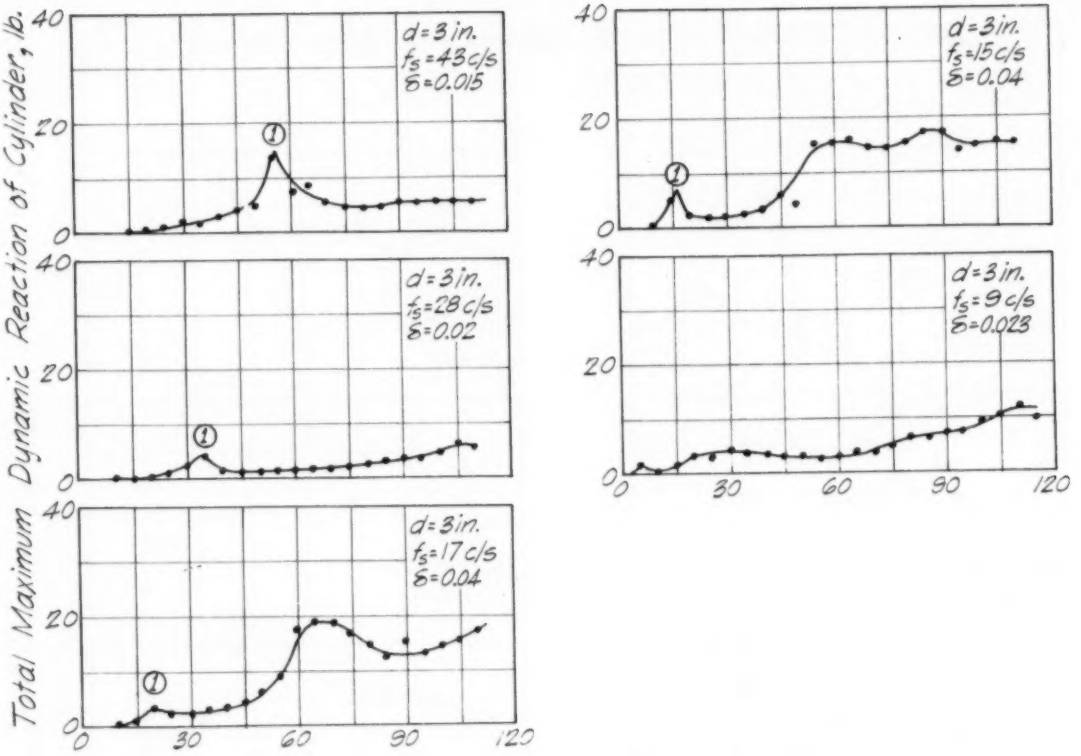


Fig. 9 - Dynamic Response Curves for 3-in. Smooth Cylinder.

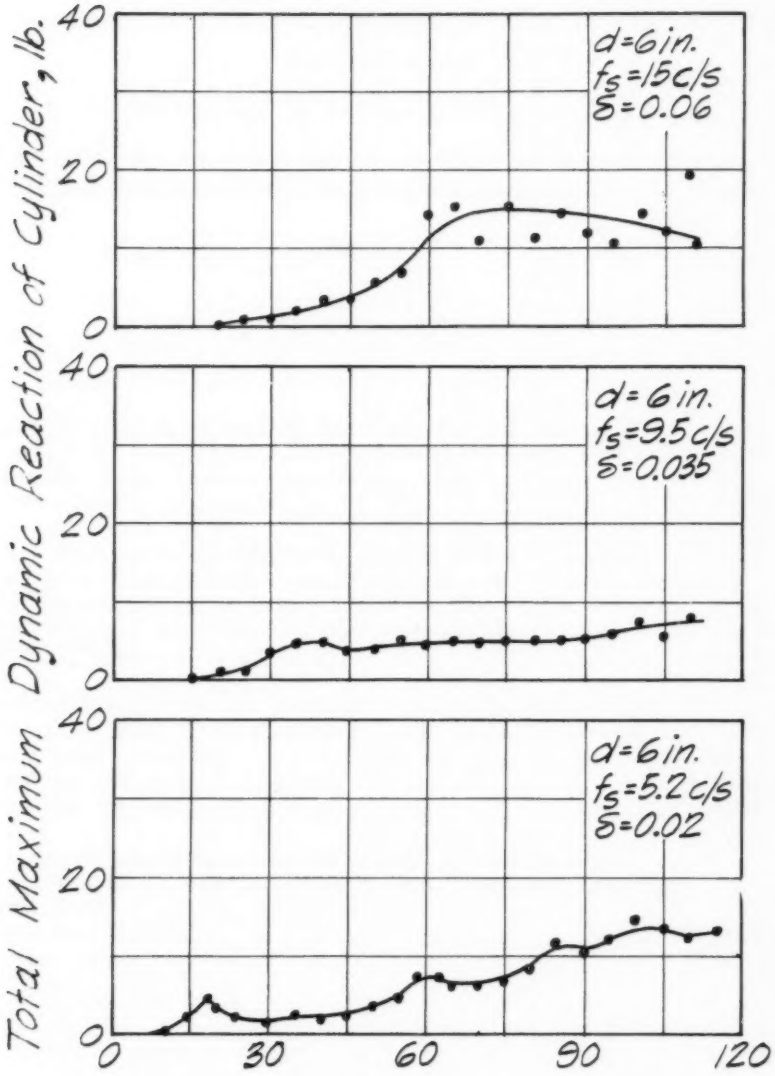


Fig. 10 - Dynamic Response Curves for 6-in. Fluted Cylinder.

Journal of the
ENGINEERING MECHANICS DIVISION
Proceedings of the American Society of Civil Engineers

CONTENTS

DISCUSSION
(Proc. Paper 1154)

Page

Lateral Buckling of Rolled Steel Beams, by R. A. Hechtman, J. S. Hattrup, E. F. Styer, and J. L. Tiedemann. (Proc. Paper 797. Prior discussion: none. Discussion closed.)
Corrections . . . . . 1154-3

Some Observations on Open Channel Flow at Small Reynolds Numbers, by Lorenz G. Straub, Edward Silberman, and Herbert C. Nelson. (Proc. Paper 1031. Prior discussion: none. Discussion closed.)
by Wallace M. Lansford and James M. Robertson . . . . . 1154-5
by C. J. Posey . . . . . 1154-13

Lateral Bracing Forces on Beams and Columns, by William Zuk. (Proc. Paper 1032. Prior discussion: none. Discussion closed.)
by Robert V. Hauer . . . . . 1154-15
by Chesley J. Posey . . . . . 1154-16
by C. M. Segedin . . . . . 1154-18

Minimum-Weight Design of a Portal Frame, by William Prager. (Proc. Paper 1073. Prior discussion: none. Discussion open until March 1, 1957.)
by Robert L. Ketter . . . . . 1154-21

Note: Paper 1154 is part of the copyrighted Journal of the Engineering Mechanics Division of the American Society of Civil Engineers, Vol. 83, No. EM 1, January, 1957.

Discussion of
"LATERAL BUCKLING OF ROLLED STEEL BEAMS"

by R. A. Hechtman, J. S. Hattrup, E. F. Styer, and J. L. Tiedemann
(Proc. Paper 797)

CORRECTIONS.—In Figs. 9 and 10 curves that are presently labeled "From Eq. 7" should be labeled "From Eq. 2." Also, Eq. 2 should be changed so that the term $L^3$ is replaced by $L^2$.

Discussion of
"SOME OBSERVATIONS ON OPEN CHANNEL FLOW AT SMALL REYNOLDS NUMBERS"

by Lorenz G. Straub, Edward Silberman, and Herbert C. Nelson
(Proc. Paper 1031)

WALLACE M. LANSFORD,* M. ASCE, and JAMES M. ROBERTSON,** M. ASCE.—This very concise presentation of an extensive study of laminar and turbulent flow in open channels is most welcome. Since the writers' interest in open channel flow has primarily been in connection with the turbulent flow regime, their discussion of the laminar flow results presented will be limited. Comments on the turbulent flow aspects will be more extensive. With regard to the theoretical relations presented for viscous laminar flow in elliptical, rectangular and 90 degree triangular open channels, it should be noted that these are contained in the theoretical results presented by Boussinesq in 1868(1) for viscous flow in rectangular and elliptical conduits. In applying these to the appropriate open-channel cases, one assumes no effect of the free surface. In turbulent flow, this assumption is not quite correct and the maximum velocity usually lies below rather than on the free surface.

Did the authors' measurements of the velocity distribution in the case of laminar flow include a determination of the location of the filament of maximum velocity? It would be most interesting to know if this occurs on, or below, the free surface. For turbulent flows, the occurance of the maximum filament below the surface has been variously attributed to air resistance surface tension, secondary currents or some effect of turbulence. Observations of the occurance or non-occurance of this phenomenon in laminar flow would at least represent the case of no turbulence. They would tell us about the importance of turbulence and could well shed some light on this intruiguing but elusive question.

Studies of open-channel flow, although not as extensive as those reported by the authors, have been under way in the Fluid Mechanics and Hydraulics Laboratory of the University of Illinois for a number of years.(2,3) These have been mostly concerned with the turbulent flow regime at mild slopes. The following presentation of the Illinois' data is included as it directly supplements the authors' work.

The mean flow relations in a smooth 90 degree triangular flume at Reynolds numbers up to 45,000 are presented by the authors in Figs. 2 and 5. The results obtained by W. M. Owen(2) on a similar smooth wooden channel at Reynolds numbers from 20,000 to 275,000 are presented in Fig. 1 in comparison with the Minnesota data and smooth pipe relations. Baring any systematic errors, it would appear that at the higher Reynolds numbers the friction for triangular channels falls below the Blasius relation for smooth pipes, as given by Eq. (9a).

* Prof. of Theoretical and Applied Mechanics, Univ. of Illinois, Urbana, Ill.
** Prof. of Theoretical and Applied Mechanics, Univ. of Illinois, Urbana, Ill.

The open channel flow studies at Illinois have also been concerned with the nature of the turbulent flow in the triangular channel roughened with sand grains. This type of roughness was chosen because it more nearly simulates the roughness type about which we know so much in pipe flow, i.e., Nikuradse's sand grain roughness.(4) Figure 1 also includes a comparison of the pipe and open channel variation in friction factor with Reynolds number and relative roughness (k/2R). In contradiction to Owen's(2) conclusion, from some of the same data, these results show a transition region between the smooth and fully rough conditions for open channel flow. Differences from the pipe results are apparent. Thus, the present sand grains appear to be effectively rougher than Nikuradse's (by about a factor of 1.4) and fully rough flow seems to occur at a lower Reynolds number. The first of these observations is not particularly unexpected since the sand grains used in the flume were not as closely packed as Nikuradse's were.

A better understanding of the nature of the flow is obtained through studies of the velocity distribution. Thus, in Fig. 6, the authors present velocity traverses obtained for turbulent flow in the smooth 90 degree flume. Similar measurements in the roughened triangular flume have been taken at Illinois by D. B. Y. Chen.(5) These measurements were made in the same 55 foot flume used by Owen.(2) The sand grain roughness was not identical, but the same sized grains were attached in the same fashion. That the roughness was effectively the same is evident from the general agreement of friction factors in Fig. 1. More baffling was added at the entrance of the flume to improve flow symmetry. The velocity measurements were taken at a station 45 feet from the head bay, with a pitot-static tube (diameter 0.106 inches). For a flow depth of 0.518 feet, velocities were measured at 32 locations; while for a depth of 0.788 feet, 48 locations were used. The reliability of the velocity measurements was verified through comparison of integrated discharges with those obtained by weight. The integrated discharges were quite consistently smaller by about 2.75 percent.

The results obtained for the smaller depth and roughness ($^{2R}/_{k} = 294$) are shown as contour plots in Fig. 2. The symbols on the upper plot represent the locations at which velocities were actually obtained. The differences between the several plots are most apparent when one considers the maximum velocity in magnitude and location. It is seen from this figure that as the Reynolds number increases, the ratio of the maximum velocity to the average velocity increases and this maximum is found nearer the free surface. All thirty traverses taken were analyzed by noting the ratio of maximum to average velocity $^{w_m}/_{\bar{w}}$ and the ratio of the depth of the maximum velocity location to depth of flow $\epsilon$. The results are summarized in Table I and, in general, agree with trend shown in Fig. 2. However, the measurements were mostly taken in the region of rough conduit where the friction factor presumably depends only upon relative roughness and not Reynolds number. Variation of the velocity ratio with the relative roughness, as found by Nikuradse in rough pipes, is not evident from these data due either to lack of precision or effect of the free surface.

Five of the velocity traverses taken by Chen were analyzed to determine velocity profiles in the rough flume in a manner similar to those presented by the authors in Fig. 6 for the smooth condition. Profiles have been obtained on the center line and on normals to the side walls passing through the point of maximum velocity. In this latter case, values of the velocity were determined from velocity contours sketched with the aid of the measured data.

The resultant velocity profiles are presented in Fig. 3. Comparison of the profiles on the center line and the normal lines indicates similar effects to those shown in the authors' Fig. 6. The mean lines passing through the data have the following equations:

for the normal:

$$\frac{w}{\bar{w}_*} = 8.3 + 5.75 \log \left(y/k\right)$$

for the center line:

$$\frac{w}{\bar{w}_*} = -4.85 + 10.5 \log \left(y/k\right)$$

This form of equation, rather than an exponential form as used by the authors, is chosen to permit comparison with Nikuradse's pipe work. In making this comparison, the first equation above is found to be very close to Nikuradse's equation for the velocity profile in fully rough pipe flow. Such similarity is coincidental since it has already been noted that the roughness heights of the sand grains used correspond to higher values of Nikuradse[6] sand grain roughness. Another factor influencing these results is the variation in wall shear stress around the periphery of the flume. Thus, for the center line traverses, the effective shear must be much less than the mean value used to compute $\bar{w}_*$.

Some idea as to the variation in the wall shear stress around the wetted perimeter of the flume has been obtained from the velocity measurements nearest the side walls. For each such measurement, the Nikuradse rough pipe velocity profile equation,* corrected for the different effective roughness height of the sand grains, was utilized to calculate the value of the local shear stress velocity $w_*$. The square of the ratio of $w_*$ to the mean shear stress velocity $\bar{w}_*$ yields the ratio of wall shear stress to the average or $\tau_w/\gamma RS$. The indicated variation in wall shear stress up the side of the flume is presented in Fig. 4. Although there is considerable scatter and traverse A appears out of line, a definite trend is apparent for the wall shear stress variation.

For rectangular rough channels, Keylegan[6] has analyzed Bazin's data in a similar manner to obtain the peripheral variation in wall shear. He notes that the shear has a maximum value at the midpoint of the bottom and minima at the corners. With this information, he then verifies the agreement between Bazin's velocity traverses and the Nikuradse velocity equation. It is the writers' opinion that more such studies of shear and velocity distributions in turbulent open channel flow will advance our basic understanding of the phenomena involved.

It is hoped that this presentation and discussion will aid in giving a clearer insight into some phases of open channel flow, thus supplementing the excellent coverage of the author's paper.

---

* From a detailed analysis of Nikuradse's velocity measurements near the wall, this equation has been found to apply for values of $w_*k/\nu$ greater than 4.4. For the traverses analyzed, $\bar{w}_*k/\nu$ was not less than 8.4. This implies an error when $w/\bar{w}_*$ is less than 0.52 ($\tau_w/\gamma RS$ less than 0.23).

TABLE I

Summary of Maximum Velocity Data

From Triangular Flume With Rough Sides

| d ft. | k ft. | S | $\overline{w}$ fps | $\frac{2R}{k}$ | Re | $\frac{k\overline{w}_*}{\upsilon}$ | $\frac{w_m}{\overline{w}}$ | $\epsilon$ |
|---|---|---|---|---|---|---|---|---|
| 0.788 | 0.00125 | 0.0005 | 1.293 | 444 | 144000 | 8.4 | 1.164 | 0.238 |
| 0.788 | 0.00125 | 0.001 | 1.785 | 444 | 202000 | 11.8 | 1.240 | 0.195 |
| 0.788 | 0.00125 | 0.002 | 2.56 | 444 | 290000 | 17.0 | 1.268 | 0.031 |
| 0.518 | 0.00125 | 0.0005 | 0.989 | 294 | 74360 | 6.9 | 1.175 | 0.212 |
| 0.518 | 0.00125 | 0.001 | 1.398 | 294 | 104000 | 9.8 | 1.204 | 0.169 |
| 0.518 | 0.00125 | 0.002 | 1.988 | 294 | 146000 | 13.6 | 1.232 | 0.135 |
| 0.788 | 0.0025 | 0.0005 | 1.235 | 206 | 135600 | 16.5 | 1.184 | 0.290 |
| 0.788 | 0.0025 | 0.001 | 1.747 | 206 | 190000 | 30.8 | 1.264 | 0.197 |
| 0.788 | 0.0025 | 0.002 | 2.431 | 206 | 287000 | 35.5 | 1.211 | 0.042 |
| 0.518 | 0.0025 | 0.0005 | 0.908 | 134 | 65200 | 13.5 | 1.231 | 0.254 |
| 0.518 | 0.0025 | 0.001 | 1.275 | 134 | 94000 | 19.1 | 1.181 | 0.212 |
| 0.518 | 0.0025 | 0.002 | 1.863 | 134 | 134000 | 26.6 | 1.240 | 0.171 |

---

$\overline{w}$ = average velocity, fps

$w_m$ = maximum velocity, fps

$\epsilon$ = depth to maximum velocity filament divided by depth of flow (d)

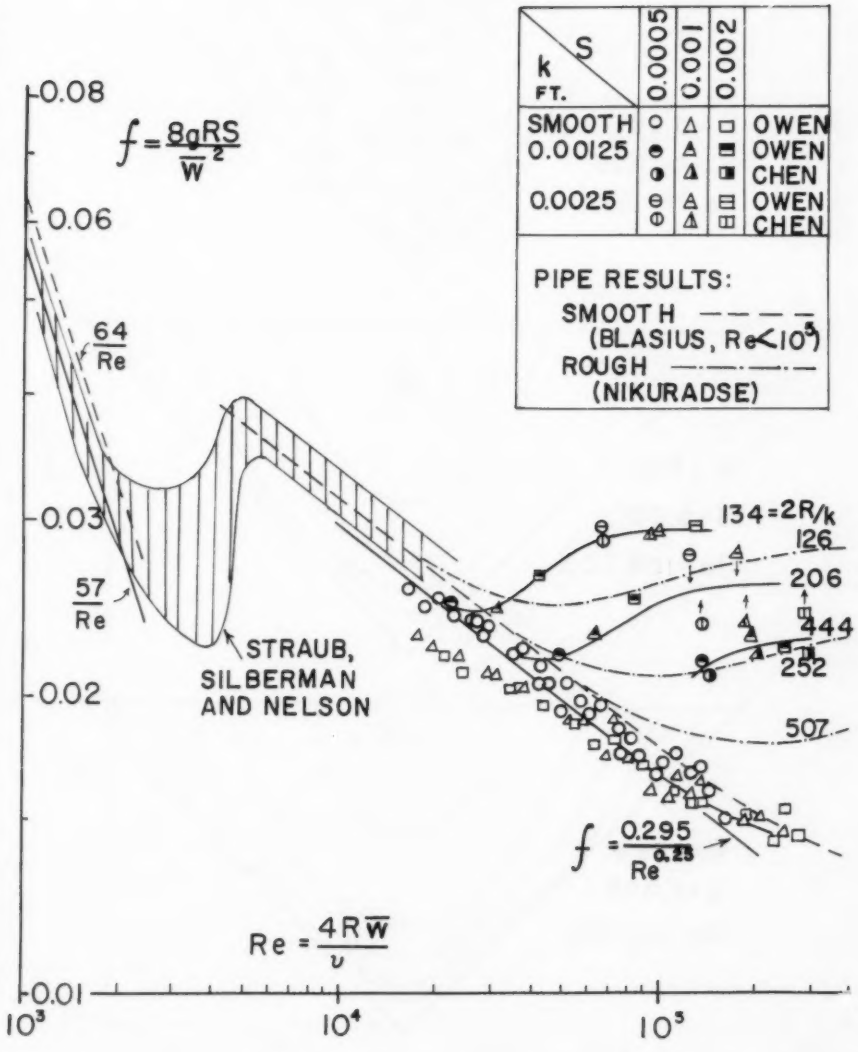


FIG. 1 FRICTION FACTOR IN 90-DEGREE FLUME COMPARED WITH PIPE RESULTS

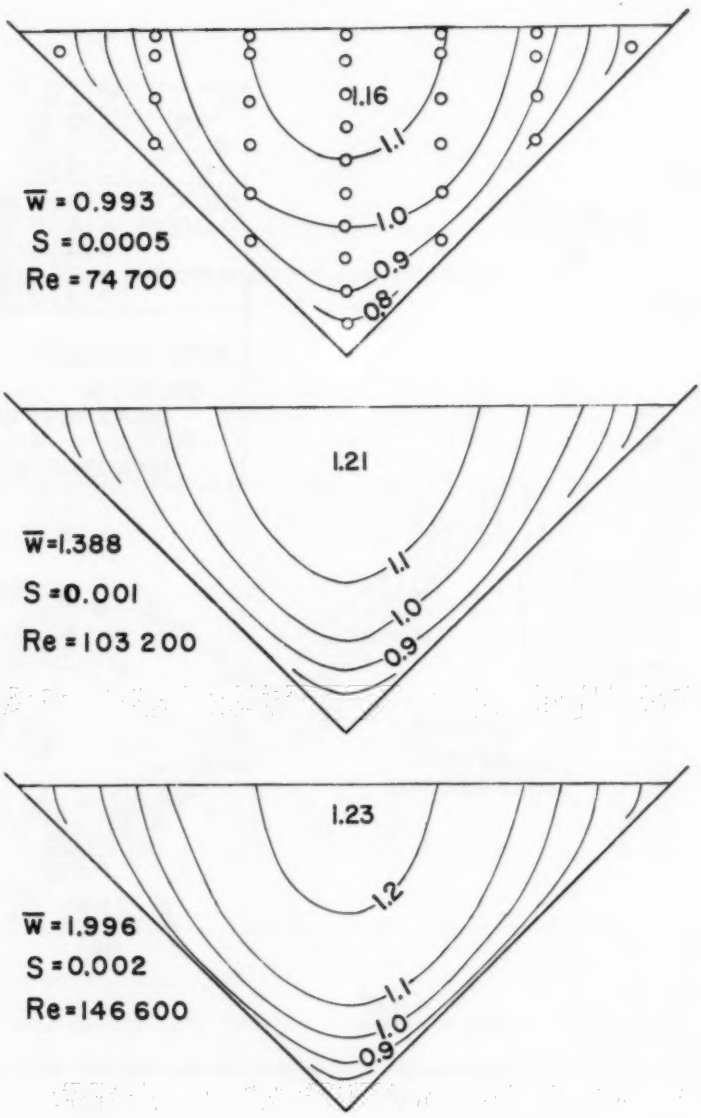


d = 0.518 FT k = 0.00125 FT

FIG. 2 VELOCITY CONTOUR PLOTS FOR THREE REYNOLDS NUMBERS

| TRAVERSE | SYMBOL | |
|---|---|---|
| | ℄ | N |
| B | × | × |
| C | + | + |
| D | ▽ | △ |
| E | ○ | ● |
| F | ◇ | □ |

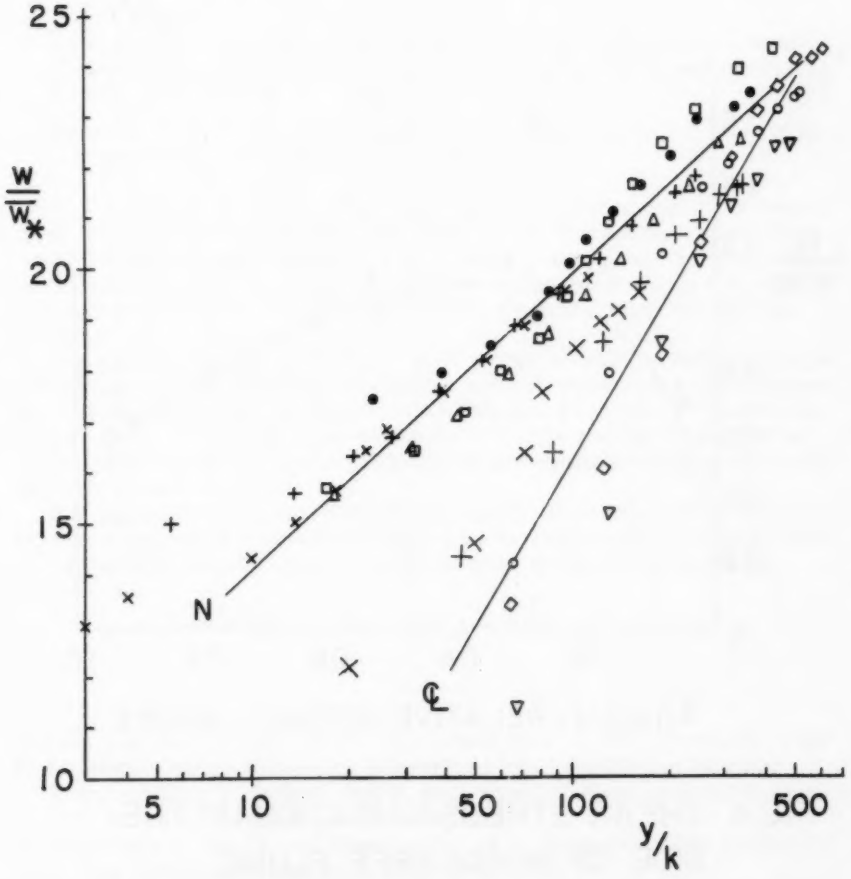


FIG.3 VELOCITY PROFILES FOR ROUGH TURBULENT FLOW IN TRIANGULAR FLUME

| TRAVERSE | A | B | C | D | E | F |
|---|---|---|---|---|---|---|
| DEPTH - d | 0.788' | 0.518' | 0.518' | 0.788' | 0.788' | 0.788' |
| ROUGH. - k | 0.0025' | 0.0025' | 0.00125' | 0.00125' | 0.00125' | 0.00125' |
| SLOPE - S | 0.001 | 0.001 | 0.001 | 0.0005 | 0.001 | 0.002 |
| SYMBOL | ○ | × | + | △ | • | □ |

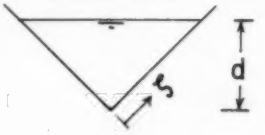


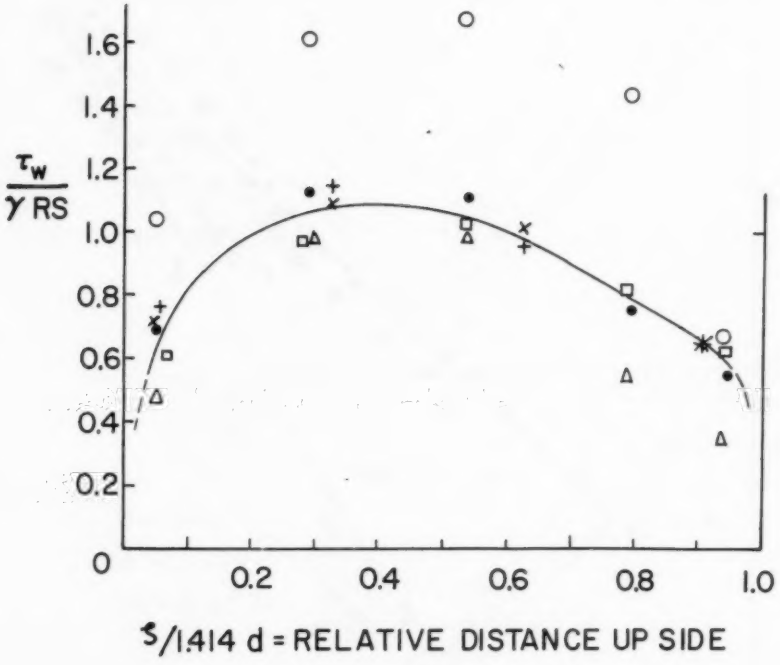


FIG.4 SHEAR STRESS VARIATION UP THE SIDE OF 90-DEGREE FLUME

REFERENCES

1. Boussinesq, J. "Memorie sur L'Influence des Frottements dans les Mouvements Reguliers des Fluides," Journal de Mathematiques Pures et Appliqués, Series 2, Vol. 13, 1868, pp. 377-424.
2. Owen, W. M. "Correlation Between Pipe Flow and Uniform Flow in a Triangular Open Channel," Trans. Am. Geoph. Union, Vol. 34, 1953, pp. 213-219.
3. Owen, W. M. "Laminar to Turbulent Flow in a Wide Open Channel," Trans. ASCE, Vol. 119, 1954, pp. 1157-1164.
4. Nikuradse, J. "Laws of Flow in Rough Pipes," V.D.I. Forschungsheft 361, 1933, Translated by NACA, TM 1292, 1952.
5. Chen, D. B. Y. "A Study of the Velocity Distribution in an Open Channel Having a Triangular Cross Section," M. S. Thesis, University of Illinois, Urbana, Illinois, 1955.
6. Keulegan, G. H. "Laws of Turbulent Flow in Open Channels," Jour. of Res. of NBS, Vol. 21, Dec. 1938, pp. 733-735.

C. J. POSEY,[1] M. ASCE.—The writer questions part of one of the conclusions, in which it is stated that "The entire effect of shape in laminar flow may be computed theoretically." If it is meant to imply that the theory based on the Navier-Stokes equations is applicable to the extent that it will yield an accurate picture of the velocity distribution, there is good evidence to the contrary.

The author's data shown in Fig. 3 show a considerable deviation from the theoretical which is evidently systematic, and not haphazard. Data obtained by Ellis B. Pickett show deviations of comparable magnitude.[2] Theoretical studies based on differential equations that describe the behavior of actual fluids more precisely than do the Navier-Stokes equations yield significantly different results.[3,4,5]

It is reasonable to expect that velocity distributions which differ appreciably from geometrical similarity might still have very nearly the same overall rate of friction loss. This could explain the agreement shown in the author's Fig. 2.

---

1. Prof. and Head of Dept. of Civ. Eng., State Univ. of Iowa, Iowa City, Iowa.
2. "A Direct Optical Method for Measuring Fluid Velocities in Laminar Flow," by Ellis B. Pickett, thesis, Department of Mechanics and Hydraulics, State University of Iowa, August, 1950.
3. "Experience, Theory, and Experiment," by C. Truesdell, State University of Iowa Studies in Engineering, Bulletin 36, 1956.
4. "Hydrodynamics of non-Newtonian Fluids," by R. S. Rivlin, Nature, Vol. 160, 1947.
5. "Overdetermination of the Speed in Rectilinear Motion of Non-Newtonian Fluids," by J. L. Erickson, Quarterly of Applied Mathematics, Vol. 14, 1956.

Discussion of
"LATERAL BRACING FORCES ON BEAMS AND COLUMNS"

by William Zuk
(Proc. Paper 1032)

ROBERT V. HAUER.[1]—The theory of elastic stability does not establish a requirement of strength for a member bracing a column or a beam which is free from imperfections and loaded concentrically. In order to provide the designer with any information of this sort, the author enforces a solution by assuming an initial crookedness of the member to be braced.

It seems doubtful to the writer whether much is gained by such a procedure, as its net result is only to replace the usual thumb rule—namely, to assume a bracing force equal to a certain percentage of the force in the main member—with another thumb rule assumption about the magnitude of the initial crookedness. Such an accidental deviation from the straight line is only one of the many differences between the actual physical conditions and the idealized assumptions upon which any structural design is necessarily based, and, therefore, should be taken care of by a properly chosen safety factor.

Furthermore, the artificial approach which the author chooses for the problem in question is not necessary at all. For, the theory of elastic stability does furnish the designer with some requirement regarding a bracing member. This requirement is not one of a certain strength, but one of a minimum stiffness.

For instance: If a column with a total length L is braced at mid-height, an investigation of the elastic line shows that the unsupported length can be assumed to be 1/2 L only under the condition that the spring constant of the bracing member is at least equal to $4\ P_c/L$, where $P_c$ is the critical load under which the braced column loses its stability. If the spring constant is less, the critical load, i.e., the capacity of the column, becomes smaller (but it does not become greater, if the spring constant increases). Similar results are obtained in all other cases of bracing.

Generally, the stiffness requirement for the bracing member is not hard to fulfill, as the following numerical example shows: A 10 WF 33 column with a total length of 28 feet is divided into two equal lengths of 14 feet by a bracing member. Assuming the steel having a modulus of elasticity of 30,000 kips per sq. in., a yield point of 40 kips per sq. in. and a proportional limit of 27 kips per sq. in., there exists in the inelastic range the following approximate relation between the slenderness ratio l/r and the critical stress $f_c$:[2]

$$f_c \text{ (in kips per sq. in.)} = 40 - \frac{1}{844}(l/r)^2$$

This gives for the example in consideration $f_c = 31$ kips per sq. in. or $P = 31 \times 9.71 = 301$ kips.

1. Structural Engr., Albert Kahn, Inc., Detroit, Mich.
2. Friedrich Bleich: Buckling Strength of Metal Structures, McGraw-Hill Book Company, Inc., New York, Page 53, Equ. 63.

In order that this computation be correct, the spring constant of the bracing member must be at least

$$k_1 = \frac{4\,P_c}{L} = \frac{4 \times 301}{28} = 43 \text{ kips per ft.},$$

or 3.58 kips per in. In other words, under an axial load on the brace of only 3.58 kips the bracing member is allowed to give as much as a full inch, which shows that even a rather flexible lateral support is sufficient to brace the column properly.

In more complicated cases, as in a half through bridge, where the top chord is braced by open frames, the influence of the flexibility of the lateral supports upon the capacity of the top chord must be carefully investigated, regardless of any more or less fictitious loads which are assumed to act horizontally on these supports. For, a requirement of stiffness can never be replaced by a requirement of strength.

CHESLEY J. POSEY,[1] M. ASCE.—The writer wonders whether it is advisable to attempt to specify the force that lateral bracing must supply. In Fig. A, consider column AB which has frictionless hinges at each end and also a hinge at its midpoint, C. Points A and C are restrained from moving in the horizontal direction by braces DA and EC. Assuming for the time being that the dead load of member EC can be neglected, how should it be designed? It is seen immediately that the stress in EC given by the ordinary analysis of statics is zero, but that the member cannot be dispensed with, for then the column will buckle at the hinge C, and collapse. To say that the member must be strong enough to carry its own weight and conform to the specification requirements for minimum slenderness ratio is begging the question.

Of course fabrication and erection difficulties would not permit points A, C, and B to lie exactly on a straight line. Assume that point C is out of line by a small distance $\delta$. A triangle-of-force solution applied to the free-body diagram for joint C shows that member C must now supply a force

$$F = \frac{2P\delta}{s} \qquad \text{(a)}$$

This relationship, graphed in Fig. B, is approximate in that it will only hold as long as $\delta$ is small compared with $\ell$. However, lack of linearity should not be noticeable until $\delta/\ell$ is 0.05 or more, a value much greater than is likely to occur. When lack of linearity does appear, however, it will require a larger value of F than that given by Eq. (a).

Fig. B shows the total force that member EC must provide, depending upon the amount of slight misalignment of the joints. Without making an assumption as to how large the misalignment might be, it is impossible to fix the magnitude of the force that member EC must be designed for.

If member EC is subjected to a force, however, it will deflect. The relationship between F', the total stress in EC, and the deflection due to that stress is

$$F' = \frac{AE\delta}{l}$$

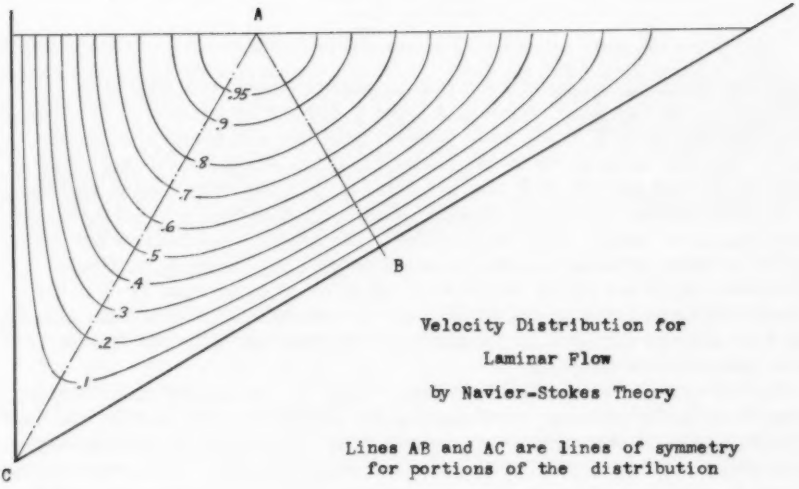


Velocity Distribution for
Laminar Flow
by Navier-Stokes Theory

Lines AB and AC are lines of symmetry
for portions of the distribution

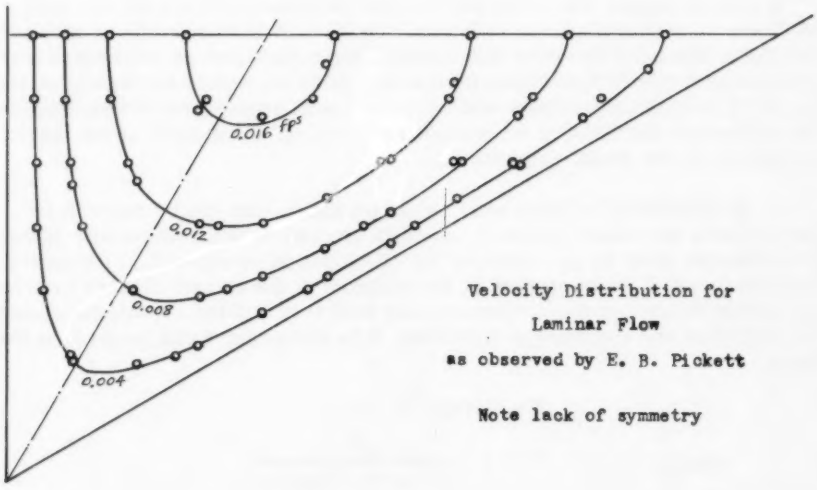


Velocity Distribution for
Laminar Flow
as observed by E. B. Pickett

Note lack of symmetry

F' is the force that member EC can supply when joint C is moved a distance $\delta$ from its unstressed position. If now we design member EC so that

$$\frac{AE}{l} = \frac{2P}{s}$$

it will be just able to supply the force necessary to hold the joint C in equilibrium for any small value of $\delta$. But $\delta$ can not be permitted to become large, for the force F required to prevent buckling will eventually become larger than the value given by the linear equation, while the force F' that member EC can provide will become smaller than the linear value as soon as the proportional limit is exceeded. Evidently this design is not safe, and some margin of safety must be provided. The design requirement for member EC is seen not to be a strength requirement, but rather a "stiffness" requirement, since the factor which must be safely greater than 2P/s is the ratio of the axial force to axial deflection in member EC. This axial stiffness would be slightly different in tension and compression. It is the smaller value that must be adequate.

For the example of the author's Fig. 10, the writer agrees that the minimum value of the stiffness coefficient of the elastic support is $P/\ell$, and that a limiting value 50% greater is practical. This is a simple and basic requirement which could be made the basis of specifications, and the writer sees no reason to shift to a strength requirement which has no validity unless definitely related to the specification governing the permissible initial eccentricity. If the fabrication alignment does not meet specifications, the margin of safety of the strength requirement is encroached upon.

It may be argued that a lateral bracing specification based solely upon stiffness is inadequate because failure might occur before the force reached the value demanded by the initial eccentricity. That such an extreme brittleness could occur with ordinary structural materials seems extremely unlikely, but if it is thought to be possible, safety could be assured by requiring that the necessary stiffness be maintained for loads up to say 200% of the value demanded by the initial eccentricity.

C. M. SEGEDIN.[a]—There are one or two points that can be made in connection with the author's Case 1, in which he considers a column with initial crookedness given by $y_0 = a\sin(\pi x/L)$. He gives in equation (1.1) the lateral bracing force, F, to be applied at the midpoint of the column if there is to be no further deflection there when an axial load P is applied. If this expression is simplified and rearranged somewhat, it is found that F can be given in the form

$$F = (4\pi Pa/\pi^2 L)\, f(u)$$

where

$$f(u) = \frac{u^3}{3(1-4u^2/\pi^2)(\tan u - u)}$$

and

$$u = \tfrac{1}{2} p L,\quad p^2 = P/EI.$$

a. Senior Lecturer in Math., School of Eng., University College, Auckland, N. Z.

f(u) of course depends, non-dimensionally, on P, EI and L, but evaluation yields the result that it is a steadily increasing function of u - at least until tanu = u - and it is found that

$$f(0) = 1,\ f(\tfrac{1}{2}\pi) = \pi^4/96 = 1.015,\ f(\pi) = \pi^2/9 = 1.097.$$

These values of u correspond to the cases (a) no axial load, (b) axial load equal to the first Euler load, $P = EI\pi^2/L^2$, and (c) axial load equal to the second Euler load, $P = 4EI\pi^2/L^2$, at which the column in this case buckles. Thus for the range of practicable values of P, f(u) is remarkably constant and we have the result that F is proportional to a, as pointed out by the author, and approximately proportional to P and 1/L.

Increased stability may be achieved if the slope of the column at the midpoint is kept zero. In this case buckling occurs when

$$\tan u = u, \text{ namely, } u = 1.430\pi \quad \text{or } P = 8.18\pi^2EI/L^2,$$

and it is easily shown that no torque need be applied at the midpoint to prevent the tendency of the column to turn there.

This suggests a related problem for which the buckling load is again $P = 8.18\pi^2EI/L^2$ in which the column, simply supported at each end, is assumed to have an initial crookedness given now by $y_o = a\sin(2\pi x/L)$. If further deflection and slope are both kept zero it can be shown that the bracing torque, M, applied at the midpoint must be

$$M = (6Pa/\pi)F(u)$$

where

$$F(u) = \frac{u^2\tan u}{3(1-u^2/\pi^2)(\tan u - u)}$$

F(u) is not so conveniently constant for different values of u but here M is relatively insensitive to L at least for small axial loads. Throughout, for the initial crookedness now assumed the lateral bracing force is zero.

Discussion of
"MINIMUM-WEIGHT DESIGN OF A PORTAL FRAME"

by William Prager
(Proc. Paper 1073)

ROBERT L. KETTER,* J.M. ASCE.—In discussing the problem of the minimum-weight design of portal frames, it should be pointed out that seldom if ever will a "real" structure be subjected to only one condition of loading. It is therefore necessary to determine (or check) for each of the possible loading configurations the required sized of the component parts of the frame. The problem becomes even more involved for the case of multiple span structures.

As a second and final point of this discussion, it is desirable to show how well the $\alpha = 2/3$ used by the author checks currently available structural sections. In Figure 1 is plotted to a log-log scale the weight per foot of members versus the plastic modulus (which is proportional to the full plastic moment, $M_p$) for each of the rolled WF shapes. As indicated, within a given range of nominal depth of section, weight increases approximately as the plastic modulus raised to the 0.91 power. Considering the lower extremities of these sections available (that is, the most economical sections), if the weight is less than about 40 lbs. the weight increases approximately as the 0.55 power of the plastic modulus. For those cases where the weight is greater than 40 lbs., $W = k(M_p)^{0.63}$ seems to be a better approximation. The $\alpha = 2/3$ value used by the author is a reasonable value for the overall range of available wide flange shapes.

* Research Asst. Prof., Fritz Eng. Lab., Lehigh Univ., Bethlehem, Pa.

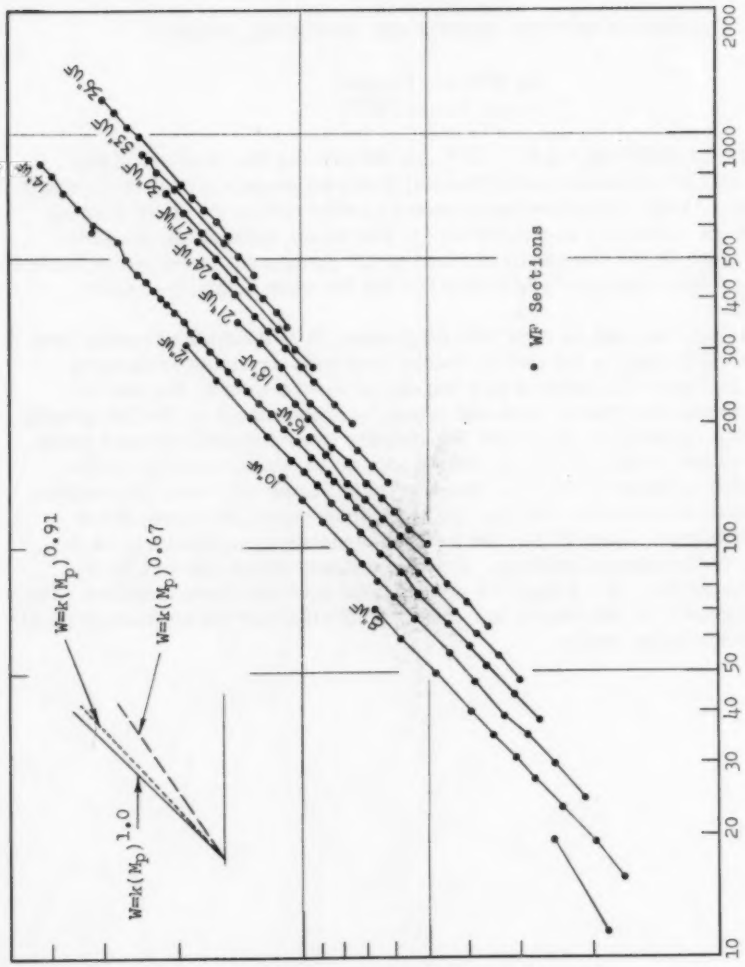
WEIGHT PER FOOT OF MEMBER
PLASTIC MODULUS, Z (in.³)
• WF Sections
W=k(Mp)^1.0
W=k(Mp)^0.67
W=k(Mp)^0.91
14"WF
12"WF
10"WF
8"WF
500
400
300
200
100
50
40
30
20
10
2000
1000
500
400
300
200
100
50
40
30
20
10

FIGURE 1

Paper 1157 EM 1

Journal of the
ENGINEERING MECHANICS DIVISION
Proceedings of the American Society of Civil Engineers

# A PRESSURE LINE CONCEPT FOR INELASTIC BENDING

Frank Baron,[1] M. ASCE
(Proc. Paper 1157)

## SYNOPSIS

The concept of the pressure line, useful for arches and rigid frames, is developed for quickly estimating the effects of plasticity on the behavior of structural elements subjected to axial and flexural loads. An initial estimate, obtained by means of an elementary theory of mechanics, is adjusted to fit the conditions of plasticity.

A procedure is presented for quickly estimating the effects of non-linear stress-strain relationships on the behavior of structural elements subjected to axial and flexural loads. The procedure consists of obtaining an initial estimate by means of an elementary theory of mechanics and adjusting the estimate to fit the conditions of a theory of plasticity. In this way, the results of both theories are available for comparisons and for further studies as in problems of ultimate load analyses and inelastic buckling.

Figures 1 and 2 show a cross-section of a differential element subjected to an axial load, P, and a moment, M, about a centroidal axis of the section. For convenience of this discussion, the cross-section is assumed to have an axis of symmetry as shown. The effects of a shear, Poisson's ratio, residual strains, and local instability of projecting elements of the cross-section are herein neglected.

The elementary theory of mechanics is summarized in Figure 1 wherein the stress in a fiber is defined as

$$s_o = s_a + s_b \qquad (1)$$

and where $s_a = P/A$ and $s_b = Mx_c/I$. The distribution of stress across the section is linear and satisfies the requirements of statics; namely,

Note: Discussion open until June 1, 1957. Paper 1157 is part of the copyrighted Journal of the Engineering Mechanics Division of the American Society of Civil Engineers, Vol. 83, No. EM 1, January, 1957.

1. Prof. of Civ. Eng. Univ. of California, Berkeley, Calif.

$$\sum s_o da = P \tag{2}$$

$$\sum s_o x_c da = M \tag{3}$$

Among the assumptions of the elementary theory are a linear distribution of strains across the section and a linear stress-strain relationship for the material. The angle-change between adjacent cross-sections is stated in terms of strains, stresses, and moment as follows:

$$\Delta\phi_o = \frac{\Delta\epsilon}{h} ds = \frac{\Delta s_b}{E_o h} ds = \frac{M}{E_o I} ds \tag{4}$$

where $\Delta\epsilon$ designates the difference in the strains of the extreme fibers, $\Delta s_b$ the difference in the stresses of the extreme fibers, and $E_o$ the modulus of elasticity.

In the theory of plasticity discussed herein, the requirements of statics and of geometry are the same as those in the elementary theory of mechanics. In each theory the distribution of stresses across the section must satisfy the requirements of statics; namely,

$$\sum s\, da = \sum s_o\, da = P \tag{5}$$

$$\sum s\, x_c da = \sum s_o x_c da = M \tag{6}$$

And in each theory the distribution of strains across the section is assumed to be linear. However, in the theory of plasticity it is assumed that the stress-strain relationships for the fibers of a member subjected to a simultaneous axial and flexural load may be non-linear and are the same as those obtained from simple tension and compression tests. In Figure 2, the stress-strain relationship of the material is represented by curve AOB and is assumed to be the same for each longitudinal fiber.

The stress in a fiber as given by the theory of plasticity may be interpreted as equal to the stress given by the elementary theory plus a correction stress to account for the non-linear stress-strain characteristics of the material. Thus,

$$s = s_o + s_c \tag{7}$$

The results of the theory of plasticity are compared in this way in Figure 2 to those of the elementary theory of mechanics. The ordinates bounded by the stress-strain curve AOB are in accordance with the theory of plasticity whereas those bounded by the straight line CD are in accordance with the elementary theory. The shaded diagram of Figure 2 represents the differences in the results of the two theories or correction stresses as defined in Equation 7.

The diagram of correction stresses shown in Figure 2 must satisfy the following conditions:

1. No load or moment is to be contributed by the diagram of correction stresses, that is

$$\Sigma s_c da = 0 \quad (8)$$

$$\Sigma s_c x_c da = 0 \quad (9)$$

2. A linear distribution of strains across the section must be observed.
3. The correction stresses must account for the non-linear stress-strain characteristics of the material.

In reverse order of above, item 3 is satisfied since the correction stresses are represented by the ordinates bounded by the straight line CD and the stress-strain curve AOB. Item 2 is satisfied since the abscissas of the stress-strain curve and the dimensions of the cross-section are drawn to linear horizontal scales. Consequently, the distribution of strains across the section is linear. The scale selected for the dimensions of the cross-section is in agreement with the values of the strains in the extreme fibers. For other values of strains in the extreme fibers than those indicated in the Figure, the horizontal scale is either reduced or magnified in proportion to the difference in the strains of the extreme fibers.

The correction stresses indicated in Figure 2 must balance or vanish. The terms balance or vanish are used here in the sense that Equations 8 and 9 are satisfied. The requirements of these Equations are restated as follows:

1. The sum of the positive correction forces must equal the sum of the negative correction forces. A correction force is equal to a correction stress times its corresponding differential area.
2. The centroid of the positive correction forces must coincide with the centroid of the negative correction forces.

The above restatement is particularly useful in pictorial studies of the effects of a non-linear stress-strain curve. This should be obvious to those already familiar with the pressure line concept for fixed-end beams and arches. A procedure of sketching may be developed herein similar to the procedure used in sketching pressure lines for fixed-end beams.(1) In a fixed-end beam, the angle-changes along the beam caused by lateral loads must balance. Thus, conditions of statics for correction forces in a short element of a member as discussed herein are analogous to the conditions of geometry for angle-changes along a fixed-end beam. If desired, these analogous relationships may be summarized as in the Column Analogy(2) except that the column now has non-linear stress-strain characteristics. In addition, the interest herein is in the correction stresses of a column and not in the correction moments of a statically indeterminate beam or arch.

Before proceeding to examples of the above procedure, we return to an inspection of Figure 2. Two modified moduli of elasticity are introduced; namely,

$$E_a' = s_a/\epsilon_a \quad (10)$$

$$E_b' = \Delta s_b/\Delta\epsilon \quad (11)$$

where $s_a$ is the average stress, $\epsilon_a$ is the strain of the fibers along the centroidal axis, and $\Delta s_b$ and $\Delta\epsilon$ are defined as previously. The values of $E_a'$ and $E_b'$ are represented in the Figure as slopes of corresponding straight lines and may be interpreted as reduced moduli of elasticity. They may also

be interpreted respectively as measure of stiffness to relative translation and to relative rotation of adjacent cross-sections.

Three examples of the pictorial procedure are given in Figure 3 and are discussed below.

Example A: Given a stress-strain curve, a cross-section, and the values of the strains in the extreme fibers. Determine the loads, stresses, angle-change per unit of length, and the reduced moduli of elasticity.

Between the values of the extreme fiber strains, draw a straight line which you consider to be the best "fit" to the stress-strain curve. Check "fit" by inspecting whether the diagram of correction forces is balanced. If necessary, revise the straight line until you are satisfied the diagram of correction forces is sufficiently balanced. Read in the Figure the values of $s_a$, $\Delta s_b$, $\epsilon_a$, and $\Delta\epsilon$. Now compute the values of load, moment, the reduced moduli of elasticity, and the angle-change per unit of length. Stresses in accordance with each theory and their differences are observed in the sketch.

Example B: Given the loads, a cross-section, and the stress-strain curve. Determine the stresses, strains, angle-change per unit of length, and the reduced moduli of elasticity.

Compute the average stress and the stresses in the extreme fibers by means of the elementary theory of mechanics. Draw horizontal lines in the stress-strain diagram consistent with the computed stresses in the extreme fibers. Between these lines, draw a straight line which you consider to be the best "fit" to the stress-strain curve. From the intersections of these lines drop verticals to the stress-strain curve. The ordinates between the straight line and the stress-strain curve represent the correction stresses to the elementary theory of mechanics. Check "fit" and, if necessary, revise the straight line. Read from the diagrams the value of $\epsilon_a$, and $\Delta\epsilon$. Now compute the values of the angle-change per unit of length and of the reduced moduli of elasticity.

Example C: Given a stress-strain curve and a cross-section of a pin-ended column subjected to a critical axial load. Consider a history of deformations as in the double-modulus theory(3) wherein an increase in strain of a fiber is associated with the tangent modulus and a decrease in strain is associated with the initial modulus. Determine the reduced modulus of elasticity and the value of L/r which is in agreement with the critical load. For illustration only, the bending is assumed to occur about the centroidal axis shown in the Figure.

Compute the average stress on the cross-section and for this value of stress draw a horizontal line intersecting the given stress-strain curve. At this intersection draw a line tangent to the curve and a line parallel to the initial slope of the curve. Consider these two lines as the stress-strain curve associated with subsequent buckling. For the critical axial load and an arbitrarily assumed moment, compute the stresses in the extreme fibers by means of the elementary theory of mechanics. Draw horizontal lines consistent with the computed stresses in the extreme fibers. Between these lines draw a straight line which you consider to be the best "fit" to the stress-strain curve associated with buckling. From the intersections of the straight line with the two horizontal lines, drop verticals to the assumed stress-strain curve. Check "fit" and proceed as in Example B to determine the desired position of the straight line. The slope of the straight line is the value of the reduced modulus of elasticity. The desired value of L/r is defined by the modified Euler equation for critical load.

For brevity, the above discussion was restricted to that of a cross-section having an axis of symmetry and subjected to an axial load and moment about an axis normal to the axis of symmetry. The pictorial procedure may be extended to the general case of an unsymmetrical cross-section subjected to an axial load and to moments about the two principal axes of the section. It may be extended to certain problems of torsion, of residual strains, and of other histories of deformations than those considered above. It may also be extended to studies of the effects of non-uniform changes in temperature or of moisture content through the thickness of a long structural member and of non-homogeneity through the thickness of the member. Many problems in the theory of elasticity which include the effects of warping of cross-sections or of non-linear distributions of strains across the sections may be studied in the same way.

If desired, the procedure may be stated more formally and a numerical or algebraic procedure may be developed for similar cases as above.

## CONCLUSIONS

The concept of the pressure line has been shown to be useful for problems of an arch with loads in the plane of the arch[1] and for structures curved in space.[4] The concept is equally useful for problems involving the inelastic deformations of structural elements.

## REFERENCES

1. "Continuous Frames of Reinforced Concrete," by Hardy Cross and N. D. Morgan, John Wiley and Sons, Inc., New York, N. Y. 1932, p. 289.
2. "The Column Analogy," by Hardy Cross, Bulletin No. 215, Eng. Experiment Station, University of Illinois, Urbana, Ill., 1930.
3. "Theory of Elastic Stability," by S. Timoshenko, McGraw-Hill Book Company, Inc., New York, N. Y., 1936, p. 156.
4. "Laterally Loaded Plane Structures and Structures Curved in Space," by Frank Baron and James P. Michalos, Transactions, ASCE, Vol. 117, 1952, p. 279.

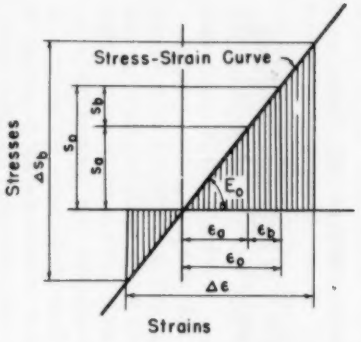


Values of stresses and strains

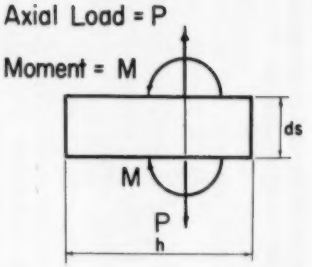


Axial and Flexural Loads

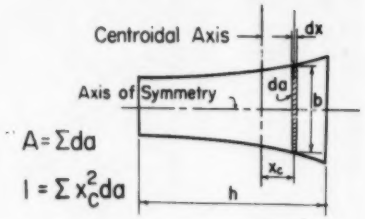


Properties of cross-section

**Stresses:** $s_o$ **Strains:** $\epsilon_o = b_o/ds$

$s_o = s_a + s_b$ $\epsilon_o = \epsilon_a + \epsilon_b$

$s_a = \frac{P}{A}$ **Modulus of Elasticity:** $E_o$

$s_b = \frac{Mx_c}{I}$ $E_o = \frac{s_o}{\epsilon_o} = \frac{s_a}{\epsilon_a} = \frac{\Delta s_b}{\Delta\epsilon}$

$\Delta s_b = \frac{Mh}{I}$ **Angle Change:** $\Delta\phi_o$

$\Delta\phi_o = \frac{\Delta\epsilon}{h}ds = \frac{\Delta s_b}{E_o h}ds = \frac{M}{E_o I}ds$

FIG.1-RELATIONSHIPS IN THE ELEMENTARY THEORY OF MECHANICS

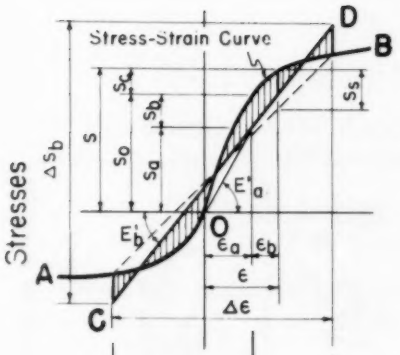


Values of Stresses and Strains

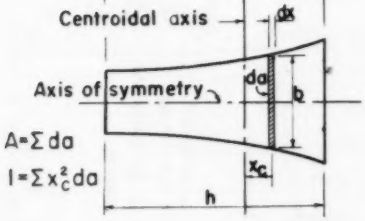


Properties of Cross-Section

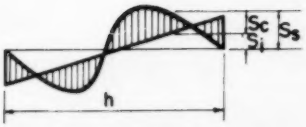


Correction Stresses to the Elementary Theory

## Stresses

$s = s_o + s_c$ $\quad \Sigma s_c\, da = 0$

$s_o = s_a + s_b$ $\quad \Sigma s_c x_c\, da = 0$

$s_a = \frac{P}{A}$ ; $s_b = \frac{Mx_c}{I}$

$\Delta s_b = \frac{Mh}{I}$

## Strains

$\epsilon = \epsilon_a + \epsilon_b$

## Modified Modulii of Elasticity

$E'_a = \frac{s_a}{\epsilon_a}$ $\quad E'_b = \frac{\Delta s_b}{\Delta \epsilon}$

## Angle-Changes

$\Delta\phi = \frac{\Delta\epsilon}{h} ds = \frac{\Delta s_b}{E'_b h} ds = \frac{M}{E'_b I} ds$

FIG.2 - THE ELEMENTARY THEORY OF MECHANICS COMPARED TO A THEORY OF PLASTICITY

Given:
The Stress-Strain Curve; $E_o = 12{,}000\ k/in^2$
Dimensions of Cross-Section; $b = 1\,in.$, $h = 18\,in.$
$A = 18\,in^2$, $I = 487\,in^4$
Extreme Fiber Strains: $\epsilon_t = 0.001\,in/in$,
$\epsilon_c = 0.0006\,in/in$ $\epsilon_a = 0.0035\,in/in$ $\Delta\epsilon = 0.0035\,in/in$
Determine $\Delta s_b$, $s_a$, P, M, $E_b'$, $E_a'$, and $\frac{\Delta\phi}{ds}$

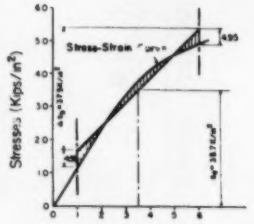

Properties of Cross-Section

Summary:
$\Delta s_b = 37.5\ k/in^2$ $s_a = 35.7\ kips/in^2$
$M = \frac{1}{h}\Delta s_b = 1{,}012\ in\text{-}kips$ $P = s_a A = 643\ kips$
$E_b' = \frac{\Delta s_b}{\Delta\epsilon} = 7{,}500\ kips/in^2$ $E_a' = \frac{s_a}{\epsilon_a} = 10{,}200\ kips/in^2$
$\Delta\phi/ds = \frac{\Delta s_b}{E_b' h} = 0.000278\ Radians/in$

Example A

Given:
The Stress-Strain Curve; $E_o = 30{,}000\ kips/in^2$
Dimensions of Cross-Section; $b = 1\,in.$, $h = 24\,in.$
$A = 24\,in^2$ $I = 1152\,in^4$
Axial and Flexural Loads, $P = 480\,k.$,
$M = 2{,}240\,in\text{-}k.$
First Compute: $s_a = \frac{P}{A} = \frac{480\,k}{24\,in^2} = 20\,k/in^2$
$\Delta s_b = \frac{Mh}{I} = \frac{2240k\ 24in.}{1152\,in^4} = 46.7\,k/in^2$
Determine: $\Delta\epsilon$, $\epsilon_a$, $E_b'$, $E_a'$, and $\frac{\Delta\phi}{ds}$

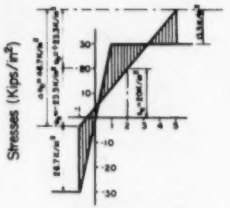


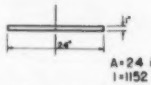


Properties of Cross-Section

Summary:
$\Delta\epsilon = 0.006\,in/in.$ $\epsilon_a = 0.002\,in/in.$
$E_b' = \frac{\Delta s_b}{\Delta\epsilon} = 7{,}780\,k/in^2$ $E_a' = \frac{s_a}{\epsilon_a} = 10{,}000\,k/in^2$
$\frac{\Delta\phi}{ds} = \frac{\Delta s_b}{E_b' h} = 0.00025\ Radians/in.$

Example B

Given:
The Stress-Strain Curve; $E_o = 30{,}000\,k/in^2$
Consider a History of Deformations
Dimensions of the Cross-Section;
$A = 5.75\,in^2$ $I = 42.5\,in^4$
Critical Axial Load; $P = -485\,kips$
$s_a = P/A = -84.4\,k/in^2$
Determine:
Reduced Modulus of Elasticity, $E_b'$ and $L/r$

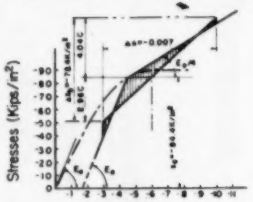


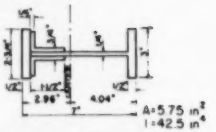


Properties of Cross-Section

Summary:
$P = -485\ kips$ $s_a = P/A = -84.4\,k/in^2$
$\Delta s_b = -78.4\,k/in^2$ $\Delta\epsilon = -0.007\,in/in$
$E_b' = \Delta s_b/\Delta\epsilon = 11{,}200\,k/in^2$
$L/r = \pi\sqrt{E_b'/s_a} = 36.3$

Example C

FIG. 3 EXAMPLES OF THE PICTORIAL PROCEDURE FOR COMPUTING THE EFFECTS OF PLASTICITY

Paper 1158 EM 1

Journal of the
ENGINEERING MECHANICS DIVISION
Proceedings of the American Society of Civil Engineers

# THE INFINITE ELASTIC BEAM ON A LINEAR VISCOELASTIC FOUNDATION

Alfred M. Freudenthal,[1] M. ASCE, and Harold G. Lorsch,[2] A.M. ASCE
(Proc. Paper 1158)

## SYNOPSIS

The infinite, elastic beam on three different types of linear viscoelastic foundations is analyzed under various loads. Initial, transient, and terminal states of beam deflection and foundation pressure are determined; conditions on the load function are stated. Numerical examples with graphs are given. The extension of the results to finite beams is discussed.

## Notation

$a_m$, $b_m$ . . . . . coefficients of Fourier series
E . . . . . modulus of elasticity of beam
I . . . . . moment of inertia of beam
K . . . . . kernel function
k . . . . . parameter having the dimension of length
L . . . . . influence length, length of half-period of load
m . . . . . integer
p . . . . . load per unit length
q . . . . . foundation pressure per unit length
t . . . . . time
x . . . . . abscissa
y . . . . . beam deflection

Note: Discussion open until June 1, 1957. Paper 1158 is part of the copyrighted Journal of the Engineering Mechanics Division of the American Society of Civil Engineers, Vol. 83, No. EM 1, January, 1957.
1. Prof. of Civ. Eng., Columbia Univ., New York, N. Y.
2. Asst. Prof. of Civ. Eng., The City College of New York, N. Y.

$\alpha_1, \alpha_2$ . . . . . reciprocal spring constants

$\phi$ . . . . . reciprocal coefficient of viscosity

$\tau$ . . . . . ratio between $\alpha$ and $\phi$, retardation time, relaxation time

$\xi$ . . . . . coordinate

## Introduction

### History

The problem of the elastic beam on a continuous foundation has been treated extensively in scientific and engineering literature ever since Zimmerman[1] gave his solution in 1888. This solution is based on Winkler's[2] assumption that the deflection at any point is proportional to the foundation pressure at that point, and does not depend on the pressure at any other point of the foundation.

Wieghart[3] was the first one to investigate the problem under the more general assumption that the deflection at any point depends on the foundation pressures along a certain length 2L of the foundation.

$$y(x) = \text{const.} \int_{-L}^{+L} q(\xi) K(|x-\xi|)\, d\xi \qquad (A)$$

Here y is the downward deflection of the beam, q the foundation pressure, and K a kernel function dependent on the type of foundation. Among others, Prager,[4] Nemenyi,[5] Marguerre,[6] Biot,[7] Reissner,[8,9] and Volterra[10] developed solutions for different kernels K, mostly through the use of Fourier integrals. Hetenyi[11] showed, however, that some of these more "accurate" solutions in two dimensions may, in effect, be poorer approximations of the actual three-dimensional problem than solutions based on the simple Winkler-Zimmermann assumption of proportionality between deflection and foundation pressure at each point.

With the recent developments in the field of soil mechanics it became evident that, for most types of soils, no kernel function $K(|x-\xi|)$ of the space coordinates alone could reproduce the actual behavior of the foundation. It appears necessary to include a function of the time in the relations between deflection and foundation pressure. Instead of being considered elastic, the foundation should therefore be approximated by a viscoelastic medium; i.e., a medium whose force-deformation relations are functions of the time.

The problem of the elastic beam supported by such a medium may be simplified by replacing the viscoelastic continuum with a series of independent, viscoelastic elements. This approximation is analogous to the usual engineering analysis of the elastic beam on an elastic foundation in which the latter is replaced by a series of independent, elastic springs.[1,2,11]

### Viscoelastic Models

The two elements whose combination represents linear viscoelastic behavior are the linearly elastic spring and the viscous dashpot filled with a liquid which obeys Newton's linear law of viscosity.[12] The motion of the

Figure 1.
Mechanical model
of Kelvin element.




Figure 2.
Mechanical model
of Maxwell element.




Figure 3.
Mechanical model
of "Standard Solid".

perforated piston inside the dashpot produces a resisting force in the liquid which is proportional to the velocity of the piston. Figs. 1, 2 and 3 show combinations of these elements to form the simplest linear viscoelastic models.

If spring and dashpot are arranged in parallel (Kelvin model, Fig. 1) the total force is the sum of the elastic and viscous forces.

$$q = (1/\alpha_2)y + (1/\phi)(dy/dt) \tag{1}$$

Here q is the force, y the deformation, $1/\alpha_2$ the spring constant, and $1/\phi$ the coefficient of viscosity. Under a constant force $q = q_0$ the deformation increases asymptotically from zero to its final, elastic value.

$$y = \alpha_2 q_0 (1 - e^{-t/\tau}) \tag{2}$$

where

$$\tau = \alpha_2/\phi \tag{3}$$

is the "retardation time;" it is defined as the time it takes for the deformation to reach $(1-\frac{1}{e})$ of its final, elastic value (Fig. 4). $\tau$ is a measure of the delay, caused by the dashpot, in attaining the elastic deformation. On removal of the force the deformation is gradually recovered. The Kelvin model thus represents delayed elasticity or after-effect.

If spring and dashpot are arranged in series (Maxwell model, Fig. 2), the total deformation rate is the sum of the elastic and viscous deformation rates:

$$(dy/dt) = \alpha_1 (dq/dt) + \phi q. \tag{4}$$

Under a constant deformation $y = y_0$ the initial force $y_0/\alpha_1$ relaxes exponentially.

$$q = (y_0/\alpha_1)e^{-t/\tau} \tag{5}$$

Here

$$\tau = \alpha_1/\phi \tag{6}$$

is the "relaxation time;" it is defined as the time it takes for the force to diminish to 1/e of its initial value (Fig. 5). For a constant force the deformation increases linearly with time. This is the simplest type of the phenomenon of creep; thus the Maxwell model represents creep and relaxation.

Fig. 3 shows the arrangement in parallel of a spring and a Maxwell element, frequently referred to as the "Standard Solid." This model combines the two previously mentioned models. If the left spring is very stiff, this model tends towards the Kelvin model; if the right spring is very soft the model tends towards the Maxwell model. Hence, the Standard Solid model exhibits a behavior in between that of a Kelvin and a Maxwell model.

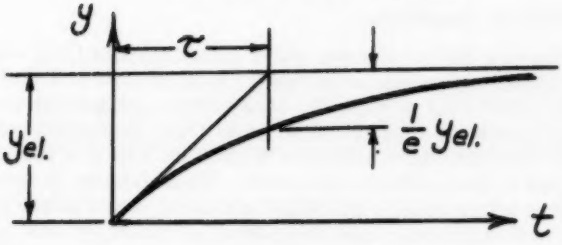


Figure 4.
Deformation-time diagram for a Kelvin element under a constant force.

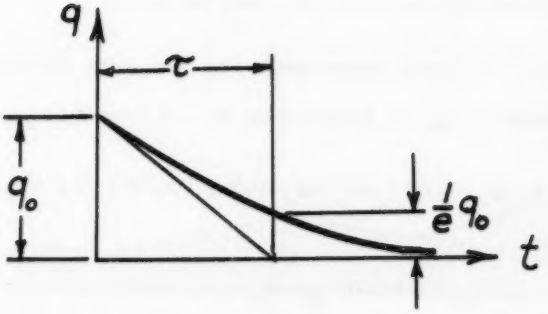


Figure 5.
Force-time diagram for a Maxwell element under constant deformation (relaxation diagram).

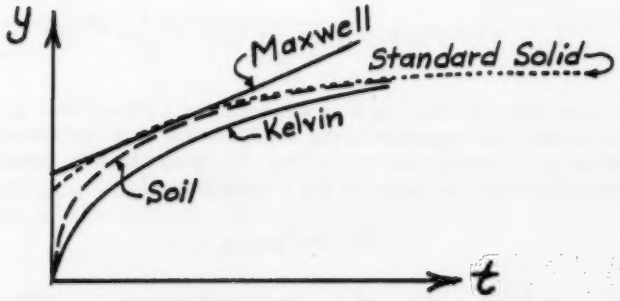


Figure 6.
Deformation-time diagrams for viscoelastic elements and soil under constant force.

Application to Beam on Foundation

The deformation of a Kelvin element under constant force (Fig. 4) approximately corresponds to the consolidation under constant load of a soil, the voids of which are filled with water. The behavior of a Maxwell element, on the other hand, is somewhat similar to that of an incompressible, cohesive soil under shear. The total deformation of a cohesive soil is a combination of deformations due to consolidation and shear. Consolidation is the predominant long-term effect under relatively light loads, while shear becomes more significant with increasing load intensities, particularly over short time intervals. Fig. 6 shows how the Standard Solid model best approximates actual soil behavior, while the Kelvin foundation approximates long-term behavior and the Maxwell foundation short-term behavior.

The present paper treats an elastic beam on various viscoelastic foundations corresponding to models of Figs. 1, 2, and 3. In all cases it will be assumed that the foundation pressure and its rate of change with time at a point depend on the deflection and its rate of change with time at that point only; in other words, the foundation will be idealized as a series of identical, viscoelastic elements, spaced uniformly under the beam.

Elastic Beam on a Linear Viscoelastic (Standard Solid) Foundation

With the notation of Fig. 3 it follows from (4) and from $y = \alpha_2 q_2$, using $q = q_1 + q_2$, that

$$(dy/dt) = \alpha_1 (dq_1/dt) + \beta q_1 = \alpha_2 (dq_2/dt) = \alpha_2 (dq/dt) - \alpha_2 (dq_1/dt).$$

This becomes

$$(dq_1/dt) + (1/\tau) q_1 = (\alpha_2 / \beta\tau)(dq/dt), \tag{7}$$

if the notation

$$\tau = (\alpha_1 + \alpha_2)/\beta \tag{8}$$

is used. The solution of this differential equation is

$$y = (\alpha_1 \alpha_2 / \beta\tau)\left(q + [\alpha_2/\alpha_1 \tau]\, e^{-t/\tau} \int_0^t q e^{t/\tau}\, dt\right) \tag{9}$$

which gives the deformation y as a function of a given force q.

The differential equation of the elastic beam on a viscoelastic foundation, loaded by an arbitrary load p(x,t) (Fig. 7), is obtained by substitution of (9) into the differential equation of the elastic beam[13]

$$EI(\partial^4 y/\partial x^4) = p(x,t) - q(x,t) \tag{10}$$

where E and I are modulus of elasticity and moment of inertia, respectively, of the beam. By differentiation with respect to t and subsequent elimination of the integral in (9), the following equation is obtained.

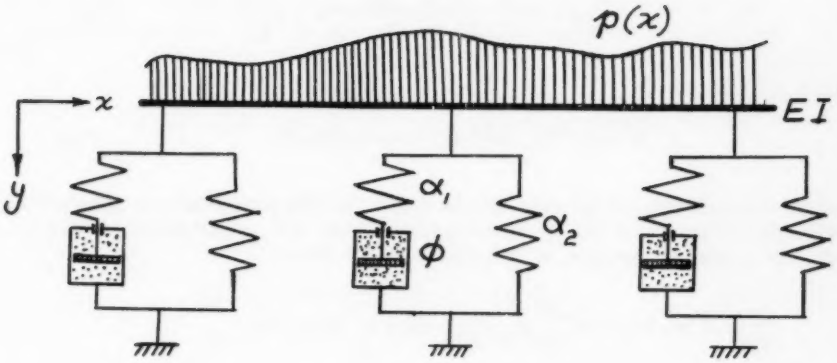


Figure 7.
Elastic beam on a linear viscoelastic
(Standard Solid) foundation.

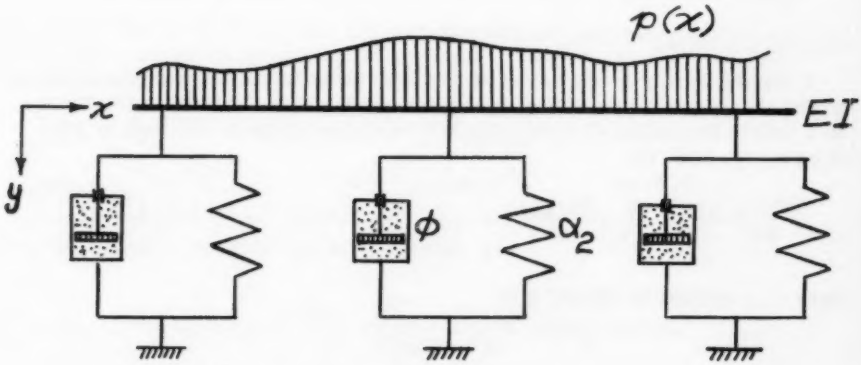


Figure 8.
Infinite elastic beam on a foundation
with after-effect (Kelvin foundation).

$$k^4 \frac{\partial^5 q}{\partial t \partial x^4} + k^4 \frac{\alpha_2}{\alpha_1} \frac{\partial^4 q}{\partial x^4} + \frac{\partial q}{\partial t} + \frac{q}{\tau} = \frac{p}{\tau} + \frac{\partial p}{\partial t} \qquad (11)$$

Here

$$k^4 = EI\alpha_1\alpha_2/(\alpha_1+\alpha_2) = EI\,\alpha_1\alpha_2/\phi\tau \qquad (12)$$

where k is a length. Whenever (11) is solved for the soil pressure q(x,t), the deflection of the beam y(x,t) can be obtained from (9). A particularly simple solution arises in the case of $(\partial^4 p/\partial x^4) = 0$ for which

$$q(x,t) = p(x,t) + \sum_{m=0}^{m=\infty} (A_m \cosh mx + B_m \sinh mx + C_m \cos mx + D_m \sin mx)\, e^{-\frac{(\alpha_1+\alpha_2)/\alpha_1 + 1/m^4k^4}{1 + 1/m^4k^4} \cdot \frac{t}{\tau}}$$

Further, simpler solutions will now be given for the case of the elastic beam on either the Kelvin or the Maxwell foundation.

## Elastic Beam on a Foundation with After-Effect (Kelvin Foundation)

### General Formulae

If the left spring in the model of Fig. 3 is made infinitely stiff ($\alpha_1 = 0$), the model changes into that of Fig. 1, and the beam of Fig. 7 becomes the beam on a Kelvin foundation (Fig. 8). Its differential equation is obtained by substituting (1) into (10).

$$\frac{\partial^4 y(x,t)}{\partial x^4} + \frac{\tau}{k^4} \cdot \frac{\partial y(x,t)}{\partial t} + \frac{1}{k^4} y(x,t) = \frac{p(x,t)}{EI} \qquad (14)$$

Here $\tau$ is defined by (3) and k by

$$k^4 = EI\alpha_2.$$

The initial condition for this beam is that the deflection is zero at t = 0. The deflection of a beam on an elastic foundation is a particular solution of (14). The solution of the homogeneous equation for (14) (right-hand side equal to zero) is obtained by setting $y(x,t) = f(x) \cdot g(t)$ which splits (14) into two ordinary differential equations that can readily be solved.

$$y_m(x,t) = (A_m \cosh mx + B_m \sinh mx + C_m \cos mx + D_m \sin mx)\, e^{-(1+m^4k^4)\,t/\tau} \qquad (16)$$

where m is a non negative integer. Hence the general solution of (14) is the sum of solutions (16) and the deflection of the beam on an elastic foundation. The soil pressure is obtained by substituting this solution in (1).

Infinite Beam Loaded by a Space-periodic Load, Invariant with Time

If the beam is loaded by a space-periodic load of period $2\pi$* which does not vary with time (Fig. 9a), the load function can be expanded in a Fourier series

$$p(x) = a_o/2 + \sum_{m=1}^{m=\infty} (a_m \cos mx + b_m \sin mx) \tag{17}$$

subject to very general conditions.(14) The coefficients of this series are given by

$$a_m = (1/\pi) \int_{-\pi}^{\pi} p(x) \cos mx \, dx \tag{17a}$$

$$b_m = (1/\pi) \int_{-\pi}^{\pi} p(x) \sin mx \, dx \tag{17b}$$

The corresponding elastic foundation pressures and deflections are

$$q_{el.} = a_o/2 + \sum_{m=1}^{m=\infty} (1/[1+m^4k^4]) (a_m \cos mx + b_m \sin mx) \tag{18a}$$

and

$$y_{el.} = \alpha_2 q_{el.} \tag{18b}$$

as can be verified from (10). Eqs. (18) thus furnish the particular solution for (14). The solution of the homogeneous equation is given by (16) with the following substitutions.

$$A_o = B_o = D_o = 0, \qquad C_o = a_o/2 \qquad A_m = B_m = 0,$$

$$C_m = \alpha_2 a_m/(1+m^4k^4), \qquad D_m = \alpha_2 b_m/(1+m^4k^4) \qquad m = 1,2,3,\ldots$$

Hence, the complete solution for the deflection is

$$y(x,t) = (\alpha_2 a_o/2)(1-e^{-t/\tau}) + \sum_{m=1}^{m=\infty} [\alpha_2/(1+m^4k^4)][a_m \cos mx + b_m \sin mx][1-e^{-(1+m^4k^4)t/\tau}]. \tag{19}$$

The foundation pressure follows by substitution in (1).

$$q(x,t) = a_o/2 + \sum_{m=1}^{m=\infty} (1/[1+m^4k^4])(a_m \cos mx + b_m \sin mx)(1+m^4k^4e^{-(1+m^4k^4)t/\tau}) \tag{20}$$

* If the period of the load is 2L instead of $2\pi$, m is to be replaced by $m\pi/L$ in all the equations that follow, except for the limits of all the sums which remain unchanged from m = 1 to m = $\infty$.

Eqs. (19) and (20) clearly show the behavior of the beam. At the instant of application of the load (t = 0) the foundation pressure is equal to the load, and the deflection is zero; the beam remains stiff at this instant, and the load is transmitted vertically through the beam and counteracted by an equal and opposite foundation pressure: $q(x,0) = p(x,0)$.*

After an infinite time interval ($t \to \infty$) foundation pressure and deflection approach their elastic values. During the transient state ($0 \leqq t \leqq \infty$) the approach to the final state for the beam on the Kelvin foundation is the faster, the larger m, k, and $1/\tau$; i.e. the smaller the period of the load (see footnote, page 8), the stiffer the beam with respect to the foundation, and the lower the viscosity of the foundation.

Infinite Beam Loaded by an Arbitrary Load, Invariant with Time

If the infinite, elastic beam is loaded by an arbitrary load which does not vary with time, the load function can be represented by its Fourier integral.

$$p(x) = (1/\pi) \int_0^\infty dm \int_{-\infty}^{+\infty} p(z) \cos[m(z-x)]\, dz \tag{21}$$

subject to very general conditions.[15] By direct analogy with the procedures used in the previous paragraph the elastic foundation pressures and deflections are

$$q_{el.} = (1/\pi) \int_0^\infty dm/(1+m^4k^4) \int_{-\infty}^{+\infty} p(z) \cos[m(z-x)]\, dz \tag{22a}$$

$$y_{el.} = (\alpha_2/\pi) \int_0^\infty dm/(1+m^4k^4) \int_{-\infty}^{+\infty} p(z) \cos[m(z-x)]\, dz \tag{22b}$$

The last equation again furnishes a particular solution for (14). The solution of the homogeneous equation is taken as the integral over m of solutions[16] setting $A_m = B_m = D_m = 0$ and determining $C_m$ such that the deflection vanishes at t=0.

$$y(x,t) = (\alpha_2/\pi) \int_0^\infty (1-e^{-(1+m^4k^4)t/\tau})\, dm/(1+m^4k^4) \cdot \int_{-\infty}^{+\infty} p(z) \cos[m(z-x)]\, dz. \tag{23}$$

As before, the foundation pressure follows from (1).

$$q(x,t) = (1/\pi) \int_0^\infty (1+m^4k^4 e^{-(1+m^4k^4)t/\tau})\, dm/(1+m^4k^4) \int_{-\infty}^{+\infty} p(z) \cos[m(z-x)]\, dz. \tag{24}$$

* This is true, provided the spreading out of the load through the thickness of the beam is not considered. Such effects are taken into account in reference 19.

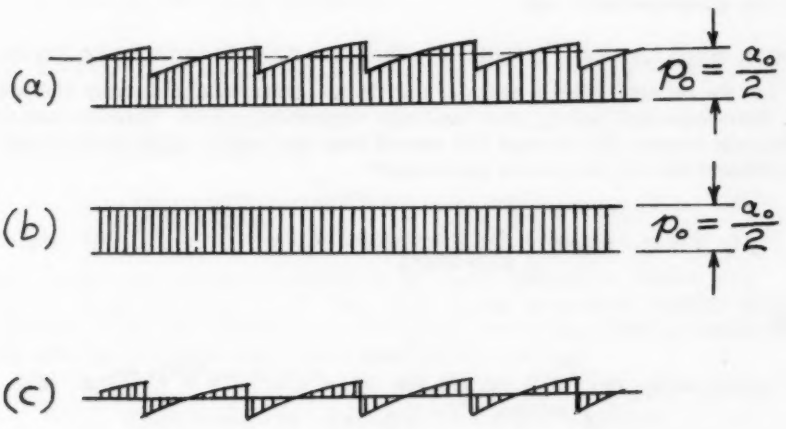


Figure 9.
a) Beam loaded by a space-periodic load p(x);
b) Average load $p_o\ a_o/2$;
c) Self-equilibrating load $p(x)-a_o/2$.

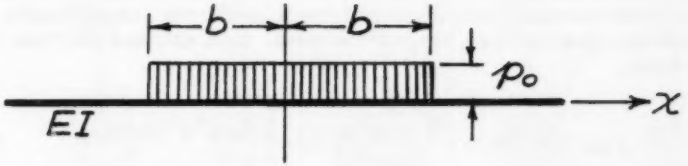


Figure 10.
Infinite beam loaded by a uniformly distributed load over a finite region.

The interpretation of the beam behavior is similar to that discussed above for the space-periodic load.

Infinite Beam Loaded by a Uniformly Distributed Load over a Finite Region

Let the infinite, elastic beam of Fig. 10 be loaded by a uniformly distributed, time invariant load $p_o$ over the finite region $-b \leq x \leq +b$. Then the second integrals in eqs. (21) through (24) extend over the limits $-b \leq z \leq +b$ only, and the integration can be readily performed:

$$y(x,t) = 2p_o\ (\alpha_2/\pi) \int_0^\infty \frac{\sin mb \cos mx}{m(1+m^4k^4)} \left(1 - e^{-(1+m^4k^4)t/\tau}\right) dm \qquad (25)$$

and

$$q(x,t) = (2p_o/\pi) \int_0^\infty \frac{\sin mb \cos mx}{m(1+m^4k^4)} \left(1+m^4k^4 e^{-(1+m^4k^4)t/\tau}\right) dm \qquad (26)$$

After an infinite time interval the parenthesis in (25) becomes equal to unity, and

$$y(x,\infty) = y_{el.} = (2p_o\alpha_2/\pi) \int_0^\infty \frac{\sin mb \cos mx}{m(1+m^4k^4)}\, dm \qquad (27)$$

is the Fourier integral of the expression for the deflection of a beam on an elastic foundation, generally found in the literature.(16) As a rule, two equations for $y_{el.}$ are given depending on whether the point under consideration is within, or outside of, the loaded region. Eq. (27) covers both cases with a single expression.

Infinite Beam Loaded by a Single, Concentrated, Constant Load

If the infinite, elastic beam is acted upon by a single, concentrated, time invariant load, the preceding Fourier integral solutions are applicable with the following substitutions: $2bp_o \rightarrow P$ and $b \rightarrow 0$. Eqs. (25) and (26) then become, respectively,

$$y(x,t) = (\alpha_2 P/\pi) \int_0^\infty \frac{\cos mx}{1+m^4k^4} \left(1 - e^{-(1+m^4k^4)t/\tau}\right) dm \qquad (28)$$

and

$$q(x,t) = (P/\pi) \int_0^\infty \frac{\cos mx}{1+m^4k^4} \left(1+m^4k^4 e^{-(1+m^4k^4)t/\tau}\right) dm. \qquad (29)$$

The last integral does not converge at $t = 0$ on account of the sharp discontinuity of load and foundation pressure at the origin at that instant. This, however, is not a serious defect of the solution because it is known that, at

t = 0, the foundation pressure equals the load.*
For $t \to \infty$ eq. (28) can be written as

$$y(x,\infty) = y_{el.} = \alpha_2 q_{el.} = \alpha_2 q(x,\infty) = (\alpha_2 P/\pi) \int_0^\infty \frac{\cos mx}{1+m^4k^4}\, dm. \quad (30)$$

This is the Fourier integral of

$$y_{el.} = (\alpha_2 P/2\sqrt{2}k)\, e^{-(x/\sqrt{2}k)} \cdot [\cos(x/\sqrt{2}k) + \sin(x/\sqrt{2}k) \quad (31)$$

which is the deformation of a beam on an elastic foundation, loaded by a single concentrated load P.(17) This again shows the general validity of the remarks concerning the behavior of an elastic beam on a (Kelvin) foundation with after-effect which were made under (V,b) above.

## Elastic Beam on a Relaxing (Maxwell) Foundation

### General Formulae

If the right spring in the model of Fig. 3 is eliminated ($\alpha_2 \to \infty$), this model changes into that of Fig. 2, and the beam of Fig. 7 becomes the beam on a Maxwell foundation (Fig. 11). Eq. (11) simplifies to

$$k^4 \frac{\partial^5 q(x,t)}{\partial x^4 \partial t} + \frac{k^4}{\tau} \cdot \frac{\partial^4 q(x,t)}{\partial x^4} + \frac{\partial q(x,t)}{\partial t} = \frac{\partial p(x,t)}{\partial t} \quad (32)$$

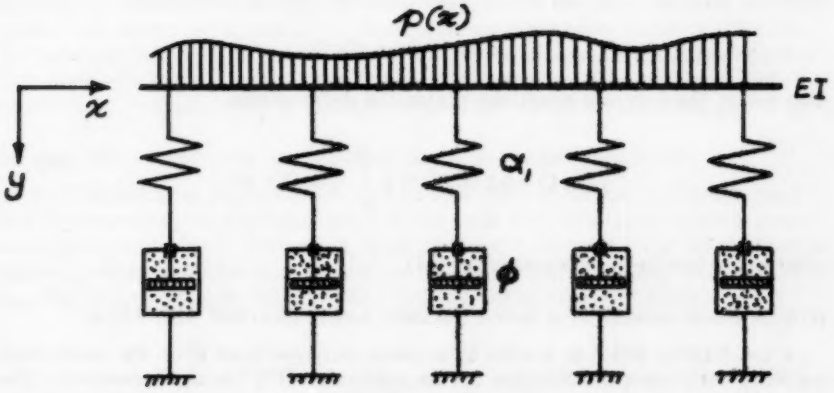


Figure 11.
Infinite elastic beam on a relaxing (Maxwell) foundation.

*Also see footnote, page 10.

where $\tau$ is defined by (6) and k by

$$k^4 = EI\alpha_1 . \tag{33}$$

If the applied loads do not vary with time, (32) reduces to

$$k^4\frac{\partial^2 q(x,t)}{\partial x^4 \partial t} + \frac{k^4}{\tau} \cdot \frac{\partial^4 q(x,t)}{\partial x^4} + \frac{\partial q(x,t)}{\partial t} = 0 \tag{32a}$$

Solutions of this equation are assumed to be of the form $q(x,t) = f(x)\cdot g(t)$ which splits (32a) into two ordinary differential equations.

$$q_m(x,t) = (A_m \cosh mx + B_m \sinh mx + C_m \cos mx + D_m \sin mx)\, e^{\left\{\frac{-t/\tau}{1+1/m^4k^4}\right\}} \tag{34}$$

Here m is a non-negative integer. The deflection y(x,t) is obtained from the foundation pressure q(x,t) by integration of (4) with respect to the time.

$$y(x,t) = \int_0^t \frac{\partial y(x,t)}{\partial t}\, dt + F(x)$$

where F(x) is an arbitrary function of x alone. It can be evaluated by considering that, at t = 0, the deflection equals the elastic deflection.

$$y(x,0) = F(x) = \alpha_1 q(x,0).$$

The use of the last two equations yields the deformation

$$y(x,t) = \alpha_1 q(x,t) + \phi \int_0^t q(x,t)\, dt \tag{35}$$

after q(x,t) has been obtained from (34).

Infinite Beam Loaded by a Space-periodic Load, Invariant with Time

If the infinite beam is loaded by a space-periodic load (Fig. 9a) which does not vary with time, the Fourier series expansion (17) can again be used. The foundation pressures are obtained by an infinite sum of solutions (34) with the following substitutions.

$A_o = B_o = D_o = 0$, $\quad C_o = a_o/2$ $\quad A_m = B_m = 0$,

$C_m = a_m/(1+m^4k^4)$, $\quad D_m = b_m/(1+m^4k^4)$, $\quad m = 1,2,3,.....$

Hence the Maxwell foundation pressure equals

$$q(x,t)=a_o/2+\sum_{m=1}^{m=\infty}\left(\frac{a_m\cos mx}{1+m^4k^4}+\frac{b_m\sin mx}{1+m^4k^4}\right)e^{\left\{\frac{-t/\tau}{1+1/m^4k^4}\right\}}, \quad (36)$$

and the beam deflection follows from (35).

$$y(x,t)=(\alpha_1 a_o/2)(1+t/\tau)+\sum_{m=1}^{m=\infty}(\alpha_1/m^4k^4)\cdot(a_m\cos mx + b_m\sin mx)\left(1-\frac{e^{\left\{\frac{-t/\tau}{1+1/m^4k^4}\right\}}}{1+m^4k^4}\right) \quad (37)$$

The behavior of the beam becomes apparent from the last equation: at the instant of load application (t=0) the deflection equals the elastic deflection (18b). After an infinite time interval ($t\to\infty$) the beam deflection is composed of two parts:

I. The deflection of a beam loaded by a uniform load equal to the average load $p_o = a_o/2$ (Fig. 9b); this is the uniform settlement of a straight, rigid beam corresponding to the uniform motion of the piston in the viscous dashpot (Fig. 2) under a constant force;

II. the elastic deflection of the beam under a self-equilibrating force system equal to the difference between the actual load and its average (Fig. 9c). This latter deflection is entirely independent of the stiffness and viscosity of the foundation, and only depends on the bending stiffness EI of the beam.

The final state of the beam, therefore, is that of a floating, elastic beam. During the transient state ($0\leqq t\leqq\infty$) the approach to the final deflection is the faster the larger m, k, and $1/\tau$. The same criteria were found to hold for the beam on the Kelvin foundation. From (36) it is apparent that the foundation pressure at t = 0 represents the elastic pressure (18a) and that, with infinite time, it approaches a constant value equal to the average load $p_o = a_o/2$.

Infinite Beam Loaded by an Arbitrary Load, Invariant with Time

For the infinite, elastic beam loaded by a time invariant, arbitrary load the Fourier integral representation of the load (21), elastic foundation pressure (22a), and elastic deflection (22b) may again be used. The Maxwell foundation pressure follows by integration over m of solutions (34) with $A_m=B_m=D_m=0$. $C_m$ is determined from the initial (elastic) state.

$$q(x,t)=(1/\pi)\int_0^\infty e^{\frac{-t/\tau}{1+1/m^4k^4}}\frac{dm}{1+m^4k^4}\int_{-\infty}^{+\infty}p(z)\cos[m(z-x)]dz \quad (38)$$

The integration (35) yields the deformation.

$$y(x,t)=(\alpha_1/\pi)\int_0^\infty\left(1-\frac{e^{\frac{-t/\tau}{1+1/m^4k^4}}}{1+m^4k^4}\right)\frac{dm}{m^4k^4}\int_{-\infty}^{+\infty}p(z)\cos[m(z-x)]dz \quad (39)$$

The variation of deflections and foundation pressures is identical to that discussed in the preceding paragraph; i.e., the initial state is that of a beam on an elastic foundation, the final state is that of a floating beam. Eqs. (38) and (39), however, are valid solutions only if, for any point x, a finite interval $x_1 < x < x_2$ exists such that

$$\int_{x_1}^{x_2} [\, p(x) - p_o \,]\, dx = 0 \qquad (40)$$

where $p_o$ is the average load on the beam.
If equation (40) is not satisfied, the beam becomes subject to an infinitely large bending moment as t approaches infinity. Obviously, no real structure can sustain infinite moments, and a redistribution of stresses will take place once the proportional limit of the material in the elastic beam has been exceeded.

Among others, the regional load discussed in (V,d) above and the single concentrated load (V,e) do not satisfy (40).

## Numerical Examples

A reinforced concrete beam, 30 in. wide and 20 in. deep, is continuously supported by a Kelvin or a Maxwell foundation. The beam is loaded by 30 x 30 in. columns every 20 ft. throughout its infinite length (Fig. 12). Each column load of 300 kips is considered uniformly distributed over the contact area. The modulus of elasticity of the concrete is 2500 kips per sq. in., the foundation modulus 0.75 kips per sq. in. per in. The last constant must be multiplied by the beam width in order to obtain $1/\alpha$, the reciprocal of the

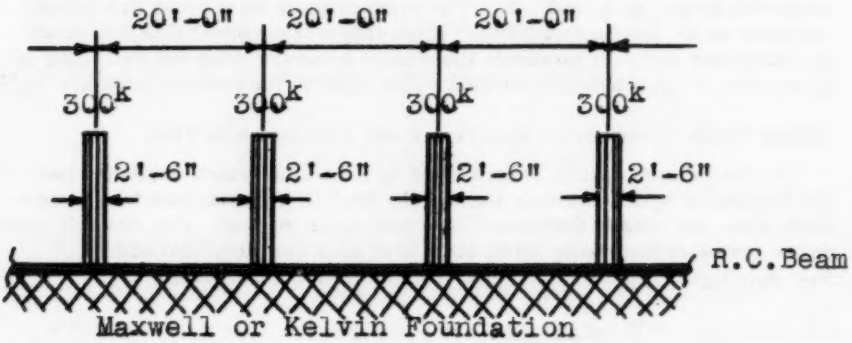


Figure 12.
Elastic beam on a viscoelastic foundation loaded by equal column loads.

elastic foundation constant used in this paper. This is due to the fact that the foundation modulus is defined as the ratio of bearing unit stress to deflection, while $\alpha$ is the ratio of deflection to bearing load per unit length.

The Fourier coefficients for the load function p(x) are determined from (17a) and (17b).

$$\left.\begin{aligned} a_m &= (40/m\pi)\,(-1)^{m/2}\,\sin(m\pi/16) \quad \ldots\ \text{if m is even} \\ a_m &= 0 \quad \ldots\ \text{if m is odd} \\ b_m &= 0 \end{aligned}\right\} \qquad (41)$$

The deflections and bearing pressures for the beam on the Kelvin and Maxwell foundations, respectively, are obtained from equations (19), (20), (36), and (37) when m is replaced by $m\pi/L$, the summations are extended over all even integers, and relations (41) are used. Bending moments in the beam are obtained through term by term differentiation of equations (19) and (37). Sufficient numbers of terms of the series were taken to make the first term omitted less than 1% of the sum of the previous terms. This somewhat arbitrary criterion limits the error to approximately 2% for series, all of whose terms are positive, and to a little over 1/2% for series with alternating positive and negative terms. The former applies to points on the beam under the columns, the latter to all other points calculated. As a rule, six terms were thus required for the bending moments and three terms for the bearing pressures and deflections.

Figs. 13 through 15 show the variations in space and time of the bearing pressure, bending moment, and deflection for the beam on a foundation with after-effect (Kelvin foundation). The corresponding data for the beam on a relaxing (Maxwell) foundation are given in Figs. 16 through 18. The variation with time of the beam behavior is shown in terms of the relative time $t/\tau$. This makes Figs. 13 through 18 valid for any value of $\phi$, provided the elastic properties of beam and foundation are those assumed above. Bearing pressures and bending moments for the beam on a viscoelastic foundation can be expressed in terms of the bearing pressures and bending moments for the beam on an elastic foundation, if the viscous property of the foundation ($\phi$ or $\tau$) and the ratio of the elastic properties of beam and foundation (k) are given. The actual values of those properties must be known, however, in order to obtain values for the deflections.

Fig. 13 shows the gradual spreading-out of the bearing pressure for the beam on the foundation with after-effect (Kelvin foundation) from the state of the rigid foundation to that of the elastic foundation. Small negative bearing pressures occur in a region between the columns during a short time after the load has been applied. Even though these small tensile stresses exceed the adhesion between beam and foundation and hence the actual bearing stress distribution changes, this change will be limited to a short initial time interval. The corresponding changes in bending moments and deflections will likewise be limited to a short period of time and will not change the long-term behavior of the beam. The upward deflections over a small portion of the beam for $t/\tau$ less than 2 (Fig. 15) are, in part, a consequence of those tensile stresses. However, even though no tensile stress between beam and foundation can be transmitted in a particular foundation, these upward deflections will not disappear completely.

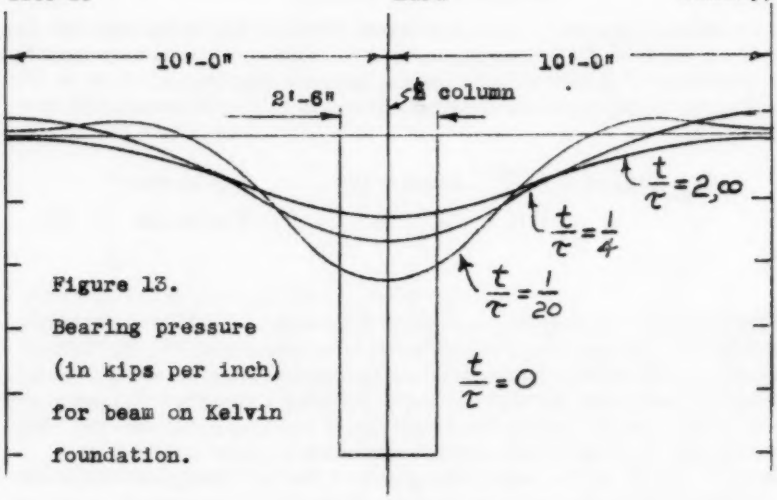


Figure 13.
Bearing pressure (in kips per inch) for beam on Kelvin foundation.

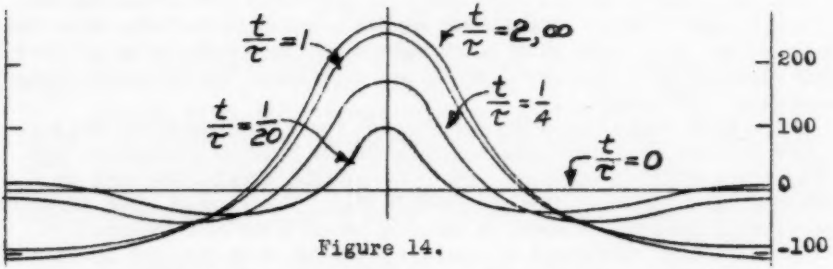


Figure 14.
Bending moment (in foot-kips) for beam on Kelvin foundation.

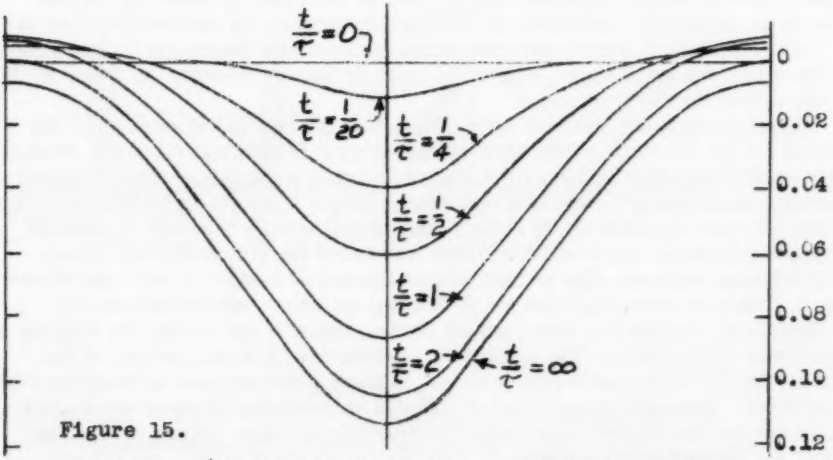


Figure 15.
Deflection (in inches) for beam on Kelvin foundation.

Fig. 14 indicates that, at some time or other, negative moments occur almost throughout the length of the beam on a Kelvin foundation. These moments are small, compared to moments for the beam on an elastic foundation ($t/\tau = \infty$), but they make it advisable to provide a nominal amount of top reinforcing steel over the entire length of a reinforced concrete beam. This is generally done in beams where such steel is needed for the proper placement of stirrups, but it is frequently omitted in beams for which no stirrups are required. The curves in Figs. 13 through 15 are not materially affected by a change in relative stiffness between beam and foundation.

The gradual flattening-out of the bearing pressure curve for a beam on a relaxing (Maxwell) foundation from its elastic to its average value is shown in Fig. 16. Fig. 17 shows how the bending moment in the beam increases as a consequence. Both bearing pressure and bending moment remain virtually constant at the quarter-points. The maximum positive bending moment increases by 57% over that for the beam on an elastic foundation, the maximum negative bending moment by 138%. This shows that, as far as stresses in the beam are concerned, it is unsafe to assume elastic behavior for a foundation in which irrecoverable shear deformations play a significant part.

If the elastic stiffness of the foundation with respect to that of the beam is decreased (k increases), bearing pressures and bending moments for the beam on an elastic foundation gradually approach those for the beam on a relaxing foundation at infinite time; i.e., those of the floating beam. For a value of k = 10 feet, their maximum difference is about 2%. (Figs. 13 through 18 are based on k = 3.22 feet) These differences become larger with increasing relative stiffness of the foundation and tend to become infinite for a perfectly flexible beam or an infinitely stiff foundation: k = 0 (Fig. 19).

Fig. 18 illustrates the steady downward motion as a whole of the beam on a Maxwell foundation on which an increase in beam flexure is superposed. An increase in k (more flexible foundation or stiffer beam) makes all the curves flatter, a decrease in k has the opposite result; neither changes the essential two-phase character of the deflection curves.

## SUMMARY

A general differential equation is derived for an elastic beam on a linear viscoelastic foundation, acted upon by arbitrarily varying loads in space and time (11). A solution is given for the special case of $(\partial^4 p/\partial x^4) = 0$. Eq. (13).

Assuming less general viscoelastic laws for the foundation, the time and space variations of foundation pressure and deflection are determined for an infinite elastic beam on a foundation with linear after-effect (Kelvin foundation)(1) and a linear relaxing (Maxwell) foundation(4) provided the loads do not vary with time. The initial state of the beam on a Kelvin foundation is the beam on a perfectly rigid foundation, the final state of the beam on a Kelvin foundation and the initial state of the beam on a Maxwell foundation is the beam on an elastic foundation, while the final state of the beam on a Maxwell foundation is the floating beam.

For the infinite beam on a relaxing (Maxwell) foundation the load function must satisfy condition (40); otherwise the moments in the beam will become infinite if the assumption of linear behavior for the beam material is maintained. Among others, the single concentrated load does not satisfy equation (40).

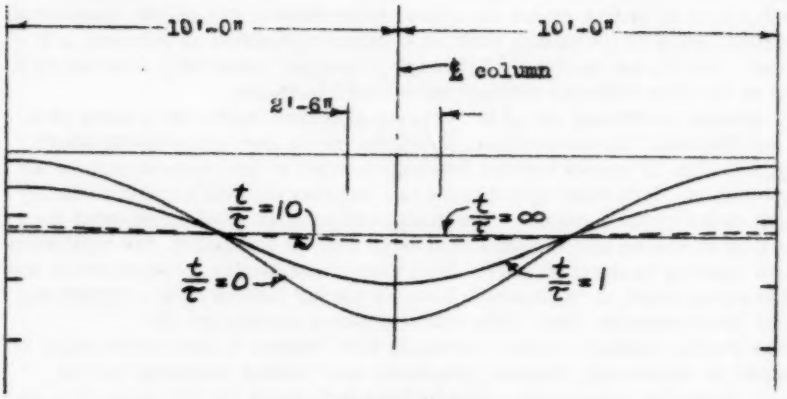


Figure 16.

Bearing pressure (in kips per inch)

for beam on Maxwell foundation.

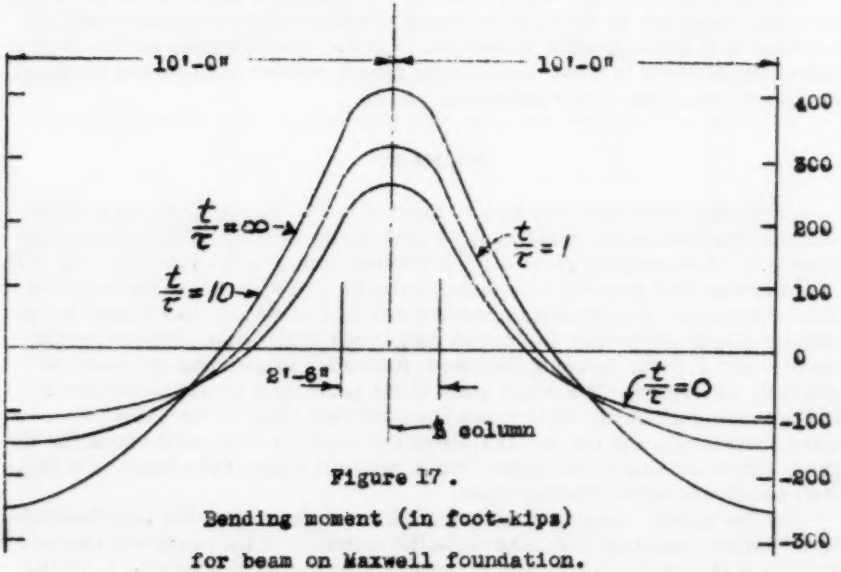


Figure 17.

Bending moment (in foot-kips)

for beam on Maxwell foundation.

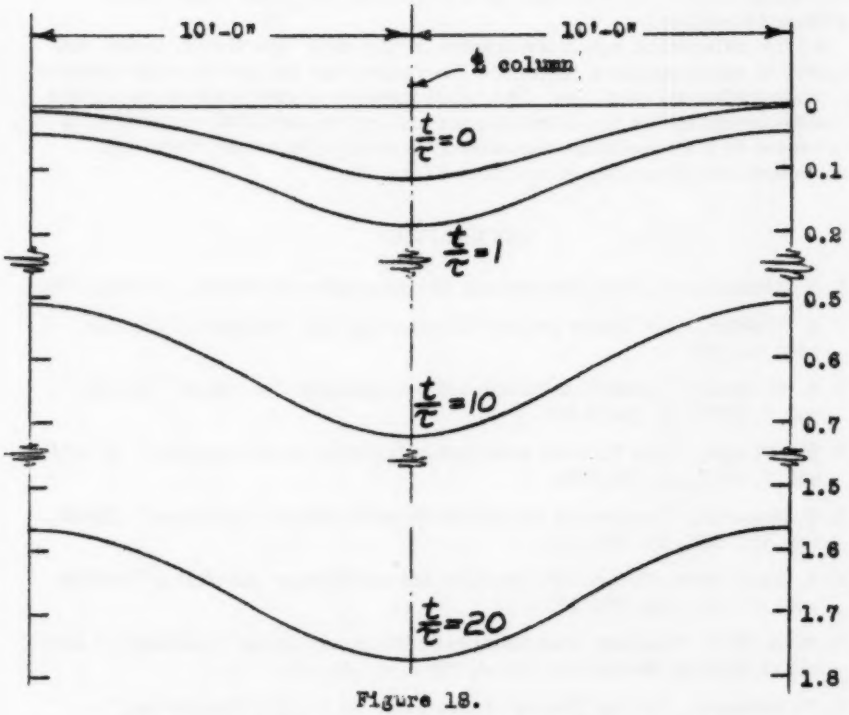


Figure 18.

Deflection (in inches) for beam on Maxwell foundation.

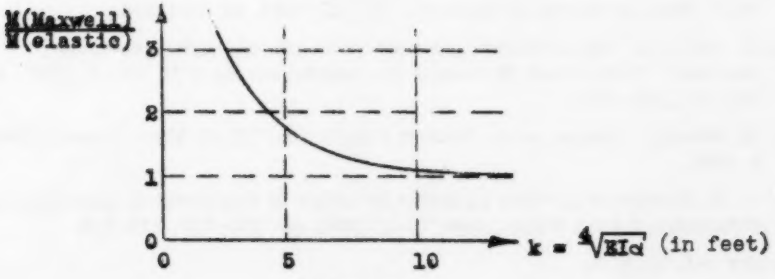


Figure 19.

Ratio of maximum negative bending moment in beam on Maxwell foundation to that in a beam on an elastic foundation as a function of relative stiffness of beam and foundation.

Graphs are given which show the behavior of an infinite, elastic beam under equally spaced column loads on a foundation with after-effect and a relaxing foundation.

All the differential equations treated in this paper are linear; hence, any number of solutions for a particular foundation may be used in superposition to obtain additional solutions. The usual methods of transition from infinite to finite beams by the use of end forces and end moments(18) is also valid for beams on a viscoelastic foundation. In general, however, these end forces and end moments are functions of the time.

## REFERENCES


1. H. Zimmerman, "Die Berechnung des Eisenbahnoberbaues," Berlin, 1888.
2. E. Winkler, "Die Lehre von der Elastizitaet und Festigkeit," Prague, 1867, p. 182.
3. K. Wieghart, "Ueber den Balken auf nachgiebiger Unterlage," ZAMM, vol. 2, 1922, pp. 165-184.
4. W. Prager, "Zur Theorie elastisch gelagerter Konstruktionen," ZAMM, vol. 7, 1927, pp. 354-360.
5. P. Nemenyi, "Tragwerke auf elastisch nachgiebiger Unterlage," ZAMM, vol. 11, 1931, pp. 450-463.
6. K. Marguerre, "Ueber den Traeger auf elastischer Unterlage," ZAMM, vol. 17, 1937, pp. 224-231.
7. M. A. Biot, "Bending of an Infinite Beam on an Elastic Foundation," Journal of Applied Mechanics, vol. 4, 1937, pp. A1-A7.
8. E. Reissner, "On the Theory of Beams on an Elastic Foundation," Federhofer-Girkman Festschrift, Denticke, Vienna, 1950, pp. 87-102.
9. E. Reissner, "On the Theory of Beams Resting on a Yielding Foundation," Proc. Natl. Academy of Sciences, vol. 23, 1937, pp. 328-333.
10. E. Volterra, "Sul problema generale della trave poggiata su suolo elastico," Rend. Acad. Nazionale dei Lincei, series VIII, vol. 2, 1947, pp. 307-311, 418-421.
11. M. Hetenyi, "Beams on an Elastic Foundation," U. of Mich. Press, 1946, p. 208.
12. A. M. Freudenthal, "The Inelastic Behavior of Engineering Materials and Structures," John Wiley, New York, 1950, pp. 220-229, 232-235.
13. See ref. 11, p. 3.
14. R. V. Churchill, "Fourier Series and Boundary Value Problems," McGraw-Hill Book Co., New York, 1941, p. 70.
15. See ref. 14, p. 89.
16. See ref. 11, pp. 15-17.
17. See ref. 11, p. 11.
18. See ref. 11, pp. 38-42.
19. G. Bosson, "The Flexure of an Infinite Elastic Strip on an Elastic Foundation," Philosophical Magazine, Series VII, vol. 27, 1939, pp. 37-50.